1991

Investigation Of Naphthacene Mobility On Silica

David Wayne Bjarneson

INVESTIGATION OF NAPHTHACENE MOBILITY ON SILICA

by

David Wayne Bjarneson

Department of Chemistry

Submitted in partial fulfillment
of the requirements for the degree of
Doctor of Philosophy

Faculty of Graduate Studies
The University of Western Ontario
London, Ontario
December, 1990

ISBN 0-315-64244-0

ABSTRACT

Photophysical and photochemical examinations of polycyclic aromatic hydrocarbons adsorbed on metal oxide surfaces provide indirect evidence for the mobility of these species. We employ Fluorescence Photobleaching Recovery (FPR) to directly measure the mobility of naphthacene on various silica gel surfaces at low coverages. On normal phase silica, the rate of diffusion is found to be invariant of the surface treatment. The diffusion coefficient is constant at 2.5×10^{-10} cm^2 s^{-1}, but the mobile fraction shows a pronounced dependence on surface treatment. These results indicate that the mobility of the same population of naphthacene is being measured in each case, but the fraction of molecules in that population changes with surface preparation.

The mobility of naphthacene is significantly greater on silica gels derivatized with long chain hydrocarbons. Both the diffusion coefficient and the mobile fraction are greatly increased. The largest values for both the diffusion coefficient and mobile fractions are found for naphthacene on silica first derivatized with C18 chains then further derivatized by coadsorption of undecanol, or normal phase silica with physisorbed myristic acid. Increased diffusion on derivatized surfaces is interpreted as the probe interaction with the coating more than the silica surface. Chemical derivatization yields heterogeneous incomplete coatings, whereas physical derivatization leads to more complete homogeneous coatings.

Photophysical investigations of naphthacene both in solution and on silica are carried out in order to examine the possibility of a

link between previous photophysical studies and direct diffusion measurements. It appears that a direct link cannot be made.

Photochemical studies of naphthacene in solution and on silica are performed from a kinetics perspective. Naphthacene photolyzes to two types of products, depending on conditions. In solution, both pathways are first order in naphthacene. On silica, the kinetics are not as simple. This lead to further development of FPR theory which previously assumed first order bleaching only. If the bleaching process is second order, little effect on the mobile fraction is seen, but the diffusion coefficient will be underestimated using the current FPR theory.

ACKNOWLEDGEMENTS

Over the last few years Dr. Nils Petersen has given much of his time and energy towards this project. I offer my deepest gratitude to him, his guidance and patience are greatly appreciated.

The graduate students of this laboratory have been the best of friends and lab mates. I thank Dr. Bruce Balcom, Paul St. Pierre, Alison Paprica and Paul Wiseman for their friendship and sharing of knowledge.

Finally, I would like to thank my family for support throughout my entire post secondary education.

TABLE OF CONTENTS

Page

Page

LIST OF TABLES

LIST OF FIGURES

LIST OF SYMBOLS

Symbol	Description
A	Attenuation
C	Concentration
$\bar{C}$	Average initial concentration
D	Diffusion Coefficient
ε	Molar extinction coefficient
ϕ	Quantum yield
f	Relative fluorescence intensity
f	Frictional coefficient
f_i	Fraction in i^{th} population
F	Absolute fluorescence intensity
g	Signal losses
I	Intensity
I_a	Rate of photon absorbance
k	Boltzmann's constant
k	Rate constant
k(r)	Radially dependent rate constant
K	Extent of bleaching parameter - first order
K′	Extent of bleaching parameter - second order
λ	Photochemical quantum yield - first order
λ'	Photochemical quantum yield - second order
ma	Myristic acid
n	Number
N	Number of data points
N′	Number of samples
^1N	Ground state naphthacene
$^1N^*$	First excited singlet state of naphthacene
$^3N^*$	First excited triplet state of naphthacene
N_2	Naphthacene dimer
P	Laser power
Q	Emission quantum yield
r	Radial distance
τ	Lifetime
τ_D	Characteristic diffusion time
t	Time
t′	Time
T	Absolute temperature
T_p	Pretreatment temperature
ω	Beam width
χ_r^2	Reduced chi-square
Xm	Mobile fraction
X	Mole fraction

LIST OF ABBREVIATIONS

Abbreviation	Description
C1	Methyl derivatized silica
C8	Octyl derivatized silica
C18	Octadecyl derivatized silica
CFM	Continuous Fluorescence Microphotolysis
CHX	Cyclohexane
CI-MS	Chemical Ionization Mass Spectroscopy
DMPC	Dimyristoylphosphatidylcholine
DPPC	Dipalmitoylphophatidylcholine
ESM	Exponential Series Method
FAB-MS	Fast Atom Bombardment Mass Spectroscopy
FEM	Field Emission Microscopy
FIM	Field Ionization Microscopy
FPR	Fluorescence Photobleaching Recovery
HPLC	High Performance Liquid Chromatography
IPA	Isopropanol
MEM	Maximum Entropy Method
MS	Mass Spectroscopy
NBD	N-methyl-4-amino-7-nitrobenz-2-oxa-1,3-diazole
NBDPE	NBD labelled phosphatidylethanolamine
OD	Optical density
PAH	Polycyclic aromatic hydrocarbon
PAHs	Polycyclic aromatic hydrocarbons
PMT	Photomultiplier tube
UV-VIS	Ultraviolet-visible

CHAPTER ONE

INTRODUCTION

Interest in surface diffusion extends as far back as the 1920's when Volmer investigated crystal growth and transport over surfaces[1]. Over the last seventy years, much interest has been focused on the motion of species adsorbed on solid surfaces[1-3]. Motion of adsorbates plays a distinct role in processes such as surface mediated reactions, heterogeneous catalysis, and some photophysical and photochemical processes in heterogeneous systems[4-14].

The vast majority of quantitative surface diffusion studies have measured the motion of a gas or a metal on metal surfaces[1-3]. Generally, the adsorbates in these systems are chemisorbed, *i.e.* they are bound to the surface with energies on the order of a hundred kilojoules per mole or more[1-3,15]. Many diverse techniques have been developed for direct measurements of surface mobility in these systems. Two microscopic techniques employed are Field Ionization Microscopy (FIM) and Field Emission Microscopy (FEM)[16]. Both techniques employ high electric fields at the end of a metal whisker, which allows for measurement of mobilities on atomic length scales. In FIM, an inert gas is ionized at the tip of the whisker and is accelerated towards a detector. The efficiency of the ionization process depends greatly on the local electric field. FEM relies on variations in the local work function to cause changes in the flux of field emitted electrons. The work function is sensitive to alterations of the surface, such as the presence of adsorbates.

These two methods use systems in equilibrium, whereas many others measure mobilities by generation of concentration gradients. Both FIM and FEM use high electric fields which can cause artifacts arising from field induced desorption. As well, neither of these two techniques give chemical or structural specificity which can complicate interpretation of some data obtained.

Other techniques have been developed to measure surface mobilities on larger length scales (μm to mm). These include Auger electron spectroscopy, laser induced desorption (LID), low energy electron diffraction (LEED), contact potential difference (CPD) methods, and a laser beam localized surface photochemistry technique[1-3,16-18]. LID, for instance, involves either one or two laser beams causing local changes in the surface concentration of the adsorbate. This results in a concentration gradient, the relaxation of which is measured over time. The laser beam typically covers areas of a few hundred square micrometers.

Application of these techniques has lead to quantitative measurements of the mobility of a score of adsorbates (gases and metals) on numerous metal surfaces. The diffusion coefficients for these systems are found to depend on temperature, surface coverage, and the strength of binding. Temperature ranges examined extend from a few degrees Kelvin to hundreds of degrees Kelvin. Surface coverages are generally high, and range from 20% of a monolayer to complete coverage and even multilayers. The optimal range of mobility for use of each of these techniques varies. A range of mobilities from 10^{-17} to 10^{-6} cm^2 s^{-1} is covered by these techniques[1-3,16].

Surface diffusion of adsorbates on metal oxide surfaces (silica, alumina) has been said to occur, but previously has not been measured directly. Evidence for the mobility of polycyclic aromatic hydrocarbons (PAHs) on silica and alumina come from various photochemical and photophysical studies[5-14]. The binding interactions for these systems are hydrogen bonding between the π electrons of the PAH and surface hydroxyl groups, and is on the order of tens of kilojoules per mole[15]. Species bound to surfaces with these weaker interactions are termed physisorbed. The goals of the photochemical and photophysical investigations were not to measure surface diffusion, but rather to examine the behavior of these species in heterogeneous environments. Many results obtained are explained by adopting an assumption of mobility on the surface. This assumption is used to explain the growth of excimer emission from pyrene on silica gel[7], and the ratio of *cis* to *trans* acenaphthylene dimers formed on silica gel upon irradiation[17]. These investigations provide indirect evidence for motion of adsorbates, but do not provide a means for quantification of the motion.

Fluorescence Photobleaching Recovery (FPR) is a suitable tool for measuring the mobility of adsorbed PAHs directly. Until now, this fluorescence microscopy based technique has been used almost exclusively with systems of great importance in the biological fields. The basis of FPR lies in the generation of a concentration gradient, and following the relaxation of the gradient as a function of time.

FPR is well suited for diffusion measurements in a time regime relatively slow compared to mobilities in non-viscous solutions. The

range of diffusion coefficients covered by this technique is from 10^{-} cm^2 s^{-1} to 10^{-7} cm^2 s^{-1}, or characteristic diffusion times in the 10^5 to 0.1 s range[19]. There are other fluorescence microscopy techniques which are suitable for faster diffusion[19].

Diffusion measurements have been performed on a variety of systems. In 1974, the first group to report on the use of fluorescence redistribution techniques investigated the mobility of rhodopsin in the retinal disk membrane[20]. In this study, Poo and Cone found the diffusion coefficient for rhodopsin to be 3.5×10^{-9} cm^2 s^{-1}. Liebman and Entine, in an independent study, found similar results for the same system[21]. Shortly after, Peters and co-workers reported the mobility of some proteins in human erythrocyte membranes to be on the order of 10^{-12} cm^2 s^{-1} [22]. Since these early studies using FPR, many groups worldwide have used and developed this technique to investigate a great variety of systems. A short description follows which gives a flavor for the variety of systems investigated, and the range of values found in the mobility parameters measured.

Some of the fastest diffusion measurements made with FPR are for various fluorescently labelled species in model or synthetic membranes. Peters and Beck measured the mobility of labelled phospholipids in both multilaminar bilayers and monolayer spreads[23]. . . dilaurylphosphatidylcholine bilayers, the diffusion coefficient of fluorescently labelled phosphatidylethanolamine (NBDPE) was measured to be 7.7×10^{-8} cm^2 s^{-1}. In the monolayer study, the diffusion coefficient was found to be a function of the surface pressure, and varied from 110 to 15×10^{-8} cm^2 s^{-1} for surface pressures in the range

of 1 to 38 mN/m. For the same probe in dipalmitoylphosphatidylcholine (DPPC) over a range of surface pressure in which DPPC exhibits a phase change, the diffusion coefficient varied from greater than 10^{-7} cm^2 s^{-1} to less than 10^{-8} cm^2 s^{-1}. In all cases the mobile fractions were found to be unity.

Recently in our lab, a systematic study on the dependence of the diffusion coefficient on probe size was carried out[24]. In this study, model membranes were used with a series of fluorescently labelled probes. Results for NBDPE in dimyristoylphosphatidylcholine (DMPC) multibilayers were in agreement with those of Peters and Beck.

When using cell membranes which have numerous structures of physiological importance, the diffusion process is found to be slower. Mobility of labelled proteins which are native in cell membranes have been measured in both cell and model membranes. A review by Edidin[25] shows that some proteins are immobile, on the time scale of the photobleaching experiment, in cell membranes, but are mobile in model membranes with diffusion coefficients of $(2 - 3)\times10^{-10}$ cm^2 s^{-1}. Data for other proteins presented in this review show an increase in mobility by a factor of 2 to 5 in model membranes over cell membranes. Good agreement between groups is reported in this review.

Weis *et al.* have used FPR in conjunction with total internal reflection to measure diffusion of a lipid hapten in lipid monolayers coated on alkylated quartz microscope slides[26]. In this study, quartz slides were first alkylated with octadecyltrichlorosilane. A second layer, consisting of DPPC with 2 mol% lipid hapten, was then deposited on the slide. The diffusion coefficient was measured to be less than

10^{-10} cm^2 s^{-1}. In two similar studies, the mobility of NBDPE on alkylated quartz supported DPPC monolayers was measured to be 2×10^{-10} cm^2 s^{-1} [27,28]. In these investigations, the fluorescent probe is removed from the glass substrate by two layers. In similar experiments performed here, the PAH probe is in contact with the first monolayer.

In the developmental stages of FPR, Axelrod and co-workers investigated the diffusion of Rhodamine 6G in water and water/glycerol mixtures[29]. In particular, they were interested in measuring the effect of the extent of photobleaching on the diffusion coefficient. By roughly doubling the extent of bleaching, they found virtually no change in the diffusion coefficient of $(1.2\pm0.2)\times10^{-6}$ cm^2 s^{-1} for the dye in water, and $(0.26\pm0.09)\times10^{-6}$ cm^2 s^{-1} for the dye in 1:1 water/glycerol. The study revealed that the diffusion coefficient does not have an apparent systematic dependence on the extent of bleaching.

Studies on many diverse systems have been reported. Generally, there is good agreement between different groups working on similar problems. Variations in reported values may occur due primarily to two sources. Systematic errors can arise from poorly aligned optics, or inaccurate determinations of the beam size. Also, when dealing with biological samples, live cell lines for example, there are some parameters that investigators cannot control which may lead to variations in mobility values.

FPR has been employed to determine mobility of numerous probes in many diverse environments. The values of D ranges from 10^{-7} to

10^{-13} cm^2 s^{-1} and the mobile fraction (Xm) has been found to range from less than 10% to unity. In this study, we employ FPR to measure the mobility of naphthacene on various silica gel surfaces. The diffusion coefficient is measured to be on the order of 10^{-9} to 10^{-10} cm^2 s^{-1}, and the mobile fraction is in the 30 to 90% range. These values fall well within the ranges reported by others who have used this technique, and represent significant mobility.

Continuous Fluorescence Microphotolysis (CFM) is another fluorescence microscopy based technique, similar to FPR. The same apparatus is employed for both techniques, but CFM does not involve imposing a large concentration gradient by using a strong bleach beam. Instead, a laser beam of moderate intensity is shone on the sample continuously. The time dependent fluorescence intensity will depend on two factors: the rate of photodestruction and diffusion of probes into the illumination area. Peters and co-workers have developed the necessary theory for extraction of both the diffusion coefficient and the rate constant for the photolysis reaction[30,31]. In the development, the assumption of first order photobleaching kinetics is assumed. Among other systems, Peters *et al.* have measured the diffusion coefficient and bleaching rate constants for 3,3'-dioctadecyloxatricarbocyanine in lipid vesicles and fluorescein isothiocyanate in a glycerol/water mixture. The measured diffusion coefficients are on the order of 10^{-8} cm^2 s^{-1}, and rate constants are on the order of 1 s^{-1} [30]. The diffusion coefficients are in good agreement with those found by FPR for the same systems.

The major goal of this thesis is to investigate the mobility of

PAHs on various silica gel surfaces utilizing FPR. This provides direct and quantitative evidence for the mobility of PAHs adsorbed on silica surfaces. The mobility of adsorbed naphthacene is studied in detail, with two other PAHs (rubrene and pentacene) examined in less detail.

In conjunction with the diffusion measurements, the photochemical and photophysical behavior of naphthacene in solution and on silica is examined. In solution, the fluorescence decay of naphthacene follows a single exponential decay law. On silica, the fluorescence decay is best described as a distribution of lifetimes. The decay data for adsorbed naphthacene are analyzed using the Exponential Series Method[32].

In solution, naphthacene photo-oxidizes to form an endoperoxide in the presence of oxygen, but dimerizes in degassed solutions upon irradiation. Both processes are found to proceed through mechanisms first order in naphthacene. The photoproducts of naphthacene are examined spectroscopically. NMR (nuclear magnetic resonance), UV-VIS (absorption spectroscopy) and MS (mass spectroscopy) data are presented for these species in this thesis.

On the surface, the kinetics of photobleaching are measured using CFM techniques. The photolysis of adsorbed naphthacene apparently does not always follow a first order pathway. Inherent in the development of the theoretical basis of FPR is the assumption of first order bleaching kinetics. To quantitate any effects on the measured diffusion parameters the theoretical aspects of FPR are extended to include effects of second order bleaching kinetics.

REFERENCES

(1) Ehrlich, G.; Stolt, K. *Ann. Rev. Phys. Chem.* **1980**, *31*, 603, and references therein.

(2) Naumovets, A. G.; Vedula Yu. S. *Surface Sci. Rep.* **1984**, *4*, 365.

(3) Kapoor, A.; Yang, R. T.; Wong, C. *Catal. Rev.: Sci. Eng.* **1989**, *31*, 129.

(4) Kropp, P. J.; Daus, K. A.; Crawford, S. D.; Tubergen, M. W.; Kepler, K. D.; Craig, S. L.; Wilson, V. P. *J. Amer. Chem. Soc.* **1990**, *112*, 7434.

(5) Francis, C.; Lin, J.; Singer, L. A. *Chem. Phys. Lett.* **1983**, *94*, 162.

(6) Turro, N. J.; Zimmt, M. B.; Gould, I. R. *J. Amer. Chem. Soc.* **1985**, *107*, 5826.

(7) Bauer, R. K.; Borenstein, R.; de Mayo, P.; Okada, K.; Rafalska, M.; *Ware, W. R.;* Wu, K. C. *J. Amer. Chem. Soc.* **1982**, *104*, 4635.

(8) de Mayo, P.; Natarajan, L. V.; Ware, W. R. *Chem. Phys. Lett.* **1984**, *107*, 187.

(9) de Mayo, P.; Natarajan, L. V.; Ware, W. R. *J. Phys. Chem.* **1985**, *89*, 3526.

(10) de Mayo, P.; Natarajan, L. V.; Ware, W. R. In *Organic Phototransformations in Nonhomogeneous Media;* Fox, M. A., Ed.; American Chemical Society: Washington, DC, 1985; Chapter 1.

(11) Bauer, R. K.; de Mayo, P.; Ware, W. R.; Wu, K. C. *J. Phys.Chem.* **1982**, *86*, 3781.

(12) Bauer, R. K.; de Mayo, P.; Okada, K.; Ware, W. R.; Wu, K. C. *J. Phys. Chem.* **1983**, *87*, 460.

(13) de Mayo, P.; Okada, K.; Rafalska, M.; Weedon, A. C.; Wong, G. S. K. *J. Chem. Soc. Chem Commun.* **1981**, 821.

(14) Bauer, R. K.; de Mayo, P.; Natarajan, L. V.; Ware, W. R. *Can. J. Chem.* **1984**, *62*, 1279.

(15) Unger, K. K. In *Porous Silica;* Elsevier Scientific Publishing Co.: New York, 1979, pp 76-7.

(16) Chabal, Y. J. *Vacuum* **1990**, *41*, 70.

(17) Butz, R.; Wagner, H.; *Surface Sci.* **1977**, *63*, 448.

(18) Zeiger, H. J.; Tsao, J. Y.; Ehrlich, D. J. *J. Vac. Sci. Technol.* **1985**, *B(3)*, 1436.

(19) Petersen, N. O.; Elson, E. L. *Meth. Enzym.* **1986**, *130*, 454.

(20) Poo, M-M.; Cone, R. A. *Nature* **1974**, *247*, 438.

(21) Liebman, P. A.; Entine, G. *Science* **1974**, *185*, 457.

(22) Peters, R.; Peters, J.; Tews, K. H.; Bahr, W. *Biophys. Biochem. Acta* **1974**, *367*, 282.

(23) Peters, R.; Beck, K. *Proc. Natl. Acad. Sci.* **1983**, *80*, 7183.

(24) Balcom, B. J. Ph. D. Dissertation, The University of Western Ontario, 1990.

(25) Edidin, M. *Curr. Top. Membr. Transp.* **1987**, *29*, 91.

(26) Weis, R. M.; Balakrishan, K.; Smith, B. A.; McConnell, H. M. *J. Biol. Chem.* **1982**, *257*, 6440.

(27) Smith, B. A.; McConnell, H. *Proc. Natl. Acad. Sci.* **1978**, *75*, 2759.

(28) Burghardt, T. P.; Axelrod, D. *Biophys J.* **1981**, *33*, 255.

(29) Axelrod, D.; Koppel, D. E.; Schlessinger, J.; Elson, E.; Webb, W. W. *Biophys. J.* **1976**, *16*, 1055.

(30) Peters, R.; Brünger, A.; Schulten, K. *Proc. Natl. Acad. Sci.* **1981**, *78*, 962.

(31) Brünger, A.; Peters, R.; Schulten, K. *J. Chem. Phys.* **1985**, *82*, 2147.

(32) James, D. R.; Liu, Y.-S.; Petersen, N. O.; Siemiarczuk, A.; Wagner, B. D.; Ware, W. R. *Soc. Photo-optical Instr. Eng. (SPIE)* **1987**, *7453*, 117.

CHAPTER TWO

FLUORESCENCE MICROSCOPY TECHNIQUES

2.1 Introduction

Fluorescence microscopy techniques have been developed and widely used in biological fields to measure the mobility of biologically important molecules in various media[1,2]. In Chapter 1 of this thesis a brief introduction was presented showing the variety of systems investigated, and the range of results obtained with Fluorescence Photobleaching Recovery (FPR).

The theory for FPR, presented by Axelrod *et al.*[3], was developed with an initial condition of first order bleaching kinetics. The photobleaching reaction has been postulated to occur between the probe molecule and excited singlet oxygen[4,5]. This process should be first order in the fluorescent probe since it is the source of singlet oxygen. Most biological systems studied have oxygen contents much greater than the concentration of the fluorescent probe. If photobleaching occurs through a pathway involving oxygen, the oxygen content should not be a rate limiting factor. A mechanism for photo-oxidation of PAHs has been postulated by Stevens and Algar[6-8]. If a similar mechanism applies in the biological samples, then the photo-oxidation is expected to be first order in the parent fluorophore. To date, no publication has appeared which addresses the possible effects of non-first order bleaching kinetics.

We are particularly interested in the kinetics of the

photochemistry with respect to the fluorescent probe only. Hence, when discussing kinetics, usually only the order with respect to the probe will be mentioned. This is not to be taken as the overall order of the chemical reaction.

We use FPR to investigate the mobility of polycyclic aromatic hydrocarbons (PAHs) adsorbed on various silica gel surfaces *in vacuo*. Most experiments are performed with naphthacene as the fluorescent probe. Naphthacene is chosen for its simple structure (Figure 2.1) and fluorescent properties (Figure 2.2). Naphthacene is a planar aromatic molecule with no functional groups. As well, naphthacene is fluorescent with a quantum yield of fluorescence (ϕ_f) of 0.21 in cyclohexane[9], and can be excited with the 476.5 nm line of an Argon ion laser.

Studies on the photochemistry of naphthacene reveal that two type of photoproducts are possible. In aerated systems, naphthacene reacts with singlet oxygen to form an endoperoxide[6-8,10-13]. This process is first order in naphthacene. In degassed systems, two naphthacene react to form a dimer[14-17]. This process has been postulated to be second order in naphthacene[18]. The primary photoproduct for naphthacene adsorbed on silica gel *in vacuo* is expected to be the dimer. As a result, a theoretical investigation into the effects of second order bleaching kinetics on the recovered diffusion parameters is carried out.

To gain a better understanding of the kinetics of photobleaching of adsorbed naphthacene, a technique similar to FPR is employed. Peters *et al.* have developed a technique termed Continuous

Figure 2.1: Structure of naphthacene.

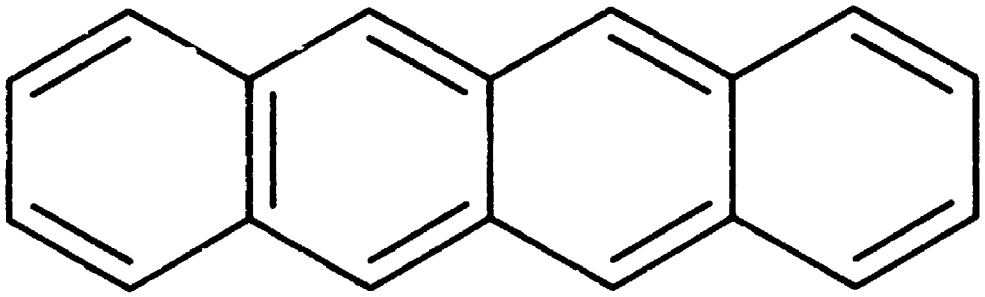

Figure 2.2: Excitation (——) and emission (– – –) spectra of naphthacene in cyclohexane. Excitation wavelength 441 nm; emission wavelength 507 nm; 9.5×10^{-6} M.

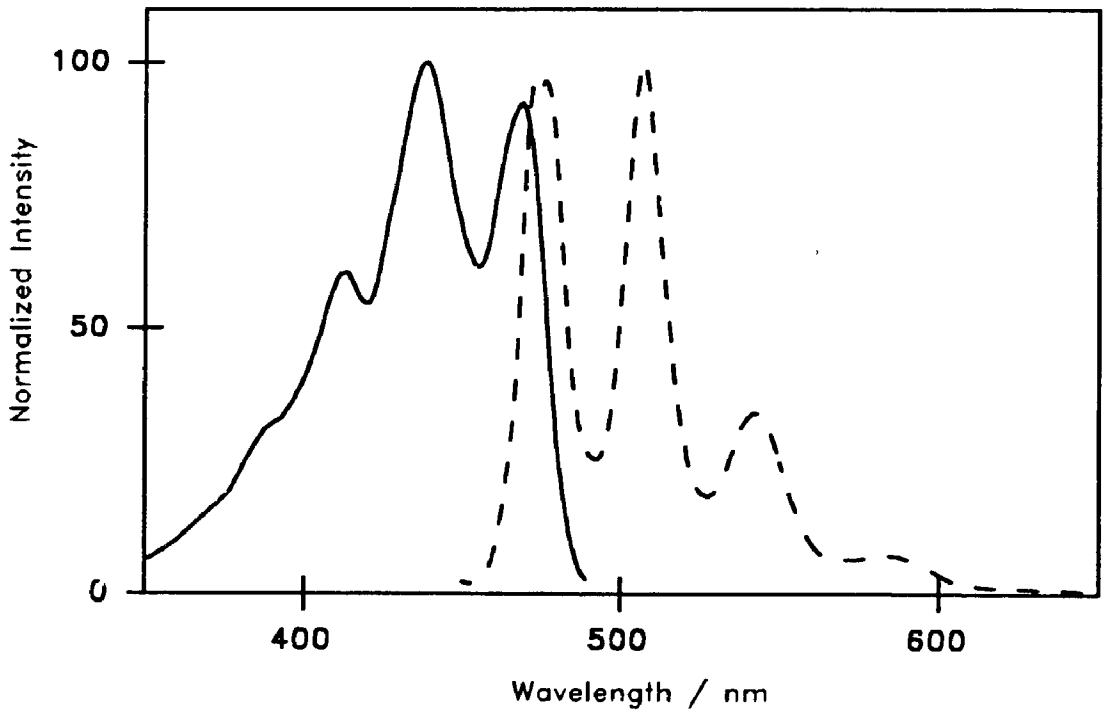
100
50
0
Normalized Intensity
400
500
600
Wavelength / nm

Fluorescence Microphotolysis (CFM)[19-21], which involves irradiating a fluorescent sample with a moderately intense laser beam, and following the decay of the fluorescence as a function of time. Two competing processes have an effect on the fluorescence intensity: photobleaching decreases the intensity while diffusion of fluorophores into the illuminated region counters the decrease. The theory outlined by Peters also assumed first order bleaching kinetics. Ferrières *et al.* further developed the theory for continuous microphotolysis for second order bleaching processes[22]. Use of this technique allows, in principle, for extraction of both the diffusion coefficient and a rate constant for photobleaching. We use CFM not to evaluate a diffusion coefficient, but to gain insight into the kinetics of the photochemistry of adsorbed naphthacene.

The remainder of Chapter 2 is a discussion on theoretical and conceptual aspects of FPR. Following the procedure of Axelrod *et al.*[3], the theory for fluorescence recovery following a second order bleach is developed. A brief discussion on CFM is also included.

2.2 Fluorescence Photobleaching Recovery Theory

The illumination source used by many groups is a laser operating in the TEM_{00} mode. This gives a Gaussian intensity profile when the laser beam reaches the sample. Many other illumination sources and illumination patterns have also been used in fluorescence redistribution experiments[23-27]. We use the spot photobleaching technique in our laboratory. The following discussion will deal with

some of the theoretical and conceptual aspects of spot photobleaching.

Fluorescence photobleaching entails creation of a concentration gradient in fluorescent molecules and subsequent measurement of the relaxation of the imposed gradient as a function of time. Simply, a typical experiment is run thus: a weak, focused laser beam (monitor beam) is shone on the surface of a fluorescent sample and the initial fluorescence intensity (F(-)) is recorded. Then a brief, intense laser pulse (bleach beam) is shone on the sample in the same spatial region. This causes a decrease in the fluorescence intensity (to (F(0)) due to rapid irreversible photolysis of a fraction of the fluorophores present. Over time, the fluorescence intensity will increase (F(t)) due to diffusion of unbleached fluorophores into the partially bleached region. The increase in intensity is measured using the weak beam, and recorded as a function of time. After most of the recovery has taken place, the weak laser beam is shut off to permit complete recovery without exposure to light. With the weak beam turned on again, the final fluorescence intensity, $F(\infty)$, is measured. This process is shown schematically in Figure 2.3. The experimental design employed to achieve the ability to irradiate the same area with two laser beams of different intensities is outlined in Figure 2.4.

2.2.1 Recovery Following First Order Photobleaching

The kinetics of photobleaching is rarely reported, and probably rarely measured. First order kinetics are generally assumed. In the

Figure 2.3: Schematic representation of an FPR experiment. The initial intensity (F(-)) of the fluorophores (o) is measured. Some of fluorophores are photolyzed to non-fluorescent products (●) by the bleach pulse , creating a concentration gradient. The intensity immediately following the bleach pulse (time zero) is F(0). Fluorophores will diffuse into the partially bleached region, increasing the fluorescence intensity as a function of time (F(t)). After a long time, the fluorescence intensity at infinite time (F(∞)) is measured.

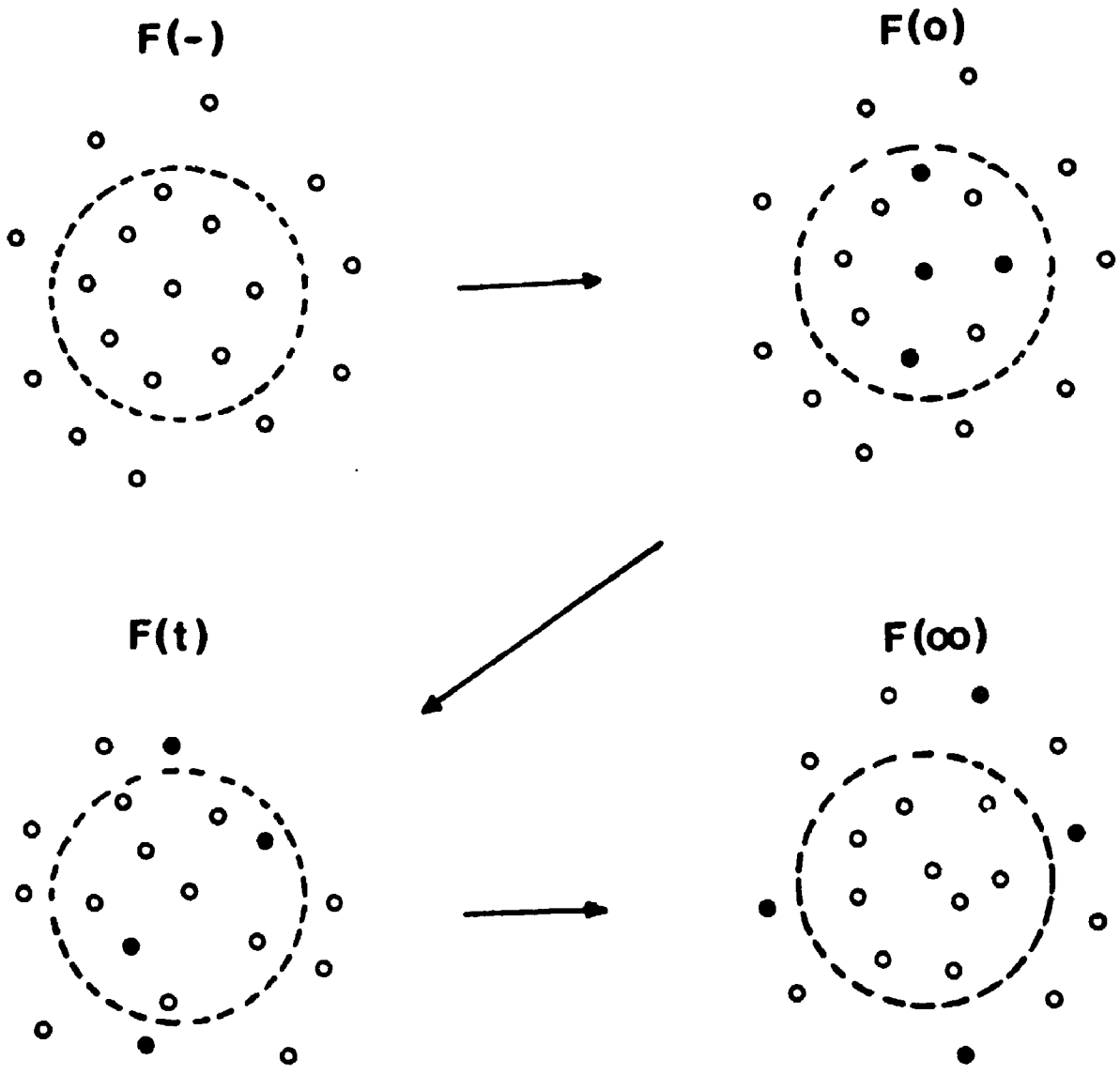
F(-)
F(o)
F(t)
F(∞)

Figure 2.4: Layout of FPR apparatus. The inset shows the beam splitters which allow for illumination of the same region with two collinear beams. The bold line after the first beam splitter represents the bleach beam, the narrow line is the monitor beam. Two shutters (S1 and S2) control when the beams reach the sample, and mirrors (M1 to M3) are used to steer the beams.

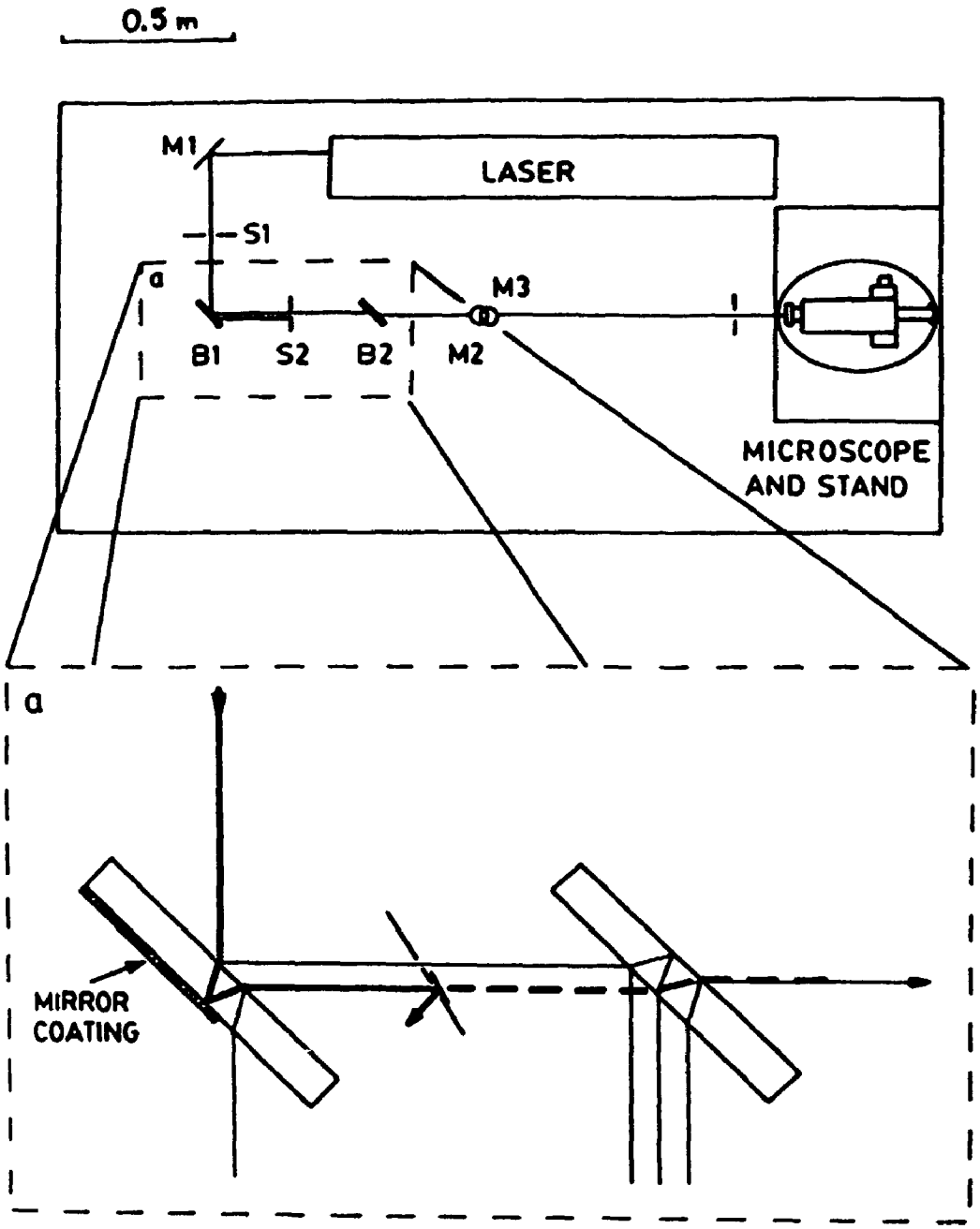
0.5 m
M1
LASER
S1
a
M3
B1
S2
B2
M2
MICROSCOPE
AND STAND
a
MIRROR
COATING

development of the theory of FPR, Axelrod *et al.* worked through the mathematics under an initial condition of first order bleaching kinetics[3]. This assumption makes the solution for the fluorescence recovery easy to derive, and easy to use. To this point in time, no report has appeared in the literature in which the effects of non-first order bleaching kinetics is investigated.

With first order kinetics, the bleaching rate is given by Equation 2.1:

$$\frac{d\,C(r,t)}{dt} = -\lambda\, I(r)\, C(r,t) \qquad (2.1)$$

where λ is a photochemical quantum yield, $C(r,t)$ is the concentration of the fluorescent probe, and $I(r)$ is the laser beam intensity profile defined by:

$$I(r) = I_0 \exp\,(-2\, r^2 / \omega^2) \qquad (2.2)$$
$$= (2\, P / \pi\, \omega^2) \exp\,(-2\, r^2 / \omega^2)$$

where P represents the laser power incident on the sample, and ω represents the width of the laser beam where the power falls to exp(-2) of its maximum value.

Integration of Equation 2.1 yields the distribution of fluorophores immediately following the bleach pulse taken to be time zero:

$$C(r,0) = \bar{C} \exp\,(-\lambda\, I(r)\, t') \qquad (2.3)$$

$\bar{C}$ represents the average prebleach fluorophore concentration and t' is the duration of the bleach pulse. Taking $K = \lambda I_0 t'$, which measures the extent of bleaching, Equation 2.3 yields the initial concentration of fluorophores in terms of K to be:

$$C(r,0) = \bar{C} \exp\left\{ - K \exp\,(-2\, r^2 / \omega^2)\right\} \qquad (2.4)$$

This initial postbleach concentration is the initial boundary condition used to solve the time dependent diffusion equation:

$$\frac{\partial C(r,t)}{\partial t} = D \frac{\partial^2 C(r,t)}{\partial r^2} \qquad (2.5)$$

The solution of Equation 2.5 for $C(r,t)$ is used to characterize the observed fluorescence recovery $f(t)$.

Detection of the fluorescence intensity is done with a photomultiplier tube. The photocurrent produced is followed as a function of time and will depend on the intensity of the laser ($I(r)$) and the concentration of fluorophores ($C(r,t)$). The position r is measured radially from the center of the laser beam, which is normal to the plane of focus. The photocurrent, $f(t)$, is defined as:

$$f(t) = (g \varepsilon Q / A) \int_0^\infty I(r)\, C(r,t)\, d^2r \qquad (2.6)$$

where g accounts for signal losses, ε and Q represent the molar extinction coefficient and quantum yield of fluorescence of the fluorophore, and A is the attenuation of the beam used in the observation. The solution for the relative fluorescence intensity, $f(t)$, under the initial conditions stated is expressed as the series:

$$f(t) = \left(\frac{g\varepsilon Q P \bar{C}}{A} \right) \sum_{n=0}^{\infty} \frac{-(K)^n}{n![1+n(1+2t/\tau_D)]} \qquad (2.7)$$

The solution is achieved by use of Fourier transform techniques, and a series expansion of Equation 2.4 in the extent of bleaching. The series expansion is valid for all values of K, but requires a greater number of terms for convergence as K increases.

2.2.2 Recovery Following Second Order Photobleaching

Inherent in the theory of FPR developed and used to date is the assumption of first order bleaching kinetics. This yields the initial boundary condition in Equation 2.4 used in the solution of Equation 2.5.

The photochemistry of naphthacene can involve formation of an endoperoxide[6-8,10-13], which is first order in naphthacene, or dimer formation[14-17], which is expected to be second order in naphthacene[18]. If the kinetics of bleaching is truly second order, then the initial boundary condition, and indeed, the series solution used to fit the data is invalid. To address this, the development of FPR theory under conditions of second order bleaching kinetics is undertaken.

Second order bleaching will proceed according to Equation 2.8:

$$\frac{d\,C(r,t)}{dt} = -\lambda' I(r)\, C^2(r,t) \tag{2.8}$$

which yields the initial boundary condition:

$$C(r,0) = \frac{\bar{C}}{1 + \bar{C}\lambda' t' I(r)} \tag{2.9}$$

where λ' represents a photochemical quantum yield for the second order bleaching reaction.

Following the procedure outlined by Axelrod *et al.*[3], the solution for the time dependent fluorescence intensity under second order bleaching kinetics is found to be:

$$f(t) = \left(\frac{g\varepsilon QP\bar{C}}{A}\right) \sum_{n=0}^{\infty} \frac{-(K')^n}{[1+n(1+2t/\tau_D)]} \tag{2.10}$$

where $K' = \bar{C}\lambda' t' I_0$. This solution requires a series expansion of Equation 2.9, which is valid only for $|K' \exp(-2r^2/\omega^2)| < 1$[27]. For

values of $|K' \exp(-2r^2/\omega^2)|$ larger than unity, the series diverges. Expressions for f(t) which are valid for all values of $K' \exp(-2r^2/\omega^2)$ are not possible with standard expansions or integral tables.

2.3 Fitting of Data

2.3.1 General Fitting Procedure

Extraction of diffusion parameters is achieved by a three parameter fit to a complete series solution for the measured time dependent fluorescence intensity. A typical example of an FPR experimental data set with the fit to the data is given in Figure 2.5. The full equation utilized in the fitting procedure is given by:

$$F(t) = Xm*F(-)*f(t) + (1-Xm)*F(0) \qquad (2.11)$$

where F(t) is the absolute fluorescence intensity at time t; F(-) is the intensity prior to the bleach pulse; and F(0) is the intensity immediately following the bleach pulse (as in Figure 2.3).

The three parameters fit are τ_D, K, and Xm, which are defined as;

τ_D is the characteristic diffusion time for recovery of fluorescence. In terms of a random walk problem in two dimensions, the relation between the root mean square displacement and characteristic diffusion time is given by:

$$\langle r^2 \rangle = 4Dt \qquad (2.12)$$

From the measured τ_D and beam width values, the diffusion coefficient is calculated as:

Figure 2.5: Sample FPR experiment. Recovery of naphthacene on dry silica gel at 0.1% monolayer. Experimental parameters: 100 ms/ch, 150 ms bleach pulse, 50 s post recovery pause. The diffusion coefficient is 2.6×10^{-10} cm^2 s^{-1}, and the mobile fraction is 0.54. Raw data are represented as points, with the fit to the data given by the solid line. The labels F(-), F(0), F(t), and F(∞) correspond to the labels in Figure 2.3.

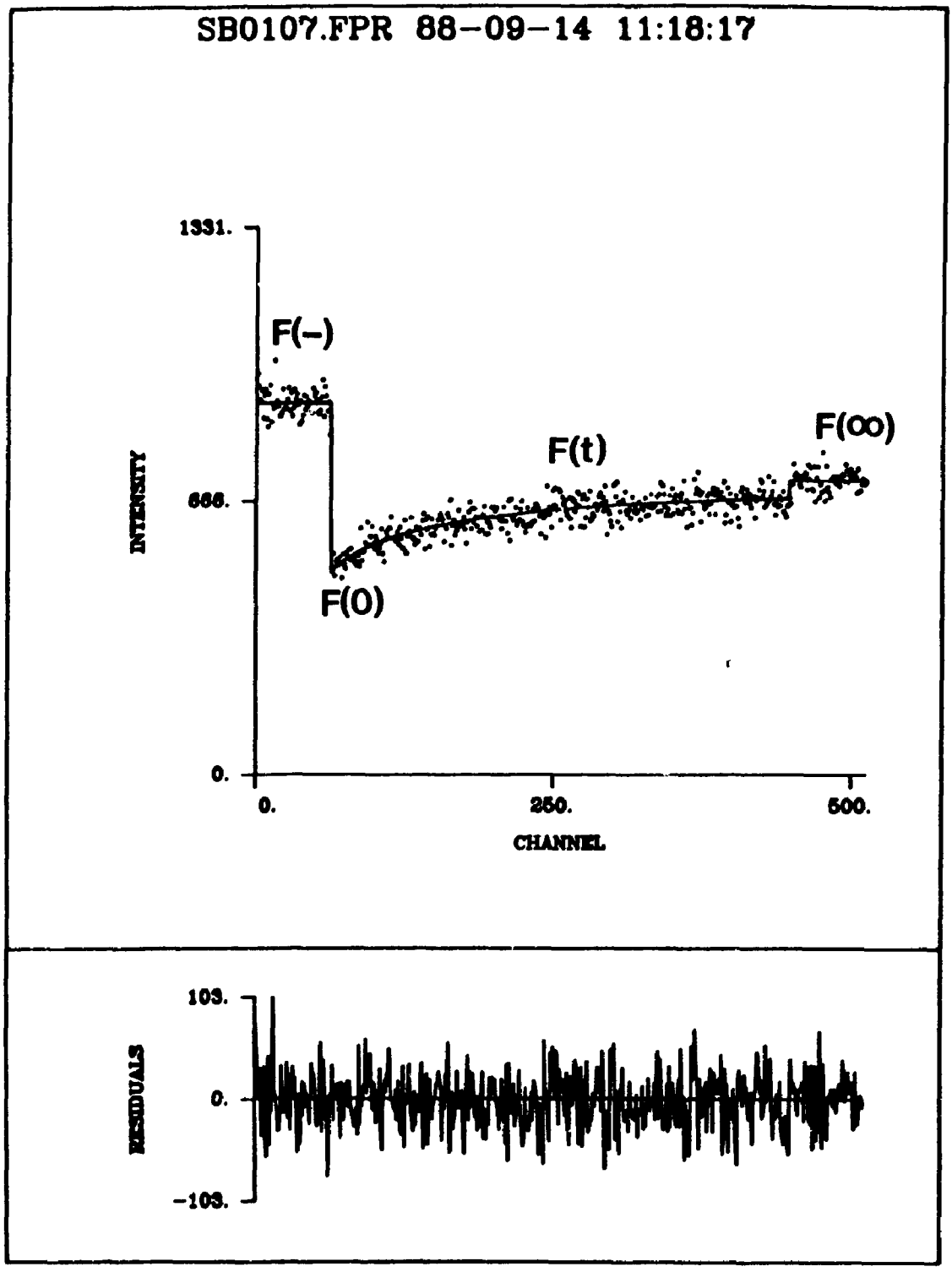
SB0107.FPR 88-09-14 11:18:17
1331.
666.
0.
INTENSITY
F(-)
F(t)
F(∞)
F(0)
0.
250.
500.
CHANNEL
103.
0.
-103.
RESIDUALS

$$D = \omega^2/4\tau_D \qquad (2.13)$$

K is a measure of the extent of photobleaching during the bleach pulse. As the extent of bleaching increases, the value of K increases. The number of terms used in the series of Equation 2.7 is truncated to a predetermined value, depending on the size of K. As K increases, the number of terms required for the series to converge increases.

Xm, the mobile fraction, represents the fraction of molecules which appear mobile on the time scale of the experiment. The mobile fraction is defined by:

$$Xm = \frac{F(\omega) - F(0)}{F(-) - F(0)} \qquad (2.14)$$

Fitting of the recovery to these parameters is achieved by smoothing the data by linear least squares to a third order polynomial, and selection of twenty eight data points from the 384 points in the recovery. Points in the early part of the recovery are weighted more heavily, to allow for a more precise calculation of τ_D, at the expense of the precision in K and Xm. This is justified since τ_D is the harder parameter to fit, and is usually the parameter of greatest interest[29].

The goodness of fit is given by calculation of a reduced chi-square value (χ_r^2) and by the residual function of the fit. Data with χ_r^2 larger than 10.0 are discarded.

2.3.2 Fitting of Data From First Order Photobleaching

Simulated data for the recovery portion of an FPR experiment following first order bleaching are generated using Equation 2.7. The prebleach and postbleach intensities are included, and random noise is added to the data. Sets of data are generated for various extents of bleaching (K) and various characteristic diffusion times (τ_D). The input values of K are calculated by:

$$K = -\ln (C(0,0)/\bar{C}) \qquad (2.15)$$

which is derived directly from Equation 2.4. Ten value of the fraction of fluorophores remaining at the center of the laser beam ($C(0,0)/\bar{C}$) and four values of τ_D (1, 5, 10, and 25 s) are used. All data are fit using Equation 2.7, assuming a beam width of 1.0 μm, and a time base of 100 ms/ch. An example of simulated data along with the fit is presented in Figure 2.6. Table 2.1 contains data recovered for simulation experiments for recoveries following a first order bleach. The recovered diffusion parameters for the three larger values of τ_D are in good agreement with the theoretical values. For τ_D set to 1 s, a time base of 100 ms/ch is too long, and the diffusion coefficient is overestimated. Table 2.2 contains the calculated diffusion parameters for τ_D = 10 s, as a function of bleaching level. Each value of D in Table 2.2 is an average from a number of simulated data sets. Each data set is generated by calling the random number generator at a different position in its period. Very good agreement is seen between the input and calculated values of K. The recovered diffusion coefficients are all equal to the theoretical value, to within 3%, and

Figure 2.6: Simulated FPR recovery. The bleaching process in the simulation is taken to be a first order process. A value of 10 s for τ_D is used. The recovered diffusion coefficient is 2.5×10^{-10} cm^2 s^{-1}, and the mobile fraction is 1.0.

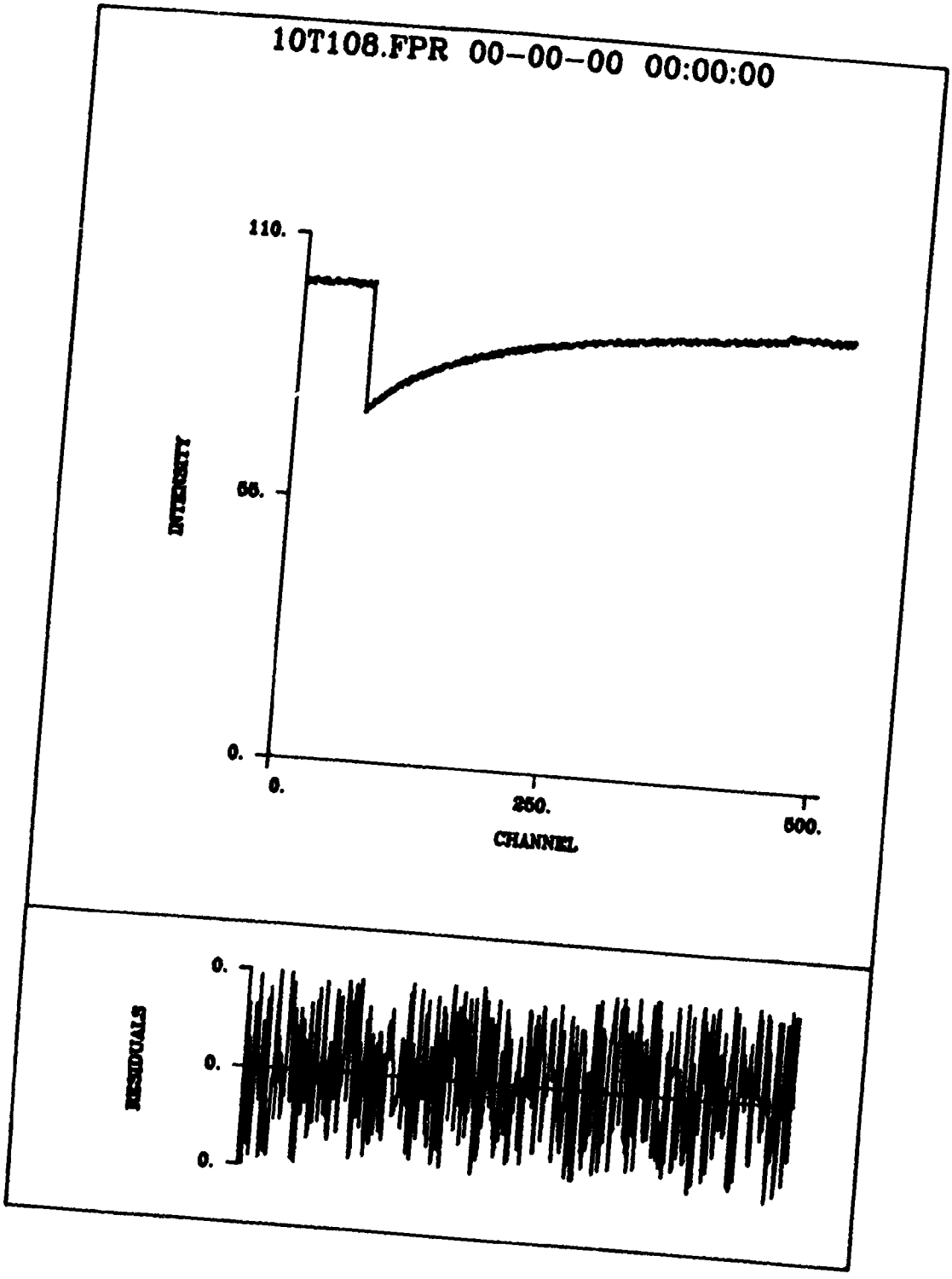
10T108.FPR 00-00-00 00:00:00
110.
55.
0.
INTENSITY
0.
250.
500.
CHANNEL
0.
0.
0.
RESIDUALS

Table 2.1: Calculated Diffusion Parameters for Simulated Recoveries Following a First Order Bleach.

τ_D/s	D^a/ $10^{-10}cm^2s^{-1}$	D^b/ $10^{-10}cm^2s^{-1}$	Xm
1.0	25.0	30.8	1.03[c]
5.0	5.00	5.50	1.04
10.0	2.50	2.55	1.03
25.0	1.00	1.02	1.01

[a]Value of D calculated from $\omega^2/4\tau_D$.

[b]Average value of D for recoveries following a first order bleaching process.

[c]Mobile fractions greater than unity are physically impossible. These are fitted parameters.

Table 2.2: Effect of the Extent of Bleaching on Calculated Diffusion Parameters for First Order Bleaching.

K_{in}[a]	K_{out}[b]	$D/10^{-10} cm^2 s^{-1}$	Xm
0.1508	0.1368	2.49	1.15[c]
0.1985	0.2024	2.57	1.00
0.2485	0.2432	2.51	1.05
0.3011	0.3017	2.55	1.02
0.3857	0.3787	2.52	1.05
0.4463	0.4512	2.57	1.02
0.5798	0.5756	2.54	1.04
0.6539	0.6583	2.54	1.02
0.6932	0.7008	2.54	1.02
1.0217	1.0049	2.54	1.01

[a]Value of K used in the simulation program.

[b]Value of K recovered from fitting of data to Equation 2.7.

[c]Mobile fractions greater than unity are physically impossible. These values are fitted parameters.

a mobile fraction of unity is calculated for each value of K.

2.3.3 Fitting of Data From Second Order Photobleaching

Recovery curves following second order bleaching for the same characteristic diffusion times, time base and beam width used in Section 2.3.2 are generated using Equation 2.10. For these data, K′ is calculated to give the same extent of bleaching at the center of the beam as those values of K used in the first order bleaching case (Section 2.3.2). The values of K′ are calculated by:

$$K' = \frac{1 - (C(0,0)/\bar{C})}{(C(0,0)/\bar{C})} \qquad (2.16)$$

which comes directly from Equation 2.9.

To determine the effect of second order bleaching on the recovered diffusion parameters, all data are fit using Equation 2.7, the solution for recovery following a first order bleach. An example of the fit to the recovery after second order bleaching is presented in Figure 2.7. The fit to the recovery after a second order bleach using Equation 2.7 is generally quite good. There are differences in the recovery curves for the two cases. The recovery portions of an FPR procedure for both the first and second order bleaching cases are compared in Figure 2.8. The curves have similar shapes, but for the second order case the initial postbleach intensity is slightly lower, due to a greater number of fluorophores being bleached in the second order case (*vide infra*).

Table 2.3 contains the average diffusion coefficients for each

Figure 2.7: Simulated FPR recovery. The bleaching process in the simulation is taken to be a second order process. A value of 10 s for τ_D is used. The recovered diffusion coefficient is 2.5×10^{-10} cm^2 s^{-1}, and the mobile fraction is 1.0.

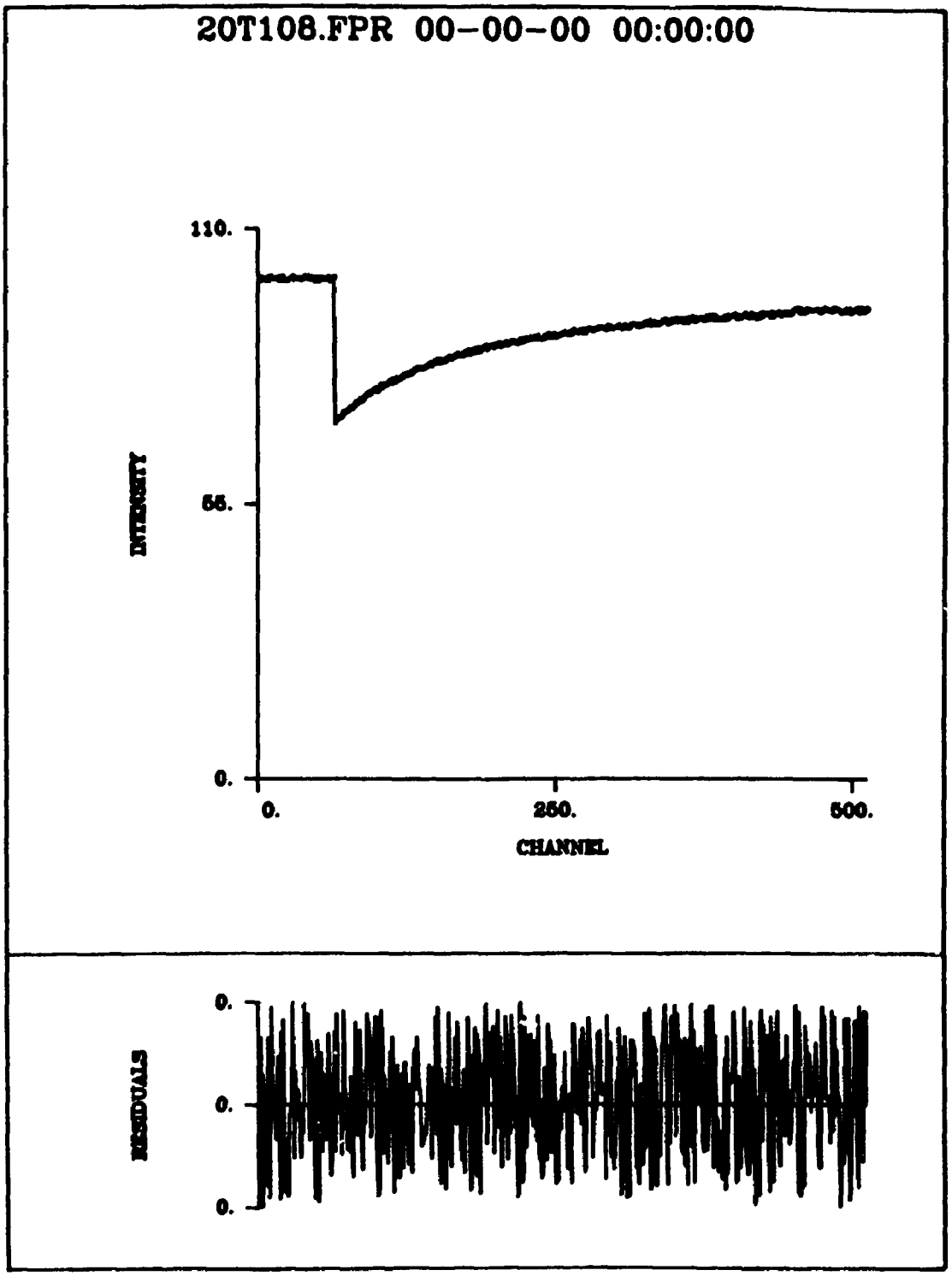
20T108.FPR 00-00-00 00:00:00
110.
55.
0.
INTENSITY
0.
250.
500.
CHANNEL
0.
0.
0.
RESIDUALS

Figure 2.8: Comparison of the recovery portions of Figures 2.6 and 2.7. The recovery profile following a second order bleach (– – –) is similar to that following a first order bleach (———). The difference in post bleach intensity is due to more fluorophores bleaching in the second order process (see Figure 2.9).

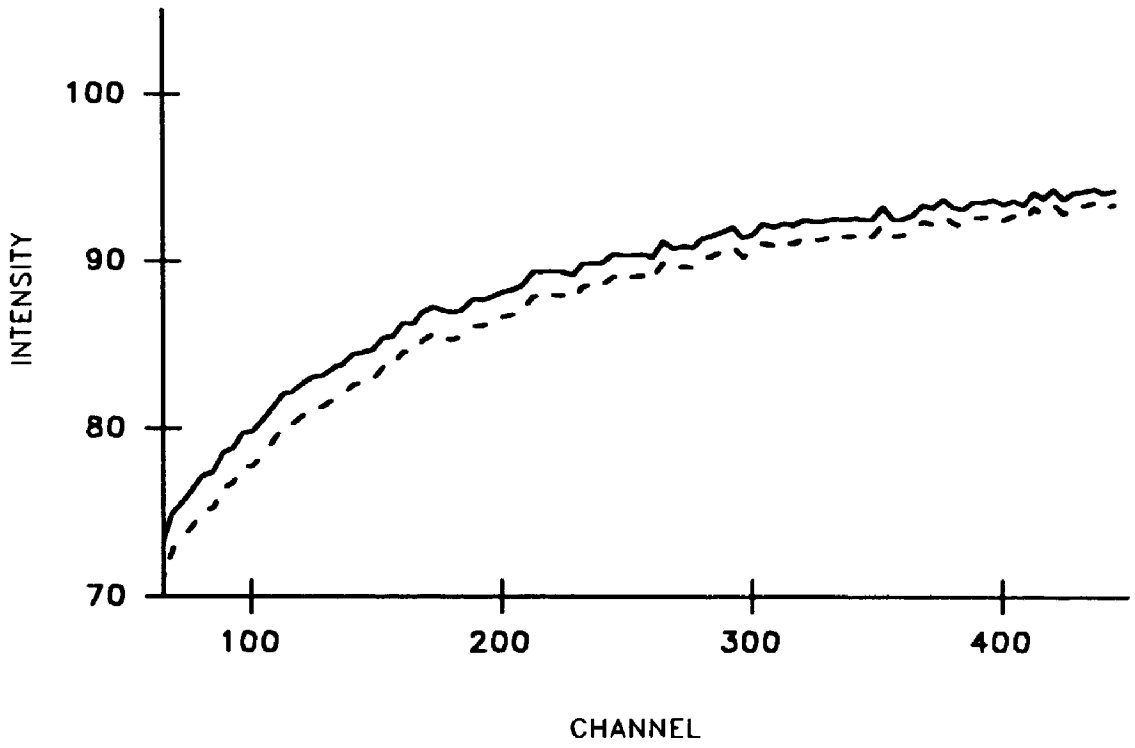
100
90
80
70
INTENSITY
100
200
300
400
CHANNEL

Table 2.3: Calculated Diffusion Parameters For Simulated Recoveries Following a Second Order Bleach.

τ_D/s	D^a/ $10^{-10}cm^2s^{-1}$	D^b/ $10^{-10}cm^2s^{-1}$	Xm
1.0	25.0	27.8	1.06[c]
5.0	5.00	4.94	1.04
10.0	2.50	2.41	1.04
25.0	1.00	0.95	1.02

[a]Value of D calculated from $\omega^2/4\tau_D$.

[b]Average value of D for recoveries following a second order bleaching process.

[c]Mobile fractions greater than unity are physically impossible. These are fitted parameters.

value of τ_D used. Fairly good agreement is seen again for the calculated values of D and the theoretical values for the three larger τ_D values. Once again the time base is too long for the fast diffusion case. The average value of D in each case is calculated from diffusion coefficients obtained by fitting data generated from a series of recoveries with various bleaching levels. No effect on Xm is observed, with the mobile fraction being unity in each case.

The calculated values of the fitted diffusion parameters as a function of bleaching level for the case with τ_D = 10 s are presented in Table 2.4. K'_{out} is a fitted parameter, and represents the extent of bleaching parameters for the first order case, since the first order theory is used. No agreement can be expected between the input and output values. In all cases, mobile fractions of unity are calculated.

The diffusion parameters calculated for valid choices of the extent of bleaching are considered further. To use Equation 2.10, the extent of bleaching at the center of the beam must be less than 50%. At low levels of bleaching (less than 30%), very good agreement between the fitted diffusion coefficient and the theoretical value is observed. As the extent of bleaching increases, the difference between these two values increases to as much as 7% The diffusion coefficient is consistently underestimated at higher bleaching levels for diffusion following a second order bleaching process.

To understand why the diffusion coefficient is underestimated it is instructive to examine the initial postbleach concentration profile. Profiles for both first and second order bleaching are shown

Table 2.4: Effects of the Extent of Bleaching on Calculated Diffusion Parameters for Second Order Bleaching.

K'_{in}[a]	K'_{out}[b]	$D/10^{-10}cm^2s^{-1}$	Xm
0.1628	0.1428	2.51	1.13[c]
0.2195	0.2093	2.50	1.00
0.2821	0.2541	2.47	1.05
0.3514	0.3179	2.48	1.02
0.4706	0.4057	2.42	1.04
0.5625	0.4878	2.45	1.02
0.7857	0.6384	2.38	1.04
0.9231	0.7256	2.33	1.02
1.0000[d]	0.7176	2.18	1.03
1.7778[d]	[e]	[e]	[e]

[a]Value of K′ used in the simulation program.

[b]Value of K′ recovered from fitting of data to Equation 2.7.

[c]Mobile fractions greater than unity are physically impossible. These are fitted parameters.

[d]These values of K′ are invalid choices since the value of K′ at r = 0 must be less than unity. Data generated with K′ = 1.0 was fit using Equation 2.7

[e]Data generated with K′ = 1.78 could not be fit with Equation 2.7.

in Figure 2.9, for various extents of bleaching. At corresponding levels of bleaching at the center of the beam, a second order bleaching process generates a wider concentration profile. Significant bleaching occurs at larger values of r for the case of second order bleaching. For a truly second order process, the bleach profiles resembles that obtained with a beam width which is larger than the measured exp(-2) value. As a result, using the first order theory to fit recoveries following a second order bleach will underestimate the diffusion coefficient due to the appearance that a smaller beam size is employed. As the extent of bleaching increases, the apparent beam width increases, as does the error in the calculated diffusion coefficient.

2.3.4 Utilization of the Two Theories

Development of the theory for fluorescence recovery following a second order bleaching process has been carried out. An analytical solution is found for the fluorescence recovery (Equation 2.10), but is valid only for small levels of bleaching. This is a great limitation as bleaching levels are frequently large. To avoid this limitation, all data can be fit using the theory developed for first order bleaching kinetics leading to a systematic error in the diffusion coefficient. The error on D varies with the extent of bleaching, and is roughly 35% at very high level of bleaching. For systems where the bleaching kinetics are second order the diffusion parameters can be determined using the first order theory, but a

Figure 2.9: Postbleach concentration profiles for first (———) and second (– – –) order bleaching processes as a function of the extent of bleaching. The effective beam radius (plotted here in units of the measured beam width ω) for the second order bleaching process is greater than than for a first order bleaching process. This leads to lower postbleach intensities, and underestimation of D when fitting data of this type with the first order theory.

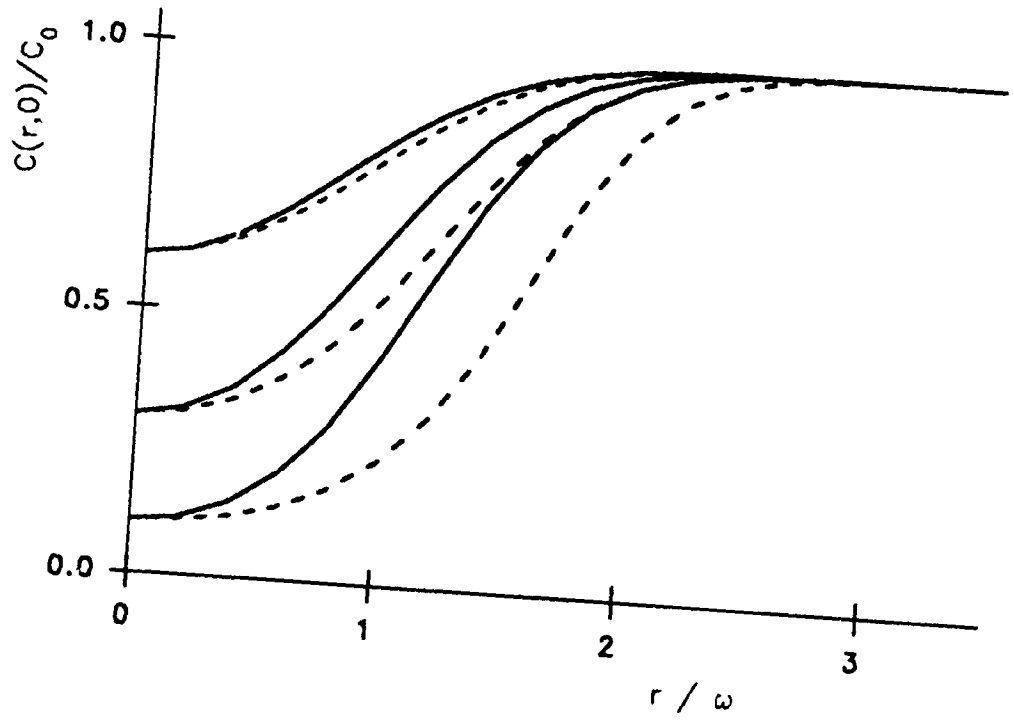
C(r,0)/C0
1.0
0.5
0.0
0
1
2
3
r / ω

correction factor should be applied to the diffusion coefficient. No effect is observed in the recovered values of the mobile fraction. Once again the mobile fraction is unity for all cases.

In a different type of experiment (Continuous Fluorescence Microphotolysis), the kinetics of bleaching for adsorbed naphthacene under various conditions is shown to be neither first nor second order. A combination of photochemical processes is occurring. On this basis, all data is fit using the first order bleaching theory, with no correction factor employed.

2.3.5 Effect of Heterogeneity on Diffusion Parameters

For heterogeneous surfaces where the fluorescent probe can experience more than one microenvironment, the calculated diffusion coefficient will be a weighted average of the diffusion coefficients in each of the environments[30].

$$D = \sum_i f_i D_i \qquad (2.17)$$

with

$$\sum_i f_i = 1 \qquad (2.18)$$

f_i represents the fraction of time the probe molecules resides in a particular environment where the diffusion coefficient is D_i. This is equivalent to weighting by the relative amounts of probe found in each environment at any particular time. This holds only for environments in which the probe can undergo fast exchange on the time scale of the FPR experiment.

2.4 FPR Technical Details

The illumination source used in this study is a Coherent Innova 70 4 W continuous wave Argon ion laser. Operated in light regulation mode, the output power is set to 100 mW at 476.5 nm (for naphthacene and rubrene) and 100 mW at 514.5 nm (for pentacene). Timing and control of the monitor and bleach beams is achieved with a Digital Equipment Corporation MINC 23 microcomputer. The intensity of the beams is reduced by the optics, as well as neutral density filters placed in the path of the laser beam before the sample. Typically 2.0 to 2.5 OD is used in these experiments. The power of the monitor beam at the sample is on the order of 1 μW, whereas that of the bleach beam is on the order of a few milliwatts.

Scattered light from the sample is cut off from reaching the detector by placing barrier filters in the path after the sample, and by an image plane pinhole assembly (Figure 2.10). The pinhole assembly also minimizes contributions of fluorophores in the path of the beam which are not in the plane of focus. A pinhole of diameter 0.4 mm convoluted with a 1.1 μm beam width will result in a volume of roughly cylindrical shape, with a long axis of 6 μm above and below the plane of focus[31]. This corresponds to a height where the intensity drops to a level of exp(-4) relative to the central intensity.

The laser beam is focused by use of a 140mm focusing lens placed before the sample and a 40× objective lens with numerical aperture of 0.75. This combination produces a beam width of 1.1μm (476.5 nm) or

Figure 2.10: Image plane pinhole assembly. Fluorescence from the sample passes the dichroic mirror and barrier filter and is focused on the image plane pinhole. Only fluorescence from the focal plane will pass through the pinhole. Fluorescence from out of the plane of focus and scattered light is stopped from reaching the detector. The bold line represents the incident laser beam.

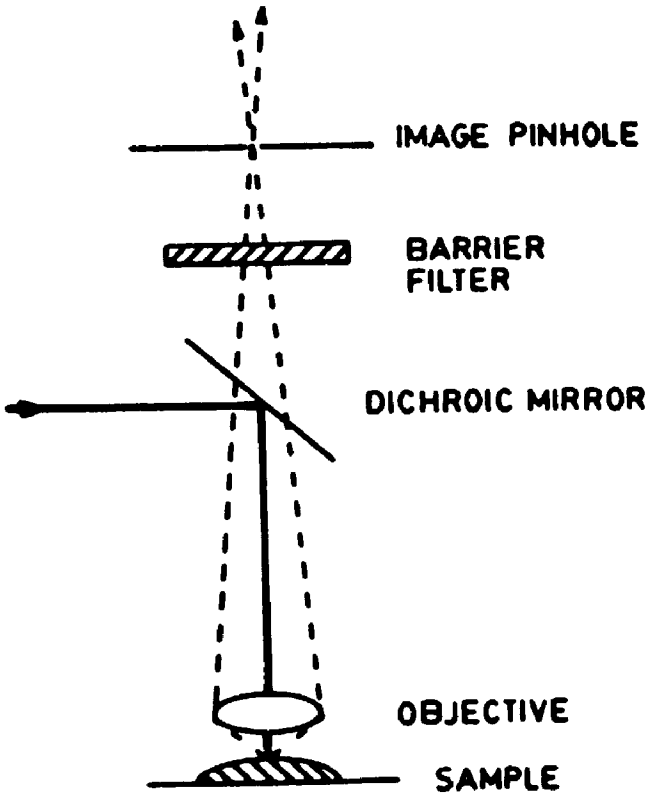
IMAGE PINHOLE
BARRIER
FILTER
DICHROIC MIRROR
OBJECTIVE
SAMPLE

1.4 μm (514.5 nm) at the focal plane.

Fluorescence emission is monitored by a Zeiss Universal epifluorescence microscope. A dry ice cooled photomultiplier tube (RCA 31034A) is fitted to the top of the optical path. The photocurrent produced is sent through an amplifier/discriminator and an A/D converter to the MINC computer. Immediate reconstruction of the data on a Digital VT 105 is done. The data can then be stored on floppy disk or discarded. The data set saved is then transferred to The University of Western Ontario's VAX 6330 for data processing and plotting. Plotting is done either on a Dataproduct's 2600 laser printer or a Calcomp 1044 widebed plotter. Both devices are driven with FORTRAN programs developed in our laboratory using the DI-3000 graphics package.

2.5 Continuous Fluorescence Microphotolysis

Peters *et al.* have developed a microfluorescence technique which yields information on the bleaching kinetics as well as the diffusion process[19-21]. This procedure, coined Continuous Fluorescence Microphotolysis (CFM), uses the same apparatus as FPR, but no bleach pulse is employed. Instead, the exposure time or the laser power, or both are increased to such an extent that photodestruction of the fluorophores is caused by the monitor beam. Over time, the fluorescence intensity will decrease due to photodestruction. This is tempered by diffusion of fluorophores from outside the irradiation area. Fitting of the data can yield both the first order rate

constant for bleaching and the diffusion coefficient. This technique has been further developed by Ferrières and co-workers to extract the diffusion coefficient and rate constant for second order photobleaching reactions[22].

We use this procedure not to measure the diffusion coefficient, but to achieve a better understanding of the kinetics of photobleaching for naphthacene on C18 derivatized silica gel.

REFERENCES

(1) Edidin, M. *Curr. Top. Membr. Transp.* **1987**, *29*, 91.

(2) Elson, E. L. *Ann. Rev. Phys. Chem.* **1985**, *36*, 379.

(3) Axelrod, D.; Koppel, D. E.; Schlessinger, J.; Elson, E.; Webb, W. W. *Biophys. J.* **1976**, *16*, 1055.

(4) Lepock, J. R.; Thompson, J. E.; Kruuv, J.; Wallach, D.F. *Biochem. Biophys. Res. Commun.* **1978**, *85*, 344.

(5) Sheetz, M. P.; Koppel, D. E. *Proc. Natl. Acad. Sci.* **1979**, *76*, 3314.

(6) Stevens, B.; Algar, B. E. *Chem. Phys. Lett.* **1967**, *1*, 58.

(7) Stevens, B.; Algar, B. E. *J. Phys. Chem.* **1968**, *72*, 2582.

(8) Stevens, B.; Algar, B. E. *J. Phys. Chem.* **1968**, *72*, 3468.

(6) Berlman, I. B. In *Fluorescence Spectra of Aromatic Molecules;* Academic Press: New York, 1965; Second Edition, p. 132.

(10) Rigaudy, J.; Sparfel, D. *Bull. Chim. Soc. Fr.* **1977**, *7-8*, 742.

(11) Lapouyade, R.; Nourmamode A.; Bouas-Laurent, H. *Tetrahedron* **1980**, *36*, 2311.

(12) Saito, I.; Matsuura, T. In *Singlet Oxygen;* Wasserman, H. H.; Murray, R. W., Eds.; Academic Press: London, 1979, Chapter 10.

(13) Bloodworth, A. J.; Eggelte, H. J. In *Singlet O* ; Frimer A. A., Ed.; CRC Press: Boca Raton, 1985, Volume II, Chapter 4.

(14) Wei, K. S.; Livingston, R. *Photochem. Photobiol.* **1967**, *6*, 229.

(15) Birks, J. B.; Appleyard, J. H., Pope, R. *Photochem. Photobiol.* **1963**, *2*, 493.

(16) Fournie, G.; Dupuy, F.; Martinaud, M.; Nouchi, G.; Turlet, J. M. *Chem. Phys. Lett.* **1972**, *16*, 331.

(17) Katul, J. A.; Zahlan, A. B.; *J. Chem. Phys.* **1967**, *47*, 1012.

(18) Livingston, R. In *Photochemistry in the Liquid and Solid States;* Daniels, F., Ed.; John Wiley and Sons: New York, 1960;pp 76-82.

(19) Peters, R.; Peters, J.; Tews, K. H.; Bähr, W. *Biochim. Biophys. Acta* **1974**, *367*, 282.

(20) Peters, R.; Brünger, A.; Schulten, K. *Proc. Natl. Acad. Sci.* **1981**, *78*, 962.

(21) Brünger, A.; Peters, R.; Schulten, K. *J. Chem. Phys.* **1985**, *82*, 2147.

(22) Ferrières, X.; Lopez, A.; Altibelli, A.; Dupou-Cezanne, L., Lagouanelle, J-L.; Tocanne, J-F. *Biophys. J.* **1989**, *55*, 1081.

(23) Koppel, D. E. *Biophys. J.* **1979**, *28*, 281.

(24) Smith, B. H.; McConnell, H. M. *Proc. Natl. Acad. Sci.* **1978**, *75*, 2759.

(25) Koppel, D. E.; Sheetz, M. P. *Biophys. J.* **1983**, *43*, 175.

(26) Lanni, F.; Ware. B. A. *Rev. Sci. Instrum.* **1982**, *53*, 905.

(27) Weis, R. M.; Krishna, B.; Smith B. A.; McConnell, H. M. *J. Biol. Chem.* **1982**, *257*, 6440.

(28) O'Neill, P. V. In *Advanced Engineering Mathematics*; Harrison, J., Ed.; Wadsworth: Belmont, Ca., 1987; Second Edition, p. 274.

(29) Petersen, N. O.; Felder, S.; Elson, E. L. In *Handbook of Experimental Immunology;* Weir, D. M., Ed.; Blackwell Scientific Publications: Oxford, 1986; Vol. 3, Chapter 24.

(30) Elson, E. L.; Reidler, J. A. *J. Supramol. Struct.* **1979**, *12*, 481.

(31) Koppel, D. E.; Axelrod, D.; Schlessinger, J.; Elson, E. L. *Biophys. J.* **1976**, *16*, 1315.

CHAPTER THREE

MOBILITY MEASUREMENTS

3.1 Diffusion on Normal Phase Silica Gel

3.1.1 Introduction

Mobility of aromatic and polycyclic aromatic hydrocarbons (PAHs) on oxide surfaces (silica, alumina, zeolites) has been said to occur since as early as 1962[1-9]. The vast majority of the data accumulated to date give indirect evidence for the motion of adsorbed species on various surfaces. Photophysical and photochemical studies of these systems predominate in this area[8-22]. One of the most commonly used probes in photophysical studies is pyrene (or a pyrene derivative) due to the advantageous photophysical properties of the pyrene moiety.

Pyrene has been adsorbed on various oxide surfaces and investigated from a photophysical point of view. On silica with high enough coverage pyrene exhibits both structured monomer fluorescence emission and structureless excimer-like emission[5,7,9-12,14]. The origin of the excimer formation has been found to be different for pyrene on dry silica and on silica with coadsorbates. On dry silica, the excimer-like emission arises from ground state complexes[7,11,12,14], whereas on silica with coadsorbates, the excimer formation is found to be a dynamic process[10,12,14]. It has been postulated that the presence of coadsorbates enhances the mobility of pyrene and diminishes the formation of ground state associations.

Recently it has been postulated that the ground state associations arise from microcrystals or aggregates of pyrene, even though emission typical of pyrene crystals is not observed[23]. The presence of microcrystalline material is consistent with some qualitative observations outlined in this thesis.

From these and other studies, bimolecular quenching rate constants for pyrene on various surfaces have been presented[8]. For pyrene on dry silica, this value is reported as 7×10^{14} dm^2 mol^{-1} s^{-1}. Adsorption of coadsorbates (water, alcohols) increases this rate constant by a factor of four for silica with decanol, and by an order of magnitude for silica coated with water providing evidence for enhanced mobility[8].

The mobility of acridine on oxide surfaces has been studied by delayed fluorescence and transient absorption spectroscopy[24]. The mobility of acridine on silica and alumina was found to have a pronounced dependence on the pretreatment temperature of the surfaces. Triplet-triplet annihilation experiments of acridine on dry silica with low pretreatment temperatures have lead to a bimolecular quenching rate constant of 8×10^{13} dm^2 mol^{-1} s^{-1}. For alumina or silica treated at high temperatures, acridine was found to be immobile, but an estimate of the rate constant for acridine on high temperature treated surfaces was given as 10^{11} dm^2 mol^{-1} s^{-1}.

Another system examined is the photodimerization of acenaphthylene adsorbed on surfaces[7,10,13]. The ratio of *cis* to *trans* dimer formed gives direct evidence as to the fraction of dimers formed through either a singlet or triplet pathway. Coadsorption of

sensitizers enhances the formation of the *trans* dimer through a triplet state pathway. The results seem to indicate that, at low surface coverages, the excited triplet state must translate in order to form the *trans* dimer. The singlet state is short lived and will decay to the ground state or undergo intersystem crossing before encountering another acenaphthylene molecule. The triplet is long lived in comparison to the singlet, and can translate farther during its lifetime, increasing the probability of interactions and formation of the *trans* dimer.

Adsorption of PAHs on oxide surfaces involves hydrogen bonding between the π electrons of the aromatic and surface silanol groups (SiOH, or chemisorbed water)[25,26]. The strength of these interactions has been found to be 17 kJ mol^{-1} [9,10], which is on the order of a typical hydrogen bond (4 - 40 kJ mol^{-1})[27]. Aza-aromatics, such as acridine, bind in a very different manner. The interactions are hydrogen bonds between the non-bonding electron pair on the nitrogen atom and surface silanol groups[24], which cause the aromatic to sit perpendicular to the surface. The two modes of binding for the various aromatics are shown in Figure 3.1.

The silica surface is composed of various types of silanol groups (SiOH, isolated, vicinal and geminal), siloxane bridges (Si-O-Si), and physisorbed water (Figure 3.2). The concentrations of surface water species can be altered by various treatments. Upon heating, concentrations of surface silanol groups and water decrease[28-31]. The silanol and water concentrations can also be increased by appropriate treatments. Heating silica in hot acid increases the silanol

Figure 3.1: Modes of binding for polycyclic aromatic hydrocarbons on silica gel. Top: PAHs with no functional groups (naphthacene shown) will bind flat to the surface. The attractive interactions are hydrogen bonds between surface silanol (SiOH) groups and the π electrons. Bottom: PAHs with functional groups with a non-bonding pair of electrons (acridine shown) will bind perpendicular to the surface. The attractive forces are hydrogen bonds between the surfaces silanol groups and the non-bonding electron pair on the nitrogen.

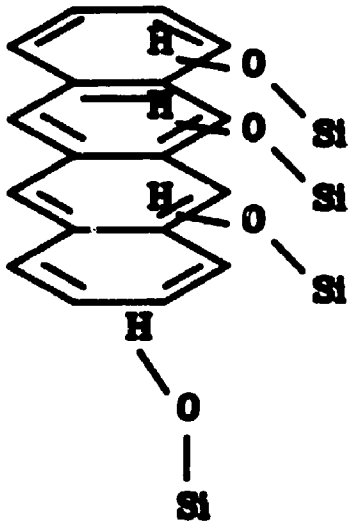
H
O
Si
H
O
Si
H
O
Si
H
O
Si

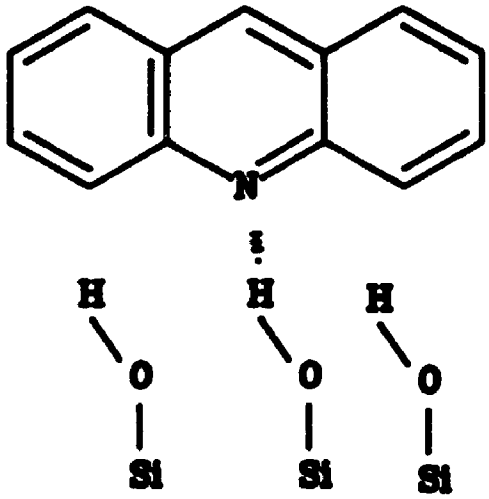
N
H
O
Si
H
O
Si
H
O
Si

Figure 3.2: Water species on the surface of silica gel. There are three type of surface silanol groups: a) isolated, b) vicinal, and c) geminal. Water can physically bind to these groups (d) via hydrogen bonding.

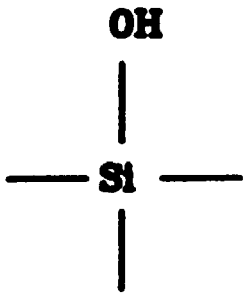

a

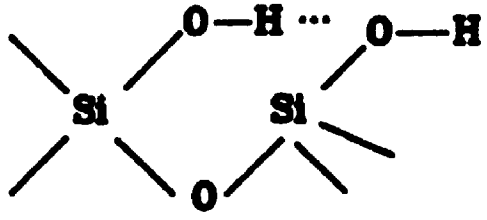

b

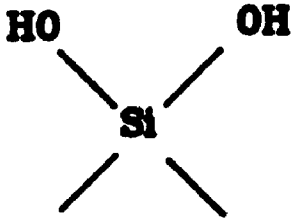

c

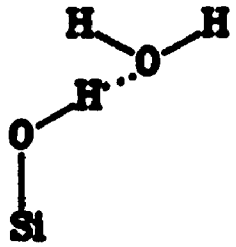

d

content[26]. Water can be added either from solutions of undried solvents, or directly to the surface. By similar treatments it is easy to change at least some of the silanol groups or physisorbed water to deuterated species. By doing so, one can look for isotope effects. Changing the concentrations of water species has been found to affect the photophysical properties of adsorbed species[8,14].

This section of the chapter deals with the mobility of naphthacene on normal phase silica gels. The effect of pretreatment temperature alone, and the effect of this with consequent addition of a small amount of water (2% of a monolayer, or 0.2 μmol m^{-2}) to the surface are presented. As well, surface concentrations of silanol groups are increased by boiling silica in concentrated nitric acid or deuterated nitric acid. Physisorption of at least monolayer coverages of water (both H_2O and D_2O) on some silica gels is also used to alter the surface.

The probe of interest used in this study is naphthacene at low surface concentrations (0.1% monolayer). Some experiments with rubrene and pentacene were also performed.

Naphthacene is shown to be mobile on normal phase silica gels. The diffusion coefficient remains virtually constant, independent of silica preparation. The mobile fraction changes dramatically with treatment.

A number of qualitative observations for these systems are also presented. For example, naphthacene forms microcrystalline domains visible in the microscope on silica gel, to varying degrees depending on preparation of the silica.

Results are discussed in terms of surface interactions (ease of desorption), surface water content (both physisorbed and chemisorbed water), surface heterogeneity and heterogeneity of the distribution of the fluorescent probe on the surface.

3.1.2 Experimental

Naphthacene (Aldrich) was recrystallized from benzene prior to use. Concentrations of degassed naphthacene solutions (obtained by bubbling with nitrogen or freeze-pump-thaw cycling in spectroscopic grade cyclohexane) were determined by absorption spectroscopy (ε = 14 000 M^{-1} cm^{-1}, λ = 471 nm)[32].

For all samples, the silica gel (Mallinckrodt, surface area 300 m^2 g^{-1}, average pore diameter 150 Å, from manufacturer's specifications) was kept in an 180^{0}C oven for at least one week prior to use. The silica was then cooled in a desiccated chamber to room temperature. Once cooled, the silica was put into a vacuum chamber (Figure 3.3) and heated under high vacuum for a period not less than four hours. Samples were normally heated overnight. The pretreatment temperature ranged from room temperature (25^{0}C) to 600^{0}C. Heating was done with a Fisher Linear Temperature Programmer, model 360, and a ceramic heater. The temperature was controlled and measured with platinel thermocouples. The silica was cooled to room temperature prior to addition of a naphthacene solution to the vacuum chamber.

Deposition of the adsorbate was achieved by either sublimation or direct solvent evaporation. Sublimation was carried out by adding

Figure 3.3: Vacuum chamber. Region A is the port to the vacuum line and stopcock; B is stoppered with a septum for introduction of solutions to the evacuated chamber. Silica is placed in a quartz chamber (C) for heating. After heating, the silica is moved to D, a 1 mm quartz cuvette, and the solution is put into C. After slow removal of the solvent, the silica is put back into C with the solid naphthacene and shaken, causing the naphthacene to sublime onto the silica surface.

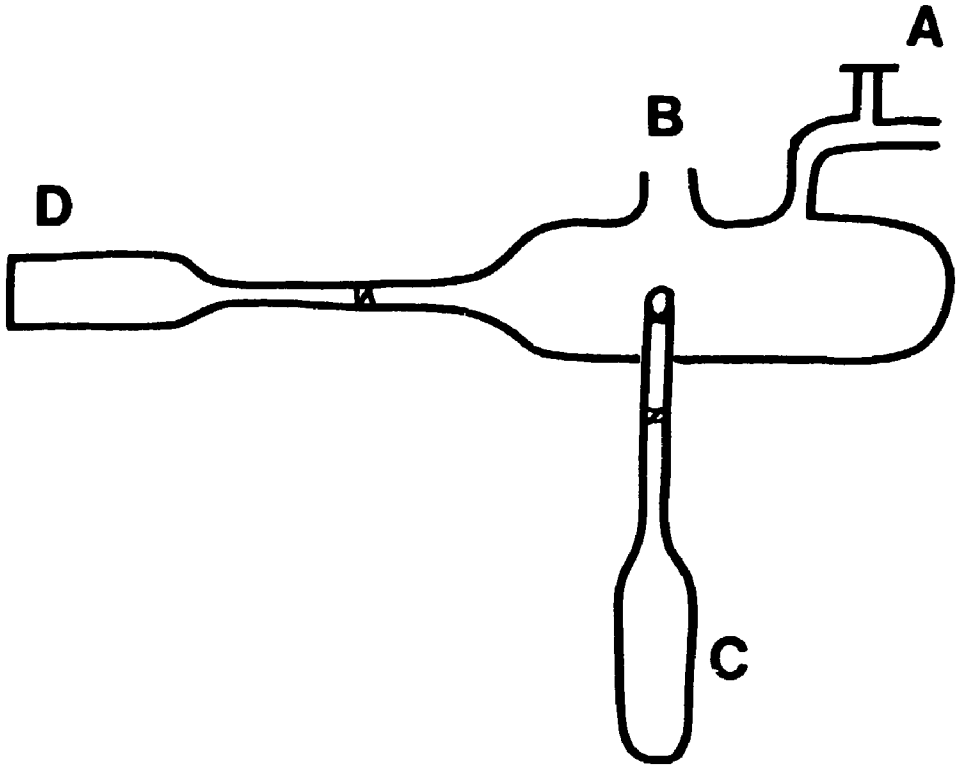
A
B
D
C

naphthacene solution to a compartment other than the one occupied by the silica. The solvent was then removed slowly by evaporation. The solid naphthacene formed and the silica were mixed and agitated for about 30 seconds. In this time most, if not all, of the naphthacene sublimed onto the silica. Samples were left on the vacuum line for another hour to approach equilibration. Deposition from solution was just that, mixing the solution and the silica and removing the solvent slowly.

Sublimation provides a way of adding the adsorbate without other alterations of the surface composition, while deposition from cyclohexane invariably leads to addition of trace amounts of water. This method was used to add water to the extent of about 0.2 μmol m^{-2} (2% of a monolayer), based on the volume of cyclohexane used in the preparation.

All samples were prepared to have a surface coverage of naphthacene to be 8×10^{-3} μmol m^{-2} or roughly 0.1%. This assumes a surface area of 60 $Å^2$ per naphthacene molecule[33] which does not account for the van der Waals radii of interaction. If we account for these the surface coverage was 0.3%.

Silica gels with increased silanol densities were prepared by boiling silica gel in nitric acid (BDH) or deuterated nitric acid (DNO_3 purchased from Sigma). Silica in a round bottom flask was mixed with enough acid to cover the silica. In the case of DNO_3, it was necessary to add a small volume of D_2O to cover the silica gel. A reflux condenser was used to minimize escape of acid fumes. The mixture was stirred slowly and heated to the boiling point of the acid

for two hours. The mixture was then diluted with doubly distilled deionized water. Initial separation of the silica from excess acid was achieved by decanting. Subsequent washing of the silica was done with water through a column, and was carried out until the eluent was neutral. The silica was initially dried in a 110°C oven overnight, and then at 180°C for at least one week prior to use in FPR experiments. Samples prepared with these silica gels ware pretreated at room temperature only.

Physisorption of H_2O or D_2O is carried out to achieve higher water concentrations. First, the silica was evacuated and heated to 250°C overnight and cooled. Then the silica was exposed to water vapor (vapor pressure 25 torr at room temperature) for two hours. This should yield at least monolayer coverages of water, due to the hygroscopic nature of silica. Physisorption of water (H_2O only) at about 10% monolayer coverage was achieved by repeatedly adding wet cyclohexane to the silica followed by slow removal of the cyclohexane. Water content in the cyclohexane was found to be 37 μg/ml by Karl Fisher titration.

The samples were sealed by a stopcock and maintained under vacuum during diffusion measurements. Mounting of the vacuum chamber on the microscope stage was achieved by use of a home made plexiglas bracket (Figure 3.4).

All measurements were made at room temperature with the sample held in a quartz cuvette with a 1 mm path length. Only the top face of the silica beads in the cuvette was used in FPR experiments.

Figure 3.4: Plexiglas bracket. Home made bracket used to mount vacuum chamber (Figure 3.3) on the stage of the epifluorescence microscope. The body of the chamber nests in the oval shape body. Wire ties are used to hold the chamber in place. The 1 mm cuvette sit above the rectangluar hole. The two holes located aboe this hole are used to mount the bracket to the stage with screws.

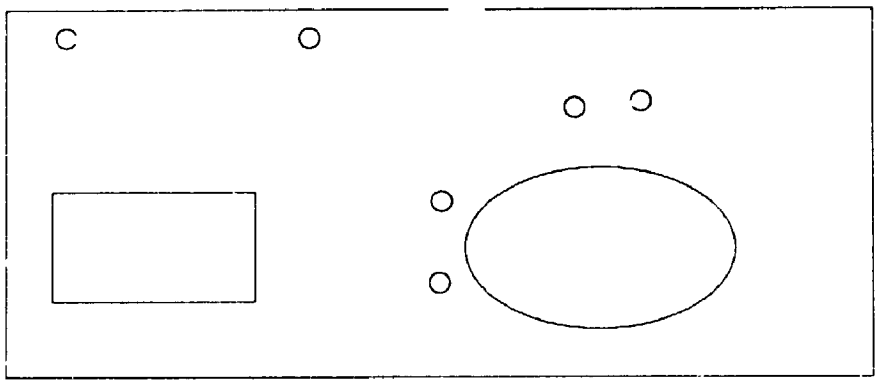

Typical FPR parameters used were 100 ms/ch, 100 to 150 ms bleach pulse, 50 s post recovery pause, and 2.1 - 2.8 OD attenuation.

3.1.3 Results and Discussion

3.1.3.1 Qualitative Observations

For all preparations, distributions in both the diffusion coefficient and the mobile fraction are recovered (*vide infra*). This is due to a heterogeneous distribution of naphthacene molecules on the surface, and to the heterogeneity of the silica surface. The heterogeneity of naphthacene coverage on the surface of the silica gel is implicit in the variation in diffusion coefficients and mobile fractions observed within the same sample. Further evidence is seen by the relative number of microcrystals of naphthacene discernible in the fluorescence microscope. Although the numbers are not quantified, it is clear that their occurrence is more frequent in samples dehydroxylated at high pretreatment temperatures. The most frequent occurrence of microcrystals is observed in some excessively hydrated samples (10% and above). In most of these cases, the fluorescence distribution in regions without microcrystals is so low that measurements are very difficult.

A corollary to excessive formation of microcrystalline domains is that the number of successful diffusion measurements decreases. The success rate is defined as the fraction of acceptable FPR procedures relative to the total number of procedures collected for any

particular preparation. In regions with large density of microcrystals, the fluorescence is predominantly from these solids. Since the microcrystals are immobile, the photobleaching experiments show so little recovery that it is impossible to get a reliable measure of the diffusion coefficient. In line with the qualitative observations outlined in the previous paragraph, the success rate for low temperature samples is almost unity while at the higher pretreatment temperatures the success rate is less than half. Generally, the success rate is greater in the slightly hydrated (2% monolayer) samples, but very low in the excessively hydrated samples.

For all the dry samples, irrespective of the pretreatment temperature, the rate of sublimation onto the silica gel is comparable. However, if the samples are left on the vacuum line for extended periods of time, there is a slow desorption which is observed as a coloration of a cotton plug positioned between the sample and the sample chamber exit port. This rate of desorption is sensitive to the silica treatment. There is virtually no desorption from the room temperature treated samples, whereas significant desorption occurs from samples treated at 600°C over a period of hours. Similar adsorption properties for heat treated silica is observed[34]. Dehydroxylated silica adsorbs less benzene from solution than untreated silica gel.

These qualitative observations point toward the same trend: samples treated at low temperatures adsorb the naphthacene with a greater number of interactions, therefore competing more effectively for the naphthacene, minimizing the tendency for naphthacene crystals

to form, and inhibiting desorption from the surface.

3.1.3.2 Quantitative Observations

Naphthacene is mobile on normal phase silica gels. An example of a photobleaching recovery experiment is shown in Figure 3.5, along with the fit to the recovery. The measured mobility parameters for naphthacene on dry silica as a function of pretreatment temperature are summarized in Table 3.1. The measured diffusion coefficient is invariant with pretreatment temperature, and is measured to be $(2.4 \pm 0.2)\times10^{-10}$ cm^2 s^{-1}. The mobile fraction shows some temperature dependence, and varies from 0.33 to 0.53. Results obtained for the mobility of naphthacene on silica with 0.2 μmol m^{-2} water added after being heated to various temperatures are outlined in Table 3.2. Little change in D is observed, but larger values of Xm (0.50 to 0.67) for corresponding pretreatment temperatures on dry silica are observed.

An increase in the extent of hydroxylation or hydration of silica is easily achieved. Increased hydroxylation is achieved by boiling silica in acid[25], whereas increased hydration is achieved by exposing silica to an atmosphere of water or to wet solvents. Both water and deuterated water are used to hydrate and hydroxylate the surface. Results for these systems are presented in Table 3.3. The results indicate that the diffusion coefficient is somewhat larger (roughly 3.8 to 4.5×10^{-10} cm^2 s^{-1} versus 2.4×10^{-10} cm^2 s^{-1}), and the mobile fraction remains in the 35 - 50% range. (It must be noted here that

Figure 3.5: Sample FPR experiment for naphthacene on dry silica gel, pretreated at 25^{0}C. Experimental conditions: 100 ms/ch, 150 ms bleach, 50 s post recovery pause. The recovered diffusion coefficient is 2.6×10^{-10} cm^{2} s^{-1}, and the mobile fraction is 0.54.

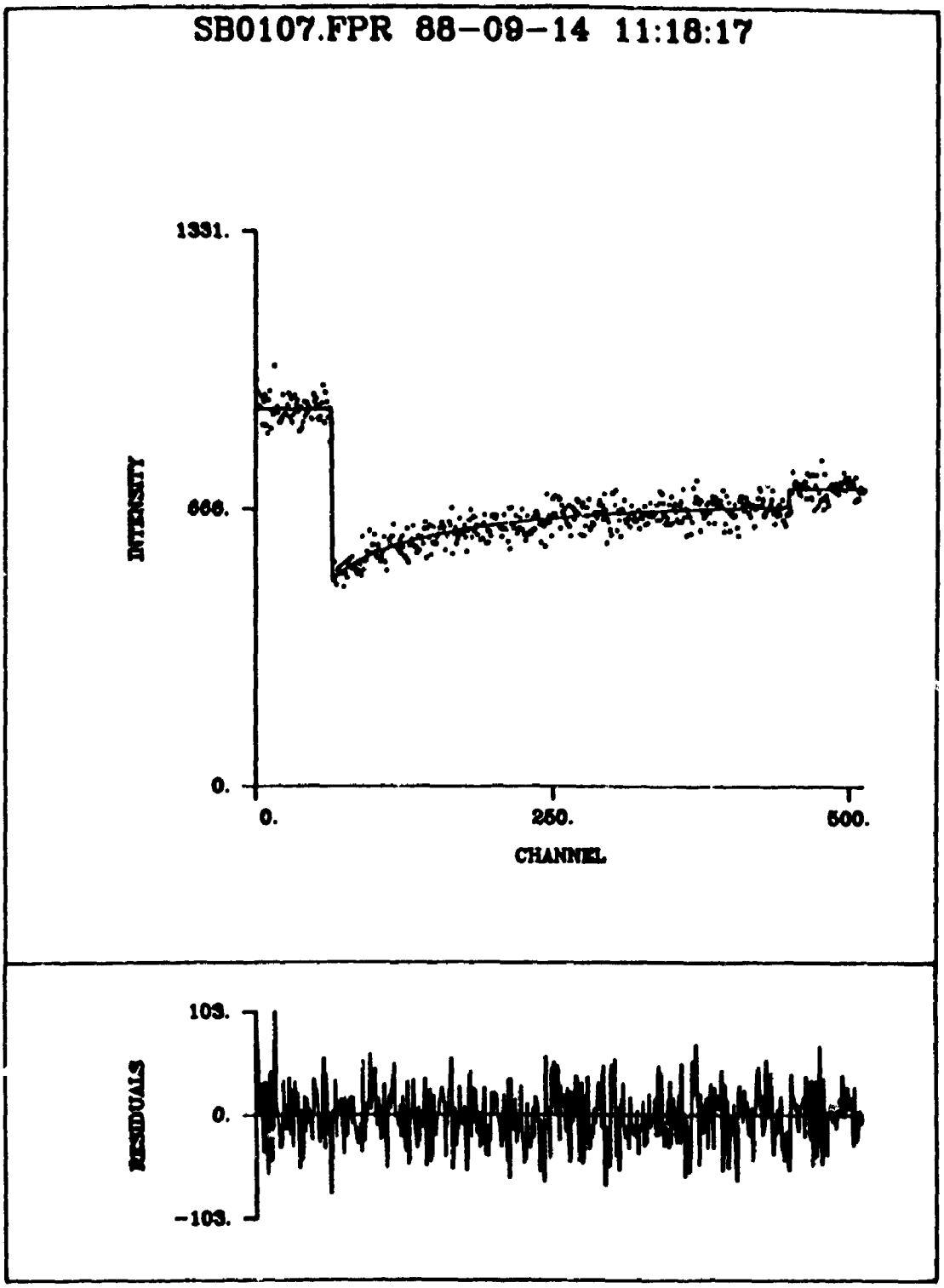
SB0107.FPR 88-09-14 11:18:17
1331.
666.
0.
INTENSITY
0.
250.
500.
CHANNEL
103.
0.
-103.
RESIDUALS

Table 3.1: Measured Diffusion Parameters for Naphthacene on Dry Silica Gel.

T_p[a] / ^{0} C	D / 10^{-10} $cm^2 s^{-1}$	Xm	N[b]	N'[c]
25	2.33 ± 0.40[d]	0.37 ± 0.04	103	7
250	2.55 ± 0.48	0.33 ± 0.04	78	6
600	2.18 ± 0.48	0.53 ± 0.07	42	3

[a] Pretreatment temperature.

[b] N is the number of FPR experiments used in the averages of D and Xm.

[c] N' is the number of samples prepared in the accumulation of the data

[d] All errors reported as the standard error of the mean at a 97.5% confidence level.

Table 3.2: Measured Diffusion Parameters for Naphthacene on Silica Gel with 0.2 μmol m^{-2} Water.

T_p[a] / ^{0} C	D / $10^{-10} cm^2 s^{-1}$	Xm	N[b]	N'[c]
25	2.83 ± 0.41[d]	0.51 ± 0.03	107	4
250	1.76 ± 0.22	0.50 ± 0.03	92	3
400	2.41 ± 0.38	0.55 ± 0.04	98	3
600	3.21 ± 0.39	0.67 ± 0.03	83	3

[a] Pretreatment temperature.

[b] N is the number of FPR experiments used in the averages of D and Xm.

[c] N' is the number of samples prepared in the accumulation of the data.

[d] All errors reported as the standard error of the mean at a 97.5% confidence level.

Table 3.3: Measured Diffusion Paramaters for Naphthacene on Silica with Increased Hydroxyl or Water Content.

Surface[a]	D / 10^{-10} cm^2 s^{-1}	Xm	N[b]	N'[c]
HY	3.90 ± 0.44[d]	0.51 ± 0.03	99	7
H_2O	3.78 ± 0.44	0.41 ± 03	93	5
DY	4.70 ± 0.60	0.37 ± 0.03	76	6
D_2O	4.26 ± 0.78	0.37 ± 0.05	39	5

[a] Type of surface used:
HY: silica boiled in concentrated nitric acid.
H_2O: silica exposed to 25 torr of H_2O for two hours.
DY: silica boiled in concentrated deutero-nitric acid.
D_2O: silica exposed to 25 torr D_2O for two hours.

[b] N is the number of FPR experiments used in the averages of D and Xm.

[c] N' is the number of samples prepared in the accumulation of the data.

[d] All errors reported as the standard error of the mean at a 97.5% confidence level.

after performing these sets of experiments, it was found that the beam profile had been distorted due to misaligned optics. As a result, the value of the calculated diffusion coefficient is expected to be larger than the real value. The effect of a distorted beam on the mobile fraction should be minimal). Trends seen within these systems with increased hydration or hydroxylation should be real since all were measured with the same distorted beam. The diffusion coefficient for naphthacene on deuterated silicas is greater than that on the non-deuterated silicas, but the mobile fraction is less. Generally, hydrogen bonds formed with deuterium are stronger than those formed with hydrogen[27]. In this case, the reverse situation is observed, since the diffusion on deuterated silica is faster.

Very little change in the diffusion parameters occurs as a result of this type of derivatization. The differences in D may be real, but this unfortunately cannot be quantified. It is clear however, that even if the differences are real the changes are small compared to differences seen when the mobility of naphthacene on an alkyl coated surface is measured. This is discussed in detail in Section 3.2.

Mobility of naphthacene on silica with increased water species is not different than that on dry silica. The mobility on deuterated surfaces ($D > 4\times10^{-10}$ cm^2 s^{-1}) appears to be greater than the mobility on non-deuterated surfaces ($D < 4\times10^{-10}$ cm^2 s^{-1}). The mobile fractions on these surfaces have the opposite trend, with less than 40% mobile on deuterated surfaces and 40 to 50% on the non-deuterated surfaces. Due to the above mentioned distortion in the beam shape, the recovered values have systematic errors. A measure of these

errors is unattainable, and quantitative evaluations of these data would be tenuous at best. All further quantitative discussions will focus on those measurements in which we have greater confidence (Tables 3.1 and 3.2).

The rate of mobility of naphthacene on silica gels with different water species in various proportions is virtually independent of the surface preparation. The mobile fraction depends greatly on the preparation. These two results suggest that the mobility of the same population is being measured in each case, but the relative proportion of naphthacene in this population changes with surface treatment. Addition of a small amount (0.2 μmol m^{-2}) of water to the surface causes an increase in the mobile fraction from 0.37 to 0.51 (Tables 3.1 and 3.2). Heating of the surface to 600^{0}C increases the mobile fraction on dry silica to 0.53. The largest value of Xm for these systems (0.67) is seen for a silica surface first heated to 600^{0}C and then exposed to a small amount of water. Heating of silica *in vacuo* causes dehydration and dehydroxylation of the surface[28-31], which causes an increase in the mobile fraction. An increase in the mobile fraction is also observed with physisorption of small amounts of water. These results are explained in terms of the relative populations of physisorbed and chemisorbed water. Heating will decrease the surface silanol concentration by dehydration. This process occurs most readily in regions where the silanol density is high, due to the dehydroxylation process involving neighboring silanol groups (Figure 3.6). These regions are those in which naphthacene would be strongly bound. A decrease in the number of these regions

Figure 3.6: Mechanism of dehydration of silica gel. Vicinal silanol groups combine to release water and form a new siloxane bridge (Si-O-Si).

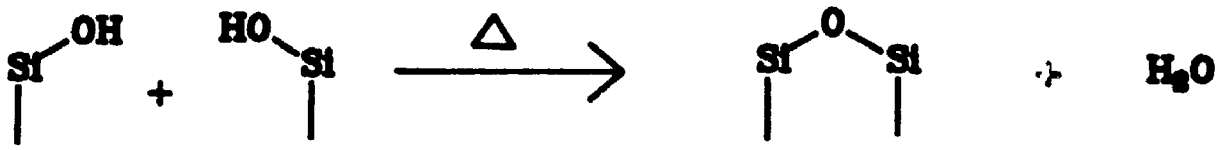
OH
Si
HO
Si
Δ
O
Si
Si
+
H_2O

will result in an increase in Xm. When water is physisorbed on the surface, it can bind to isolated silanol groups[35] or to regions of already hydrogen bonded silanol groups[26]. Regions with physisorbed water cannot bind PAHs as strongly as regions without[26]. Hence, addition of water increases Xm by blocking some of the sites where naphthacene could have been bound strongly.

Naphthacene is mobile on normal phase silica, with a rate of mobility independent of the extent of hydroxylation or hydration. This is not an artifact of the procedure. Diffusion on hydrocarbon derivatized silica yields very different values of both D and Xm (*vide infra*). The fraction of molecules free to move changes greatly with alterations to the surface.

Interestingly, a single value of D or Xm is not observed in any of the above mentioned systems. Rather, a range of values is recovered, as shown in Figure 3.7 for naphthacene on dry silica gel for various pretreatment temperatures. The distributions recovered have standard deviations which represent anywhere from 56 to 88% (for D) and 20 to 60% (for Xm) of the mean.

The width of the distributions can arise from two factors. If the data is of poor quality, with a significant level of noise, the precision of the calculate diffusion parameters is low. This leads to relatively large errors associated with each measured value, and to broad distributions. However, for measurements with only random noise, τ_D can be measured to a precision of 15%, and Xm can be measured to a precision of better than 10% for model systems. This value is somewhat higher for non-ideal systems, and has been found to

Figure 3.7a: Frequency of occurrence of diffusion coefficients (top) and mobile fractions (bottom) within intervals representing 10% of their range. These histograms show distributions of D and Xm for naphthacene on dry silica gel pretreated to various temperatures (25^{o}C diagonal bars; 250^{o}C open bars; 600^{o}C solid bars).

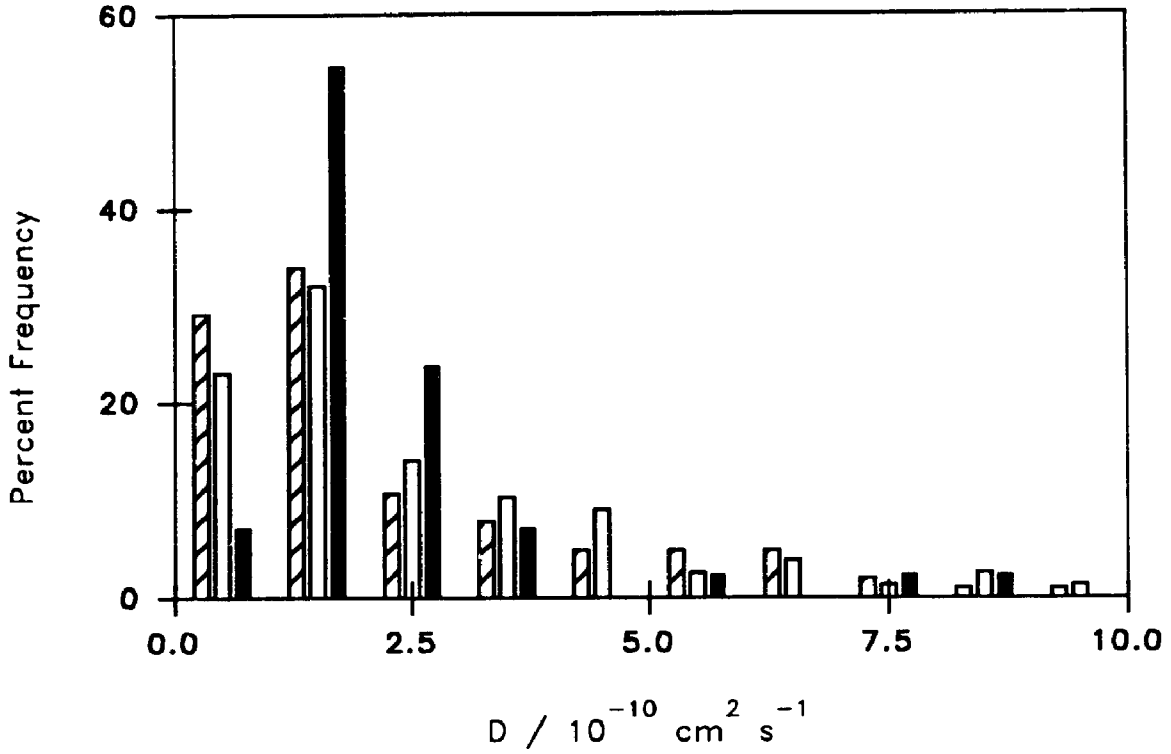
60
40
20
0
Percent Frequency
0.0
2.5
5.0
7.5
10.0
D / 10 -10 cm 2 s -1

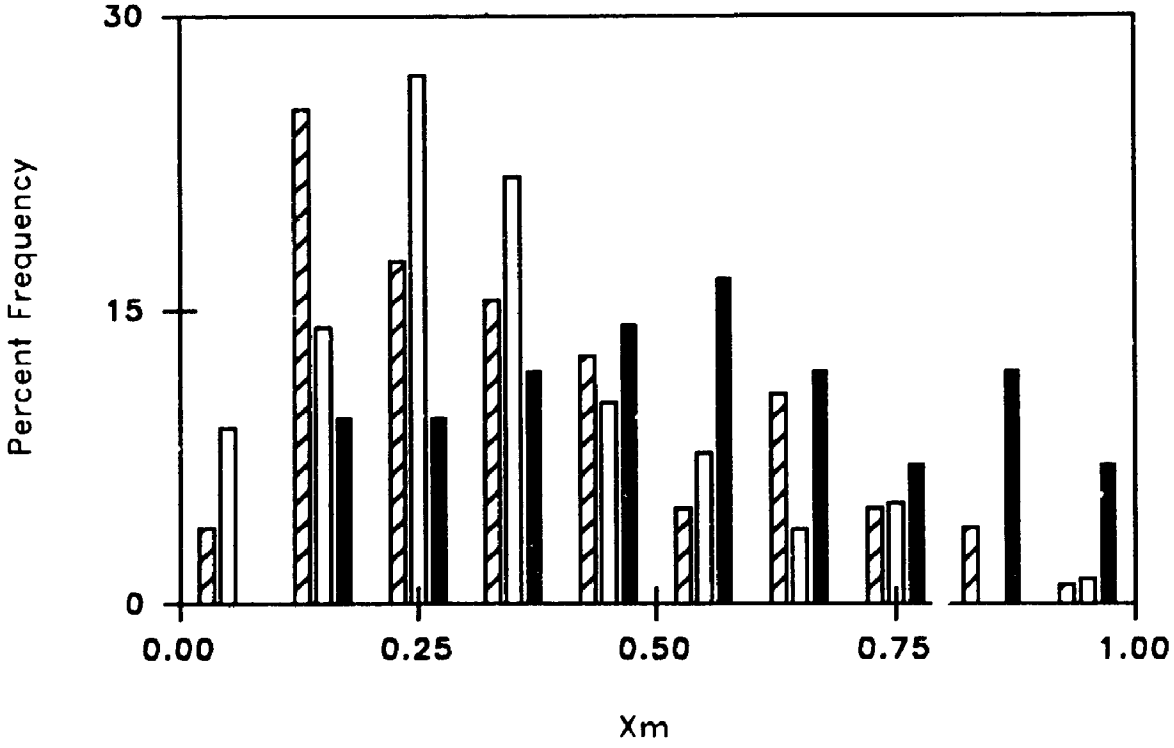
30
15
0
Percent Frequency
0.00
0.25
0.50
0.75
1.00
Xm

Figure 3.7b: Frequency of occurrence of diffusion coefficients (top) and mobile fractions (bottom) within intervals representing 10% of their range. These histograms show distributions of D and Xm for naphthacene on silica gel pretreated to various temperatures (25^{0}C diagonal bars; 250^{0}C open bars; 400^{0}C cross-hatch; 600^{0}C solid bars) followed by physisorption of 0.2 μmol m^{-2} water.

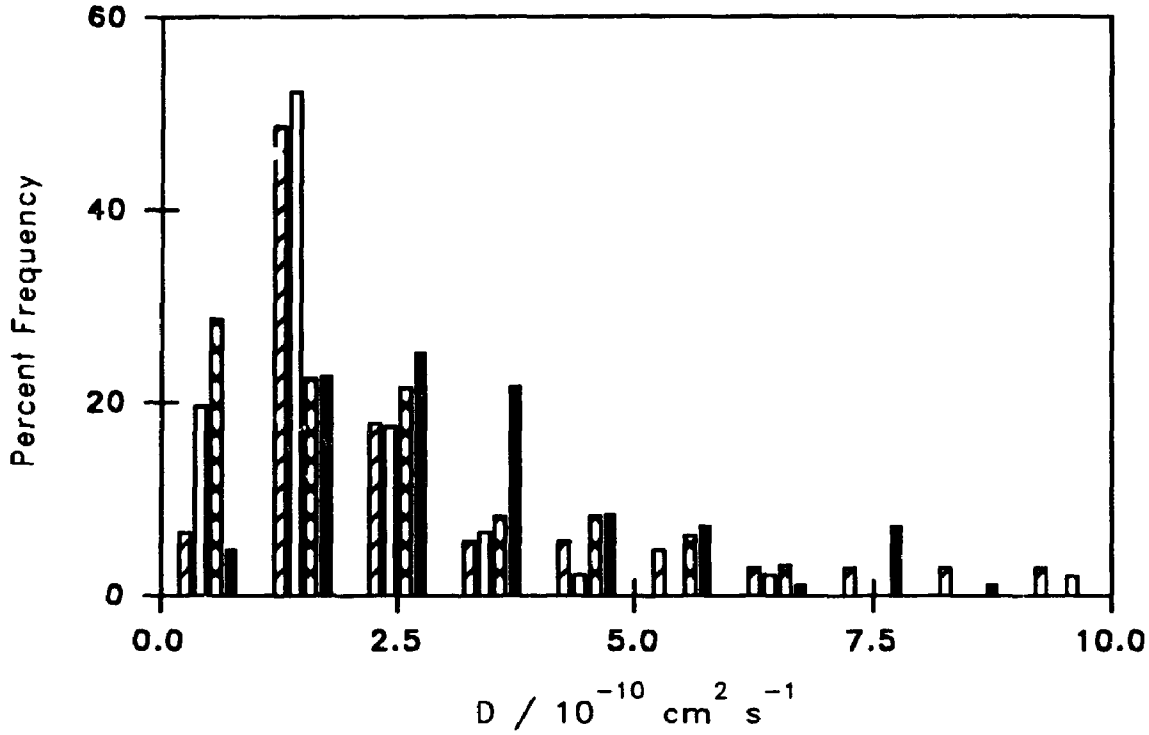
60
40
20
0
Percent Frequency
0.0
2.5
5.0
7.5
10.0
D / 10^-10 cm^2 s^-1

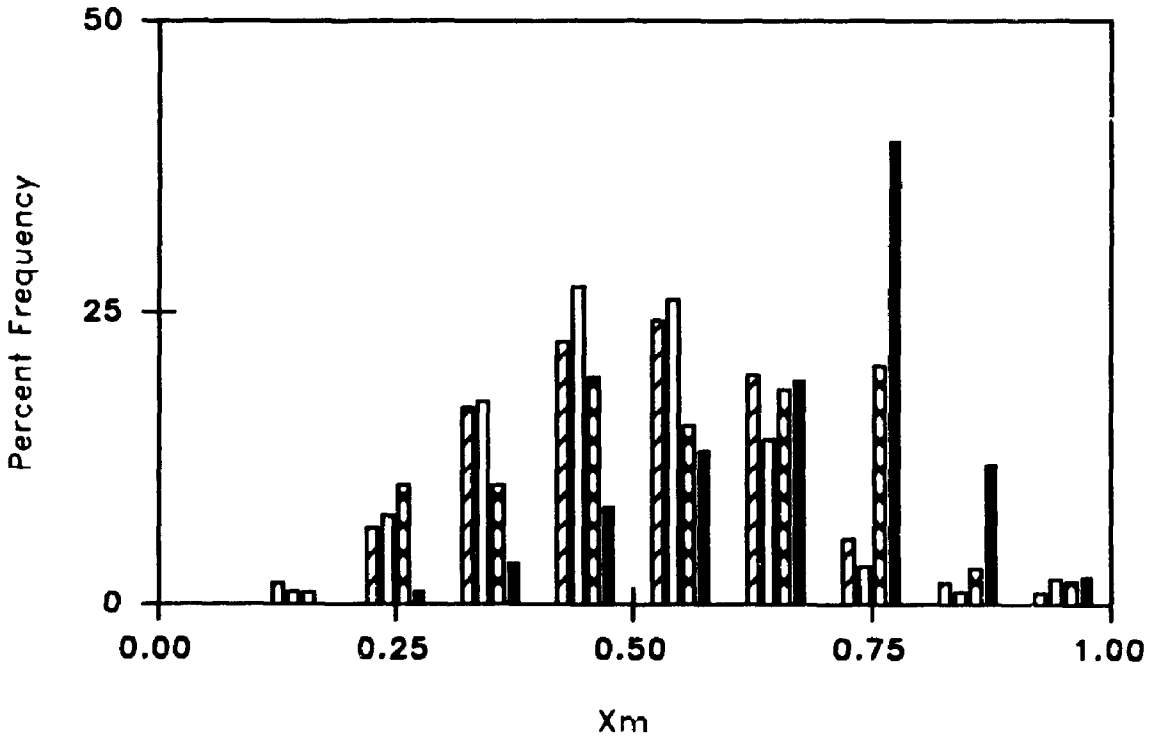
50
25
0
Percent Frequency
0.00
0.25
0.50
0.75
1.00
Xm

be as high as 20% (for τ_D) for the mobility of NBDPE in cell membranes[36]. The precision gives a measure of the population standard deviations of the recovered parameters and is much smaller than that observed. Differences in the measured values can also arise from true differences in surface populations. Standard deviations found for individual measured values are significantly smaller than the standard deviations calculated for the population mean. This suggests that the width of the distributions is due to true differences in the measured diffusion parameters. We believe the recovered widths to be a result of the surface convolution and contour. Heterogeneity of the surface exists on a molecular level, and a micrometer scale. This is reflected in the broad distributions of Xm and D.

The surface of silica gel is highly convoluted as seen in scanning electron micrographs of silica gel (Figure 3.8). The convolution allows for many microenvironments that PAHs can experience. Naphthacene has four linearly arranged aromatic rings. If naphthacene adsorbs to a flat silica surface, then there can be at most four silanol groups interacting with the π electron system. From this model there are four possible microenvironments, which are regions where naphthacene can bind to exactly one, two, three or four silanol groups. The convolution of the surface allows for many more microenvironments, one of which could be regions that have different silanol groups interacting from either side of the naphthacene molecule. This population would be immobile. Physisorption of water will also change the number of microenvironments present. The relative proportion of each of these environments will vary with

Figure 3.8: Scanning electron micrographs of silica gel.

Top: Low resolution SEM showing a whole silica bead.

Bottom: High resolution SEM of the same bead.


25kV
25kV

various treatments. Naphthacene is not mobile in all of these environments, as reflected in mobile fractions less than unity. A question arises: in which of these is naphthacene mobile? To answer this, a geometric model of silica is constructed and the relative proportions of each population were estimated[37]. The model, based on that of Peri and Hensley[38], consists of a flat surface with silanol groups distributed on an hexagonal lattice with a separation of 5Å in a random pattern determined by the total density. Each silicon site is taken to have either one silanol group (vicinal or isolated) or a geminal pair. In all cases, the number of naphthacene molecules bound to only one or two silanol groups is extremely small, with the vast majority being bound to three or four (Table 3.4).

Surface diffusion of naphthacene could occur by two simple mechanisms: desorption followed by adsorption, or sliding along the surface by alternately breaking and forming bonds with silanol groups. A naphthacene molecule bound to only one silanol group could diffuse by the desorption-adsorption model only. Molecules bound to two would not likely break two bonds simultaneously. Breaking one bond would allow for rotation of the molecule, and possible formation of new bonds with other silanol groups. This results in a translation of the center of mass. A molecule bound to three silanol groups would slide across the surface in a similar fashion. The probability of motion is decreased due to geometric constraints of the three bonds. A molecule bound to four silanol groups would be the least mobile of the four types considered here. The results in Table 3.4 show that molecules bound to three or four silanol groups make up the majority, and the

Table 3.4: Predicted Mole Fractions of Naphthacene Bound to Exactly Two (X_2), Three (X_3) or Four (X_4) Silanol Groups as a Function of the Probability (p) that a Silicon Site has a Single Silanol or a Geminal Pair of Silanol Groups.

T/°C	p	X_2	X_3	X_4
		single silanols only		
25	1.00	0.00	0.00	1.00
250	0.84	0.00	0.00	1.00
400	0.44	0.01	0.31	0.67
600	0.32	0.04	0.49	0.47
		geminal silanols only		
25	0.50	0.00	0.24	0.76
250	0.42	0.01	0.34	0.64
400	0.22	0.10	0.60	0.30
600	0.16	0.20	0.60	0.20

proportions of these populations vary with temperature. The populations with one or two bonds only are so small that they should not affect the measured diffusion values. From this simple model, it appears that the population of naphthacene molecules bound to three silanol groups is the mobile portion being measured in the FPR experiments. Those bound to four silanol groups may exchange with those bound to three, but this exchange would be slow compared to the time scale of the experiment. This hypothesis is consistent with the measured values of both D and Xm. Since the value of D remains invariant, the mobility of the same population is being measured. As well, Xm changes with treatment temperature, as predicted by this simple model. It is noted however, that the values of Xm predicted by this model are lower than measured. We attribute this to the convolution of the actual silica surface.

The mobility of other polycyclic aromatic hydrocarbons was also investigated. Specifically, measurements of the mobility of rubrene and pentacene (Figure 3.9) are attempted. Experiments with rubrene are at least partly successful. Rubrene exhibits desirable properties for a probe used in this type of study (solubility, fluorescent, can be excited by an Argon ion laser, see Figure 3.10). The distribution of rubrene on the surface is generally fairly homogeneous, with some microcrystals present. However, rubrene exhibits a wide range of mobilities. On some experiments, the recovery is virtually nil, while on others, the recovery is almost linear in time, and nearly complete. We have little confidence in the calculated parameters from these experiments. A few measurements show recoveries from which the

Figure 3.9: Structures of rubrene (top) and pentacene (bottom). Ph represents phenyl rings.

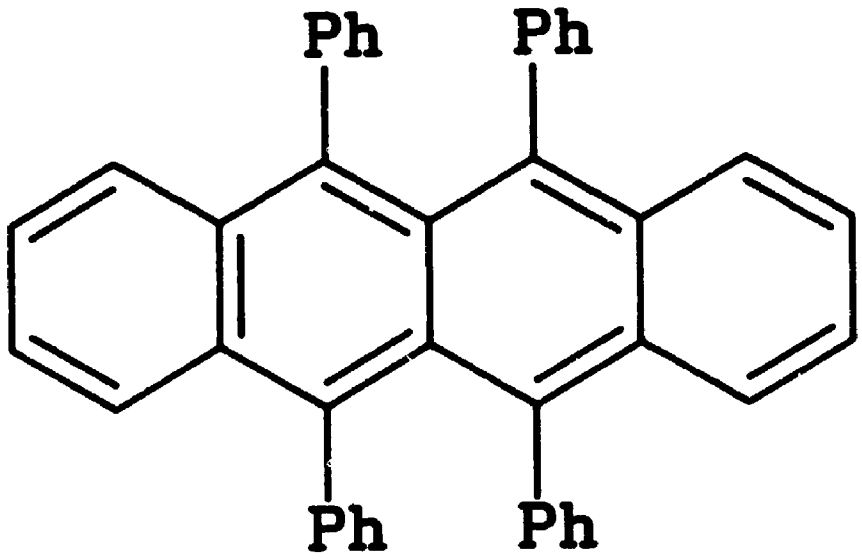
Ph
Ph
Ph
Ph

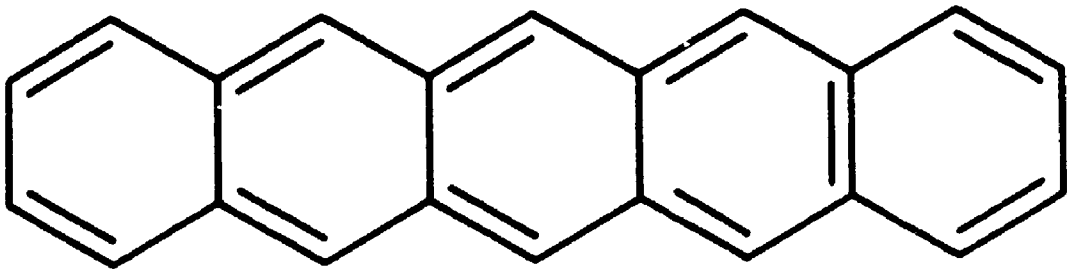

Figure 3.10: Excitation (———) and emission (- - -) spectra of rubrene in cyclohexane. Excitation wavelength 492 nm, emission wavelength 587 nm, 1.4×10^{-5} M.

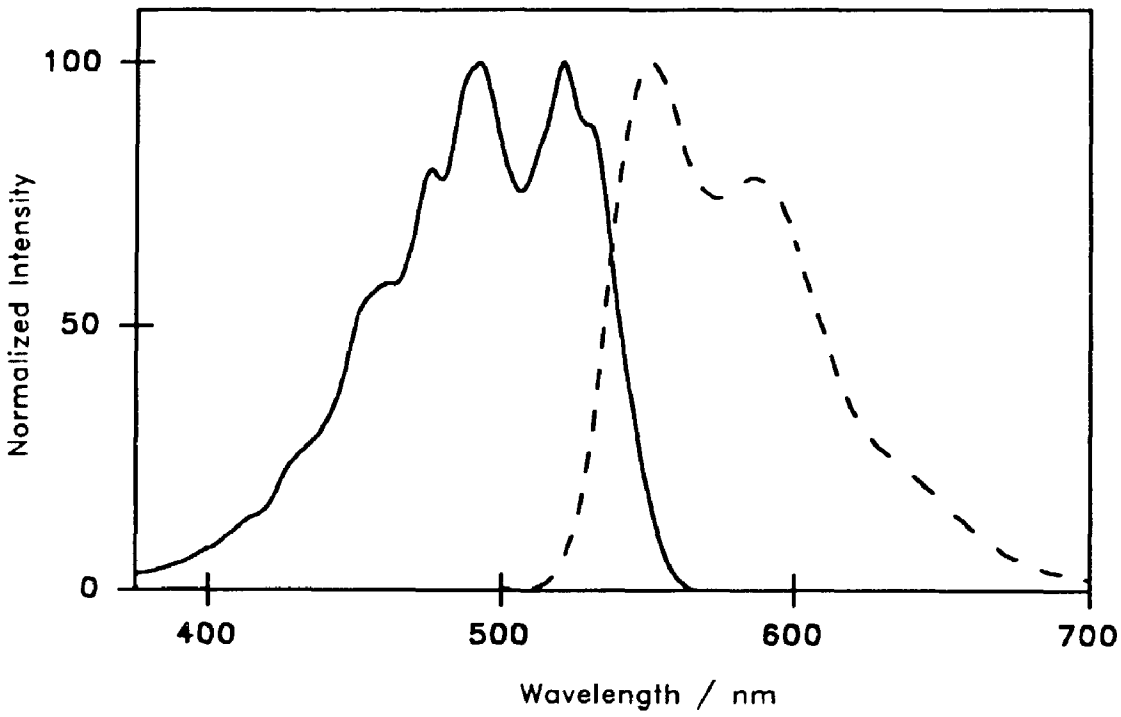
100
50
0
Normalized Intensity
400
500
600
700
Wavelength / nm

calculated parameters are believable. From these few, the diffusion coefficient is estimated to be 5×10^{-10} cm^2 s^{-1}, and the mobile fraction is near 0.4. The changes in the mobility parameters relative to values obtained for naphthacene are due to the four phenyl groups on rubrene. Based on calculations using a software package[39] on a personal computer, the phenyl rings form a dihedral angle of 81^0 to the plane of the naphthacene moiety (Figure 3.11). Not all of the phenyl rings, or the aromatic rings of the naphthacene moiety will be able to bond to the surface simultaneously. One expects that rubrene might be bound less strongly than naphthacene, and should, therefore, have a larger diffusion coefficient. The mobile fraction of rubrene should be greater than that of naphthacene since the distribution of rubrene is more homogeneous, and the binding force is apparently weaker. The mobile fractions are, however, approximately equal.

Experiments with pentacene failed for three reasons. Although pentacene is planar, and should be mobile if our hypothesis is correct, the quantum yield of fluorescence is quite low. This value is measured to be less than 5% in degassed toluene. The solubility of pentacene is also quite low in useful solvents, making appropriate volumes too large to work with. Finally, pentacene is easily oxidized[40]. If even trace amounts of oxygen are present in solution, pentacene will react quickly when exposed to light.

Figure 3.11: Spacefilled representations of rubrene. Top: Looking down on the plane of the naphthacene moiety. Bottom: Looking edge-on to the plane of the naphthacene moiety. All four phenyl rings are bent out of the naphthacene plane. Carbon represented with lines, hydrogen by the dotted regions.

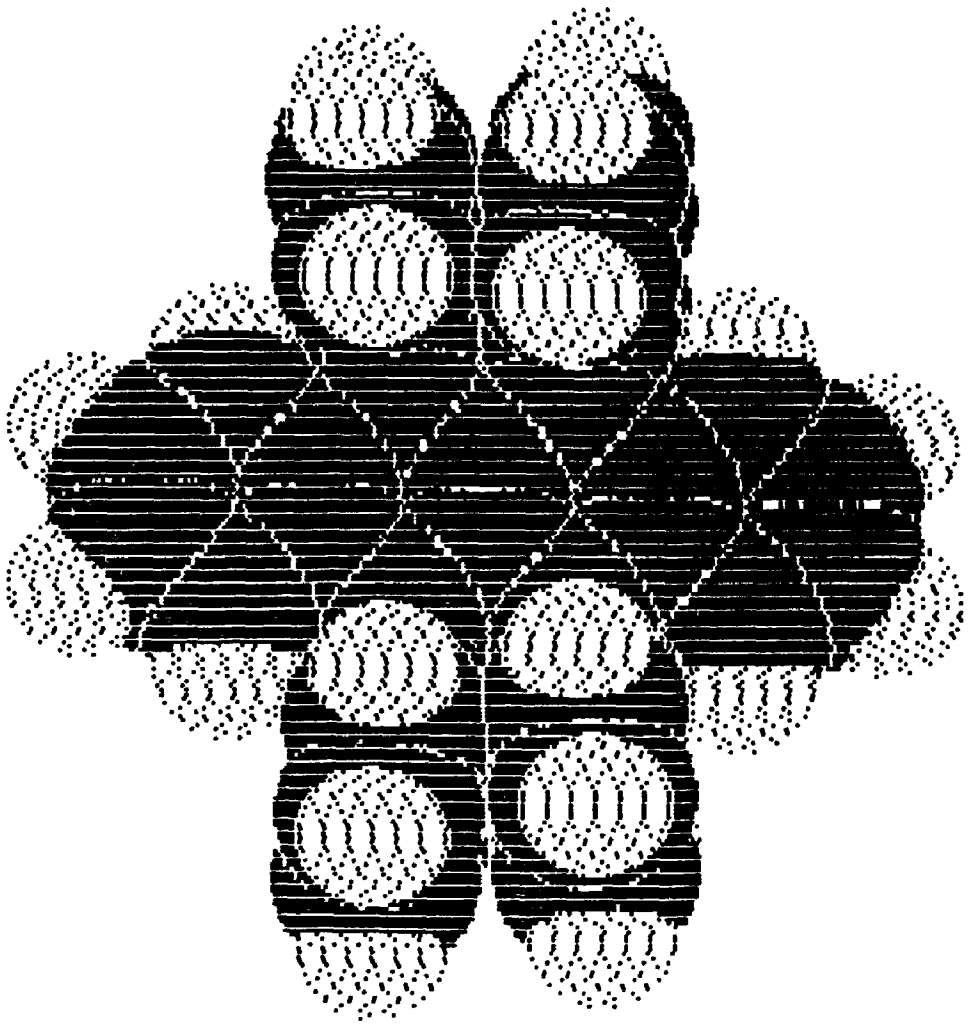

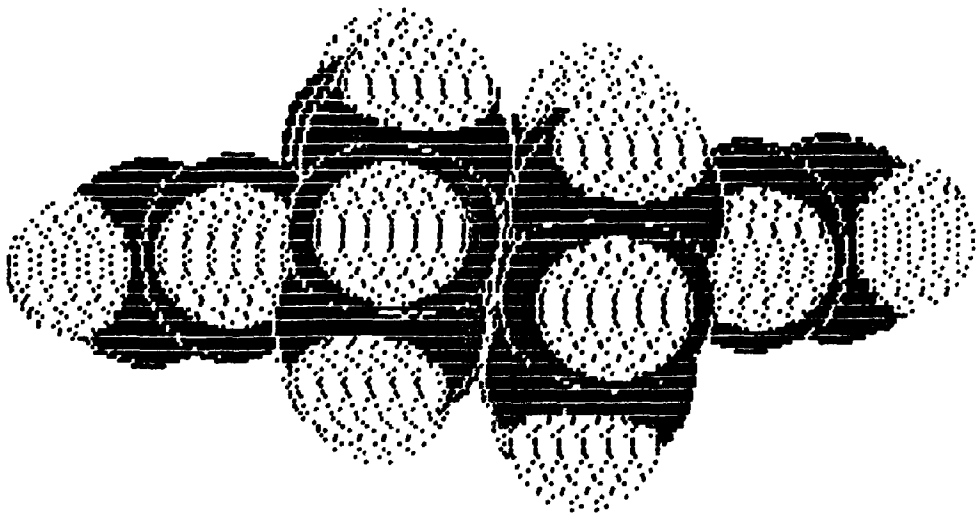

3.1.4 Conclusions

Changing the level of hydration and hydroxylation allows for qualitative and quantitative comparisons of interaction parameters between the surface and an adsorbed aromatic hydrocarbon. Many microcrystals are observed on surfaces with very low water or silanol content, or with high water content. These results indicate that water will block potential binding sites. These sites are removed by heating also. Reduction in the number of these binding sites, by heat treatment, increases the rate of desorption of naphthacene. These qualitative observations provide more evidence for the well-established idea that binding of aromatic hydrocarbons to silica must involve surface silanol groups and π electrons in the aromatic rings.

For all naphthacene samples studied in detail the diffusion coefficient is found to be virtually the same. This indicates that there is only one population of naphthacene which is mobile on the surface. The measurements also reveal that a significant fraction of naphthacene is immobile. The relative amount of the mobile and immobile populations varies with water and silanol content. We attribute this variation to the change in the fractions of naphthacene molecules which are bound to three and four silanol groups simultaneously. Those bound to three silanol groups will be mobile while those bound to four will not.

Unfortunately, there is no simple or straight forward way of comparing two dimensional diffusion coefficients to bimolecular

quenching rate constants determined for pyrene on various surfaces. Very little change in the rate of lateral motion is observed with changes to only water species on the surface. de Mayo and colleagues have reported that the rate constant can change by as much as an order of magnitude by changing only water species on silica gel[8]. Vast differences in the rate constants with no change in the diffusion coefficient are observed, and could be due to the different processes being examined in each study. The quenching rate constants are measured via time resolved fluorescence techniques (on a nanosecond time scale) , whereas the diffusion measured here is on a time scale at least nine orders of magnitude slower. Accordingly, the distance over which interactions can occur differ greatly in the two procedures.

Measurements of the mobility of other linear acenes would help to elucidate the binding mechanism with respect to the mobile fraction. If the hypothesis is correct, diffusion of anthracene should yield virtually the same diffusion coefficient, but the mobile fraction should be greater than that for naphthacene. This is due to anthracene not being able to bind to four silanol groups simultaneously. This experiment cannot be performed using an Argon ion laser, and is yet to be.

3.2 Diffusion on Chemically Bonded Layers

3.2.1 Introduction

Chemical modification of silica gel can lead to production of a hydrophobic surface. These silica gels are the basis of reverse phase chromatography. A hydrophobic stationary phase in conjunction with a relatively polar mobile phase is used for separation techniques. By what mechanism reverse phase chromatography works is open to debate. The interactions between the surface, sample and solvent are not clearly understood. Two prominent theories involve either partitioning between the two phases[41,42], or an adsorption and diffusion process on the stationary phase[43,44].

Reverse phase surfaces can be quite easily prepared. Reaction between surface silanol groups (SiOH) and an appropriate silylating agent (*eg.* octadecyltrichlorosilane) proceeds rapidly, but not necessarily to completion[45]. Steric hindrance on the surface between attached ligands can lead to a substantial number of unreacted silanol groups. This number will depend on the size of the silylating agent, among other factors. Lochmüller *et. al.* have shown that the distribution of attached ligands is heterogeneous, and one should expect regions of high and low hydrocarbon chain densities[45].

Characterization of these surfaces has been attempted using numerous techniques. Elemental analysis, thermogravimetric methods, x-ray photoelectron spectroscopy, pyrolysis gas chromatography, mass spectrometry techniques, and proton NMR are some of the techniques

used[45-48]. Various FTIR methods have been employed most often to probe the hydrocarbon surface[49,50]. Results indicate that in the absence of a solvent the hydrocarbon chains are most likely lying tangled on the surface, in a two dimensional liquid[50]. Certain peaks in the IR spectra are indicative of hydrocarbon chains in a gauche conformation. In the presence of a solvent however, the chains are free to become untangled[50].

As in the case of normal phase silica, most studies which have investigated interactions between polycyclic aromatic hydrocarbons (PAHs) and alkyl coated silica gels have employed the photophysical properties of pyrene and pyrene derivatives[45,51-54]. Data for pyrene both physically and chemically adsorbed to the surface has been obtained. Effects of temperature, coadsorbates, surface concentration and the presence of solvent have been investigated.

Some of the more pertinent results for this thesis include a diffusion coefficient and activation energies for mobility. Bogar *et. al.* have calculated an approximate diffusion coefficient for pyrene on octadecyl (C18) coated silica in contact with 75/25% v/v methanol-water mixture[51]. The value obtained by Bogar, 2.5×10^{-7} cm^2 s^{-1}, is two to three orders of magnitude larger than the diffusion coefficient obtained by us for naphthacene adsorbed on various derivatized surfaces. Indeed, Bogar has reported that with no solvent present no diffusion took place, at least on the time scale of pyrene excimer formation. Ståhlberg and co-workers have concluded that the apparent activation energy for diffusion of pyrene on C18 silica in contact with water is roughly 20 kJ/mol at ambient

temperatures[52]. From this result Ståhlberg *et. al.* deduced that the reverse phase layer had liquid like properties. The activation energy for quenching of pyrene fluorescence on decanol coated silica has been estimated to be on the order of 8 kJ/mol[8]. The difference in these two values could be due to the difference in coatings (chemisorbed versus physisorbed) or by the way the values were derived.

We show that PAHs will adsorb onto reverse phase silica gels, and are mobile. We cannot deduce whether or not the PAH partitions into or adsorbs onto the bonded layer. Qualitative results seem to indicate that naphthacene partitions into the hydrocarbon layer.

Diffusion of naphthacene occurs in these systems, even in the absence of any solvent. The rate of mobility is greater than that of naphthacene on normal phase silica. Variations in the measured parameters are observed to be a function of deposition procedure and extent of surface derivatization.

3.2.2 Experimental

All hydrocarbon derivatized surfaces used were prepared in our laboratory. The derivatization procedure used was that employed by others[55,56]. A dilute solution (0.1% v/v) of the silylating agent in 80% octane, 12% carbon tetrachloride and 8% chloroform (all from BDH) was stirred with an appropriate mass of silica gel. Enough derivatizing agent was used to give a slight excess in monolayer coverage, provided the reaction went to completion. This is based on a projected area of 20 $Å^2$ per alkyl molecule, and the assumption that

the long chain hydrocarbons are standing on the surface, and not laying flat. The reaction was typically run for 15 minutes, but one sample was prepared with a much longer reaction time (24 hours). The silica was vacuum filtered and rinsed with aliquots of chloroform, doubly distilled deionized water, and chloroform again. Before use, the silica was air cured for at least 24 hours. Hydrocarbon coated silica gels were not kept in an oven as not all coatings are thermally stable[57]. The only pretreatment temperature used for all hydrocarbon derivatized silica gels was room temperature.

Three silylating agents were used to produce reverse phase silica gels. Each derivatized surface will be identified by the number of carbons in the chain, for example C18 will be used to represent octadecyl coated silica. The three agents employed were C1 (trimethylchlorosilane), C8 (octyldimethylchlorosilane) and C18 (octadecyltrichlorosilane), all purchased from Fluka. These reagents were used without any further purification.

Myristic acid (Sigma) and 1-undecanol (Aldrich) were physically adsorbed to some silica samples. Deposition was from cyclohexane solution. In each case, the amount of hydrocarbon physisorbed was enough to give roughly one monolayer coverage. These reagents were used without further purification.

Samples used for FPR experiments were prepared in the same way as for naphthacene on normal phase silica gel. Both adsorption of naphthacene via sublimation and from solution were investigated. Some C18 silica was further derivatized by coadsorption of undecanol. The surface concentration of naphthacene was kept constant at roughly 0.1%

of a monolayer. This assumes little or no change in the surface area of the silica gel upon derivatization.

Parameters for FPR experiments with naphthacene were as follows: 75 to 100 ms/ch, 80 to 150 ms bleach pause, 20 s post recovery pause, and an attenuation of 2.11 to 2.8 OD. For experiments using rubrene as the fluorescent probe the conditions are: 75 to 100 ms/ch, 200 ms bleach pulse, 20 s post recovery pause, and 1.88 OD. Rubrene has a larger quantum yield of fluorescence than naphthacene, and requires less attenuation of the laser beam to eliminate monitor beam bleaching. Consequently, extra neutral density filters were placed between the sample and the PMT. This protects the PMT from fluorescence intensities which are too high.

3.2.3 Results and Discussion

3.2.3.1 Qualitative Observations

Adsorption of naphthacene via sublimation on the C18 silica surface yields a relatively homogeneous distribution. Typically there is some microcrystalline material present, but far less than on any of the normal phase silica gels. Adsorption from solution leads to the most homogeneous distributions, with an extremely small number of microcrystals present.

Adsorption via sublimation onto either a C8 or C1 surface yields a very inhomogeneous distribution. More crystalline material is present on C1, but even on C8 there is a significant amount. For most

samples prepared, the fluorescence intensities in regions of non-crystalline naphthacene are very low, resulting in a poor signal to noise ratio. Adsorption from solution on either C1 or C8 leads to a significant amount of microcrystalline material also. On C8, the amount is somewhat less than for sublimed naphthacene. On C1, most of the naphthacene is still crystalline.

The heterogeneity of these probe distributions are explained with respect to the interactions between the surface and the adsorbed aromatic hydrocarbon. On an underivatized surface, the attractive interactions are hydrogen bonds, and relatively strong[9,10,25]. On a hydrocarbon derivatized surface the greatest forces of attraction will be dispersion forces between the hydrocarbon chains and the aromatic molecule. The magnitude of these forces will depend on the chain length and density of the coating.

Each of the three coatings were prepared in a similar manner. Variations in the global coating density of each will occur due to varying degrees of steric hindrance, and the fact that the C18 agent can form up to three bonds with the surface. Variations in local coating density will also occur due to initial heterogeneity of the surface silanol groups prior to reaction[45].

Infrared data indicate that the C18 chains will be lying tangled on the surface[45]. This entanglement causes the surface to become fluid-like. As the chains become shorter, the degree of entanglement and extent of coverage for a given global density will decrease, yielding more regions that appear like normal phase silica. We have shown previously that microcrystals form quite readily on normal phase

silica.

As the chains become shorter, the number of interactions decreases. An extreme is reached with the one carbon chain. This very short chain will have the smallest number of interactions with naphthacene. The C8 chain is approximately as long as a naphthacene molecule, whereas the C18 chain is more than twice as long. Naphthacene will experience the greatest number of dispersion forces on the C18 surface.

These factors affect the surface distribution of adsorbed aromatics. As the coating decreases in both chain length and density, the degree of heterogeneity in the probe distribution increases.

Adsorption from solution yields fewer microcrystals. The adsorption process here is very different, as discussed above. With solvent present, the long hydrocarbon tails will not be tangled on the surface. As the solvent is evaporated, the naphthacene is trapped by the long tails as they settle back onto the surface.

Naphthacene adsorbed on C18 silica shows no evidence of desorption when left on the vacuum line overnight. Naphthacene desorbs from normal phase silica pretreated at high temperatures, as shown by coloration of a cotton plug in the vacuum chamber. An increase in the diffusion coefficient for naphthacene on C18 silica over that for naphthacene on normal phase silica indicates the strength of the interactions binding naphthacene to normal phase silica is greater than that binding naphthacene to a C18 surface. Since no desorption is detected from a C18 surface, a number of weaker interactions per naphthacene molecule must contribute more than a few

but stronger interactions on the normal phase silica. For this to occur naphthacene must be trapped in the hydrocarbon entanglement, and not adsorbed on the hydrocarbon surface. In terms of activation energies, the activation energy for diffusion of naphthacene on alkyl coated silicas is less than that of naphthacene on normal phase silica, but the activation energy for complete desorption from the alkyl coating is greater than for desorption of naphthacene from normal phase silica.

The success rate of experiments for C18 silica is only 80 to 85%. The efficiency of the photochemistry is greatly enhanced on the alkyl coated surface relative to the normal phase silica surface. With a strong bleaching pulse, quite often too many of the fluorophores are destroyed. As a result, the perturbation to the system is too large to have great confidence in the calculated diffusion parameters. Data obtained from experiments where the extent of bleaching exceeds a predetermined level are not used in further statistical analyses.

3.2.3.2 Quantitative Observations

Diffusion of PAHs occurs on a variety of derivatized silica surfaces. Figure 3.12 shows a typical FPR recovery curve along with the fit to the data for naphthacene on C18 silica with undecanol coadsorbed. The measured diffusion parameters for naphthacene adsorbed on various alkyl coated silica gels are presented in Table 3.5. As shown in Section 3.1, naphthacene is mobile on normal phase silica, and experiences at least two microenvironments, that in which

Figure 3.12: Sample FPR experiment for naphthacene on C18 silica gel further derivatized by physisorption of undecanol. Experimental conditions: 75 ms/ch, 120 ms bleach, 20 s post recovery pause. The recovered diffusion coefficient is 2.7×10^{-9} cm^2 s^{-1}, and the mobile fraction is 0.79.

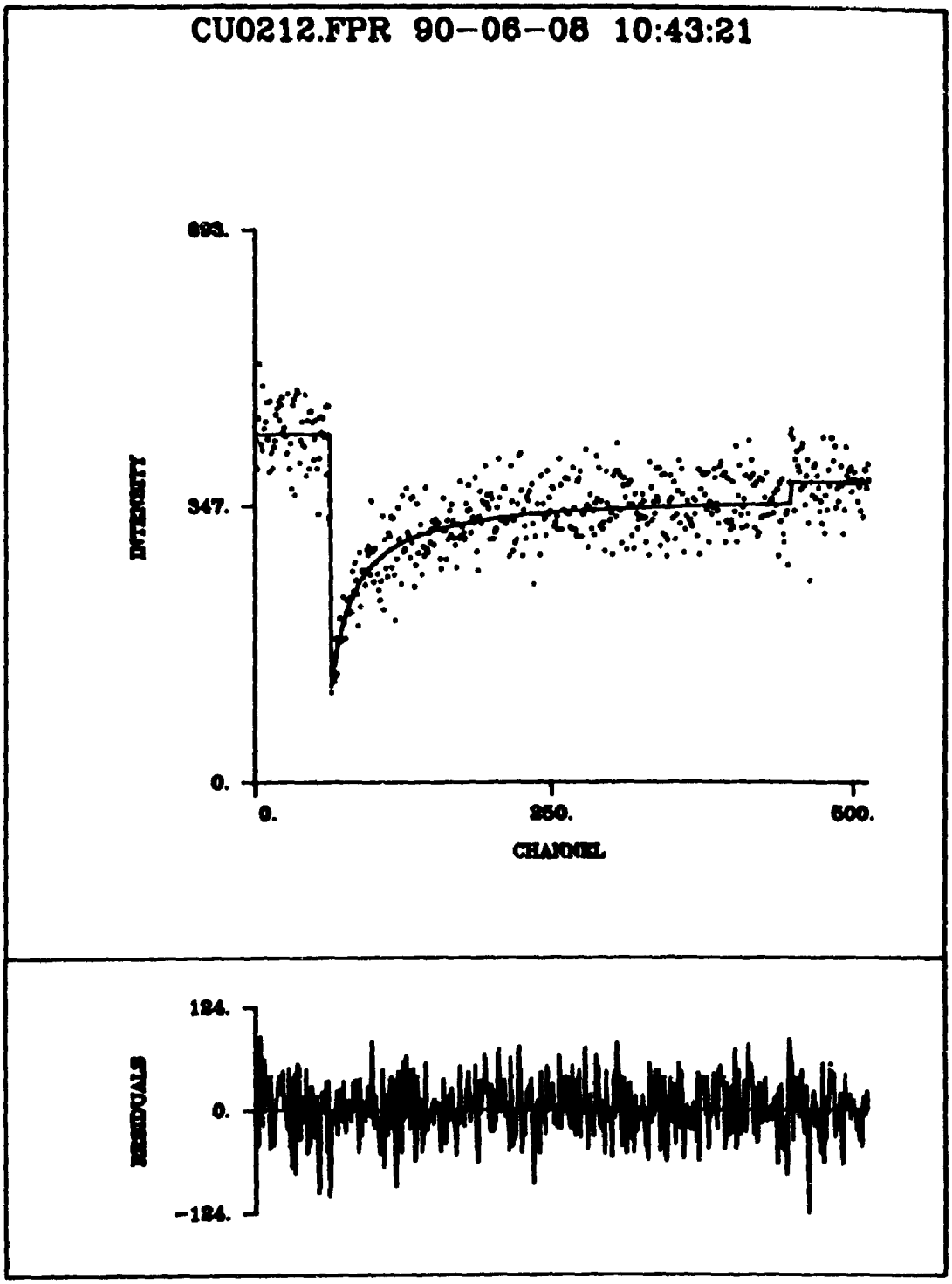
CU0212.FPR 90-06-08 10:43:21
693.
347.
0.
INTENSITY
0.
250.
500.
CHANNEL
124.
0.
-124.
RESIDUALS

Table 3.5: Measured Diffusion Parameters for Naphthacene on Chemically Derivatized Silica Gels.

Surface[a]	Method[b]	D / 10^{-10} $cm^2 s^{-1}$	Xm	N[c]	N'[d]
C8	soln.	5.03 ± 1.61	0.24 ± 0.06	13	1
C18	sub.	6.65 ± 0.41	0.50 ± 0.01	214	6
C18	soln.	6.62 ± 0.50	0.62 ± 0.01	121	3
C18	undec.	25.3 ± 1.8	0.87 ± 0.01	117	4
Silica	ma.	26.5 ± 6.1	0.75 ± 0.05	15	1

[a] Type of silica surface used. C8 is silica derivatized with an eight carbon chain agent; C18 with an eighteen carbon chain agent.

[b] Preparation: soln.: adsorption of naphthacene from solution.
sub.: adsorption of naphthacene via sublimation.
undec.: undecaonl coadsorbed on C18 silica.
ma.: myristic acid physisorbed on dry silica.

[c] N is the number of FPR experiments used in the averages of D and Xm.

[d] N' is the number of samples prepared in the accumulation of the FPR data.

[e] All errors reported as standard error of the mean at a 97.5% confidence level.

naphthacene is mobile and that in which it is not. Chemisorption of alkyl chains or physisorption of long chain alcohols provides for at least one more microenvironment. For simplicity, the derivatized silica surface is modeled to have only three environments. They are, normal phase silica where there are two naphthacene populations, a mobile one (1) and an immobile one (2), and completely alkyl coated silica, where naphthacene is assumed to be completely mobile (3). Changing the relative proportions of these three environments has a direct effect on the measured diffusion parameters.

All measured values for the diffusion coefficient of naphthacene on purely chemisorbed derivatized silica (C8 and C18) in Table 3.5 are at least twice the diffusion coefficient of naphthacene on dry normal phase silica (Table 3.1). A further increase in the diffusion coefficient is seen when long alkyl chain species are physisorbed the surface. The diffusion coefficient of naphthacene on these surfaces are an order of magnitude larger than the diffusion coefficient of naphthacene on dry silica gel. For C18 derivatized silica, the minimum mobile fraction (0.50) is roughly that of the maximum value obtained on dry silica (0.53). With physisorption of other alkyl species, the average value of the mobile fraction increases further to 0.87. The significant increases in both D and Xm show that the mobility of naphthacene in an environment very different from normal phase silica is contributing to the recovery of the fluorescence intensity in the FPR experiment. This must be the hydrocarbon environment provided by derivatization of the surface with the various alkyl chains. Chemisorption of alkyl chains will decrease

both the surface area which appears to be normal phase and the amount of naphthacene adsorbed on normal phase silica. The fraction of molecules adsorbed in the immobile environment on normal phase silica must also decrease, leading to an increase in the mobile fraction. Further derivatization of the surface by physisorption of undecanol yields a further increase in both the diffusion coefficient and mobile fraction. These changes are explained in more detail in terms of the microenvironments present.

The measured diffusion coefficient is a weighted average of all diffusion coefficients for each microenvironment present that undergo fast exchange on the time scale of the experiment (Equation 3.1):[58]

$$D = \sum_i f_i D_i \qquad (3.1)$$

Any microenvironment in which naphthacene is immobile does not belong in this category. Not only will the diffusion coefficient in these regions be much smaller than in the mobile regions, but naphthacene in these microenvironments would recover independently and should be seen as a distinct population. This would be manifest as a slow component relative to the recovery of the other components in the recovery profile. Microenvironment 1 is considered to be normal phase silica regions in which naphthacene is mobile (with fraction of molecules f_1 and diffusion coefficient D_1), and microenvironment 2 is completely alkylated silica (with fraction of molecules f_2 and diffusion coefficient D_2). An estimate of the value of f_1 (or f_2) is derived from the values of the mobile fraction for each region. Based on the measured diffusion coefficients for naphthacene on C18 silica and normal phase silica, an upper limit for the diffusion coefficient of

naphthacene in a completely derivatized environment (D_2) is calculated. The upper limit for D_2 is 3.1×10^{-9} cm^2 s^{-1}. The lower limit for D_2 is given by the measured value for naphthacene on either C18-undecanol or myristic acid derivatized silica (2.6×10^{-9} cm^2 s^{-1}). Further analysis using the upper limit of D_2 allows for an estimate of the fraction of naphthacene molecules in the alkyl phase (f_2) when adsorbed to C18 silica. This value is calculated to be 14%, indicating that the coating is incomplete.

The silylation reaction with model compounds in solution has been examined by Newman and Feher[59]. They have found the reaction was only 1% complete after 15 minutes when using similar conditions used for the derivatization of silica gel. The reaction does not go to completion for either model compounds in solution or silica gel. Experimental evidence for an incomplete coating is seen in the differences in the values of D for naphthacene on C18 versus C18-undecanol silica.

As a first approximation, the reaction is 14% complete for the silica surface after 15 minutes. The reaction may be more efficient on the surface than in solution. A sample of silica is derivatized under the same conditions, with a reaction time of 24 hours. Diffusion measurements performed on this surface gave the same results for D and Xm as those of naphthacene adsorbed on silica derivatized for 15 minutes. The reaction apparently proceeds quickly at the start, but is then retarded, perhaps due to steric hindrance on the surface.

Further derivatization of the C18 surface is achieved by

coadsorption of undecanol. Adsorption of undecanol does not depend on the availability or initial distribution of specific binding sites. On a C18 surface, undecanol could bind in regions of high C18 density, making these regions more fluid, or bind in regions of low C18 density making the overall alkyl coating distribution more homogeneous. These two ideas are expressed schematically in Figure 3.13. If undecanol preferentially binds to regions of high C18 density (Figure 3.13b), then the total area of normal phase silica will remain constant. In this scenario, an increase in D_2 is expected due to the increased fluidity, while f_2 remains constant. This assumes no changes in partitioning between normal and reverse phase silica regions with adsorption of undecanol. The net effect will be to increase D while Xm remains constant. If undecanol binds to regions of low C18 density a more homogeneous coating is expected (Figure 3.13c). This will increase f_2 while D_2 remains constant, leading to an increase in both Xm and D. Experimentally, increases in the average values of both Xm and D are observed, indicating that physisorption of undecanol leads to a more homogeneous coating than just chemisorption of C18 chains.

Binding of myristic acid on normal phase silica through physisorption leads to a homogeneous coating. The same value of D (2.6×10^{-9} cm^2 s^{-1}) and a similar value of Xm (0.75) wad obtained for normal phase silica coated with myristic acid as on C18 silica with undecanol coadsorbed. The myristic acid coating is more dense than chemisorbed C18 chains, leading to a more fluid surface, and a larger value of D.

The increase in D for naphthacene on C18 coated silica relative

Figure 3.13: Schematic representation of C18 silica gel (A), and the possible effects of undecanol coadsorption. The shaded region represent areas of low hydrocarbon density, the regions filled with lines represent areas of higher density, and therefore more fluid. Coadsorption of undecanol can either make the regions with C18 chains chemisorbed more fluid (B) or further derivatize the surface (C), making the coating more homogeneous.

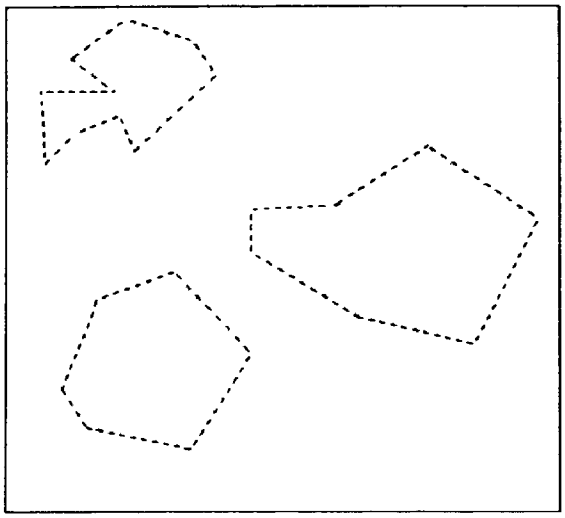

a)

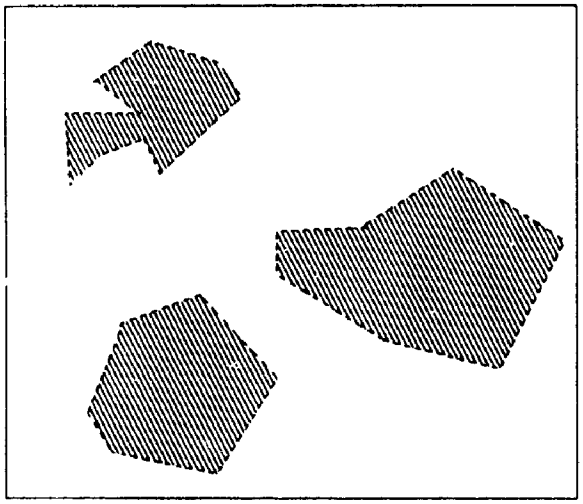

b)

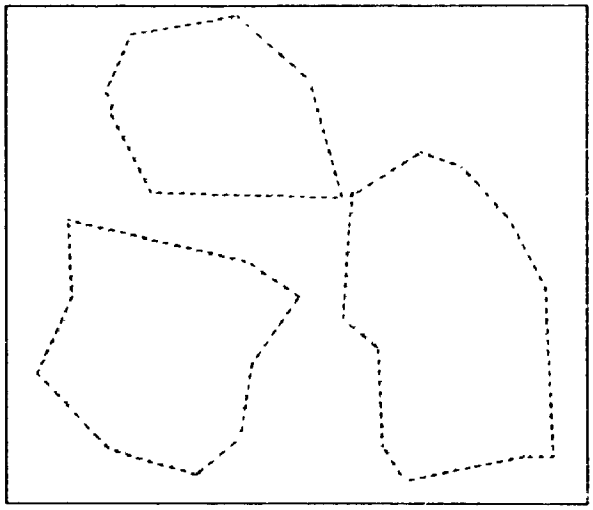

c)

to that on normal phase silica is explained by the mechanism of binding. On normal phase silica, the binding is achieved by few relatively strong interactions between silanol groups and the π electrons of the naphthacene molecule. On alkyl coated silica the individual binding interactions are weaker but larger in number.

Further increases in D with physisorption of undecanol on C18 silica are explained in terms of the microviscosity of the system (Equation 3.2):

$$D = \frac{kT}{f} \qquad (3.2)$$

k is Boltzmann's constant, T is the absolute temperature, and f is the frictional coefficient which is a function of the viscosity of the system. The addition of undecanol provides for a more uniform and less viscous coating, leading to an increase in D. The alkyl coatings are not complete, as shown by the further increase of D with adsorption of undecanol on C18 silica. The similarity of the diffusion coefficients on C8 (5.0×10^{-10} cm^2 s^{-1}) and C18 (6.6×10^{-10} cm^2 s^{-1}) silica gels and the large differences in the mobile fractions (0.25 and 0.50) indicate that for completely coated C8 surface, the diffusion coefficient should be greater than that calculated for a completely coated C18 surface. This is in accordance with the fact that shorter chain alcohols are less viscous liquids than longer chain alcohols.

In each system investigated a single value of D or Xm is not obtained. In fact, a broad distribution of values is recovered in all cases (Figure 3.14). This indicates that the probes are experiencing many microenvironments, implying that chemisorption of these reagents

Figure 3.14a: Frequency of occurrence of diffusion coefficients (top) and mobile fractions (bottom) within intervals representing 5% (D) or 10% (Xm) of their range. These histograms show distributions of D and Xm for naphthacene on C18 silica gel. Adsorption of naphthacene via sublimation (open bars) and adsorption of naphthacene from cyclohexane solution (diagonal bars).

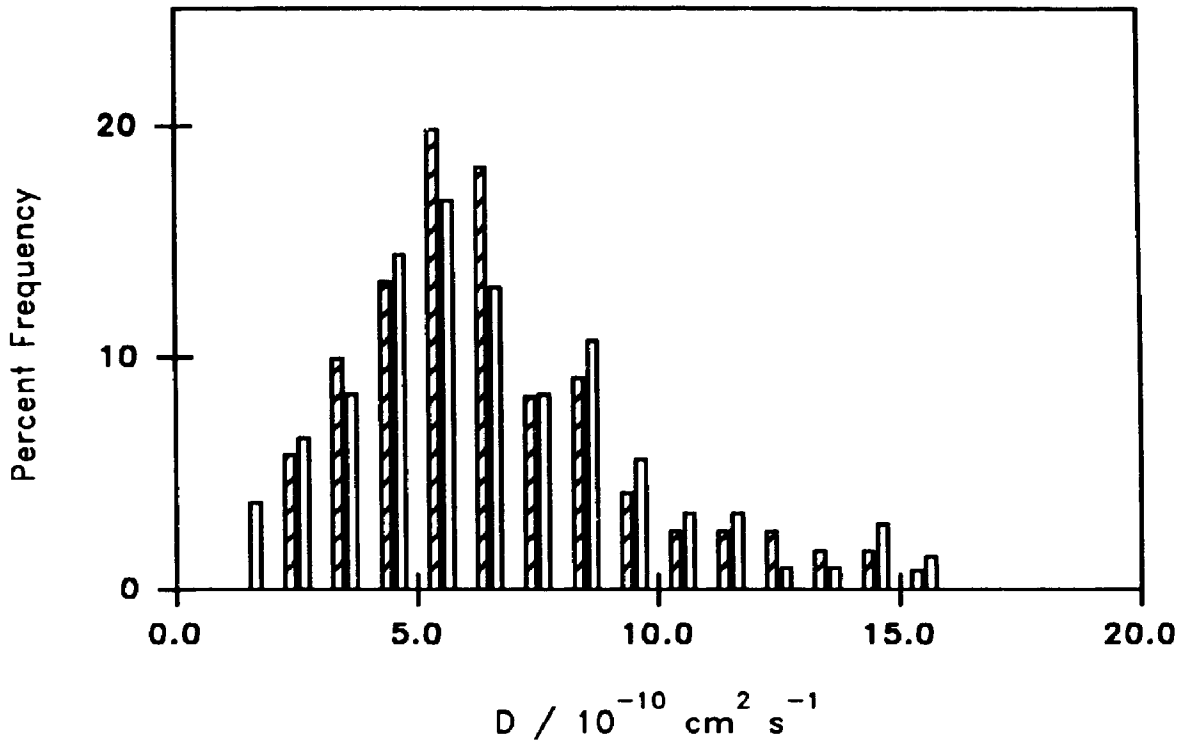
Percent Frequency
20
10
0
0.0
5.0
10.0
15.0
20.0
D / 10^-10 cm^2 s^-1

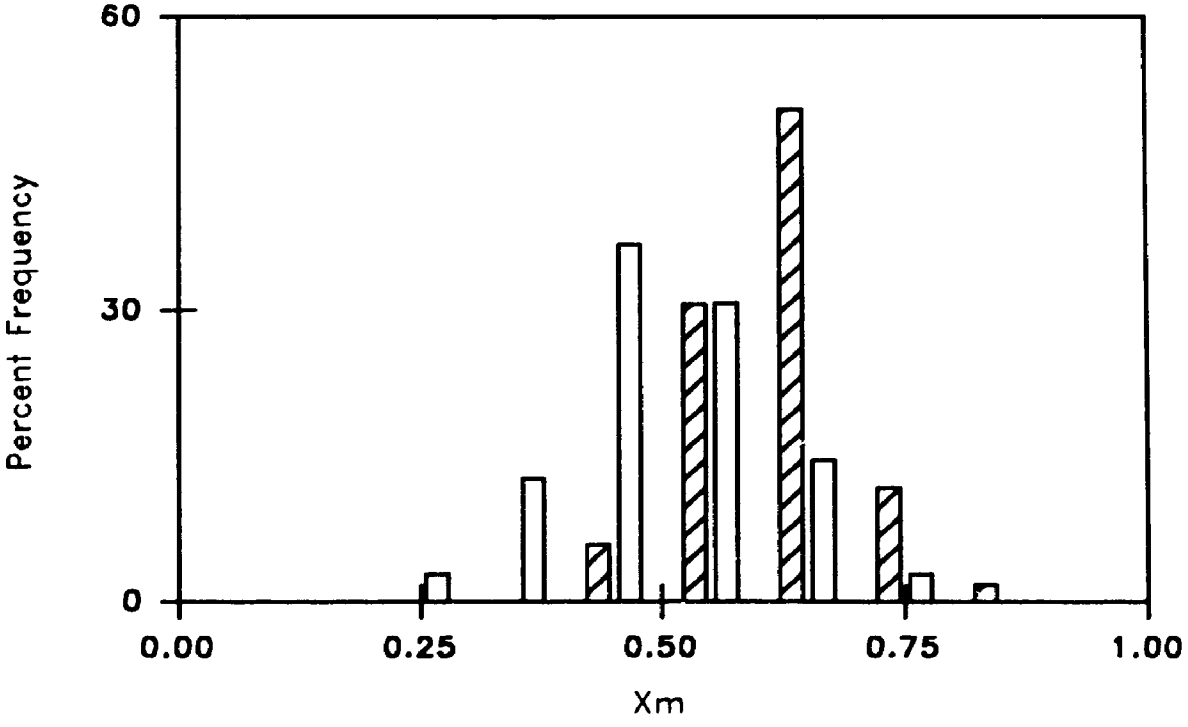
Percent Frequency
60
30
0
0.00
0.25
0.50
0.75
1.00
Xm

Figure 3.14b: Frequency of occurrence of diffusion coefficients (top) and mobile fractions (bottom) within intervals representing 10% of their range. These histograms show distributions of D and Xm for naphthacene on C18 silica further derivatized by coadsorption of undecanol. Adsorption of naphthacene from cyclohexane solution.

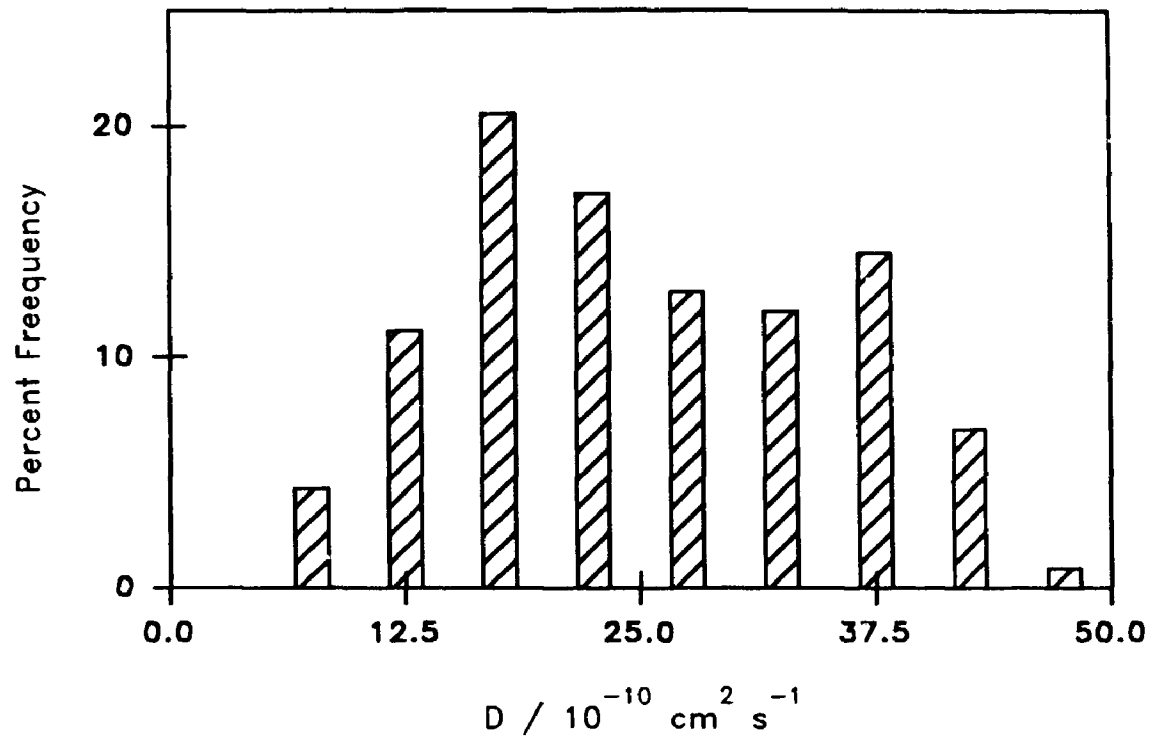
Percent Freequency
20
10
0
0.0
12.5
25.0
37.5
50.0
D / 10 -10 cm 2 s -1

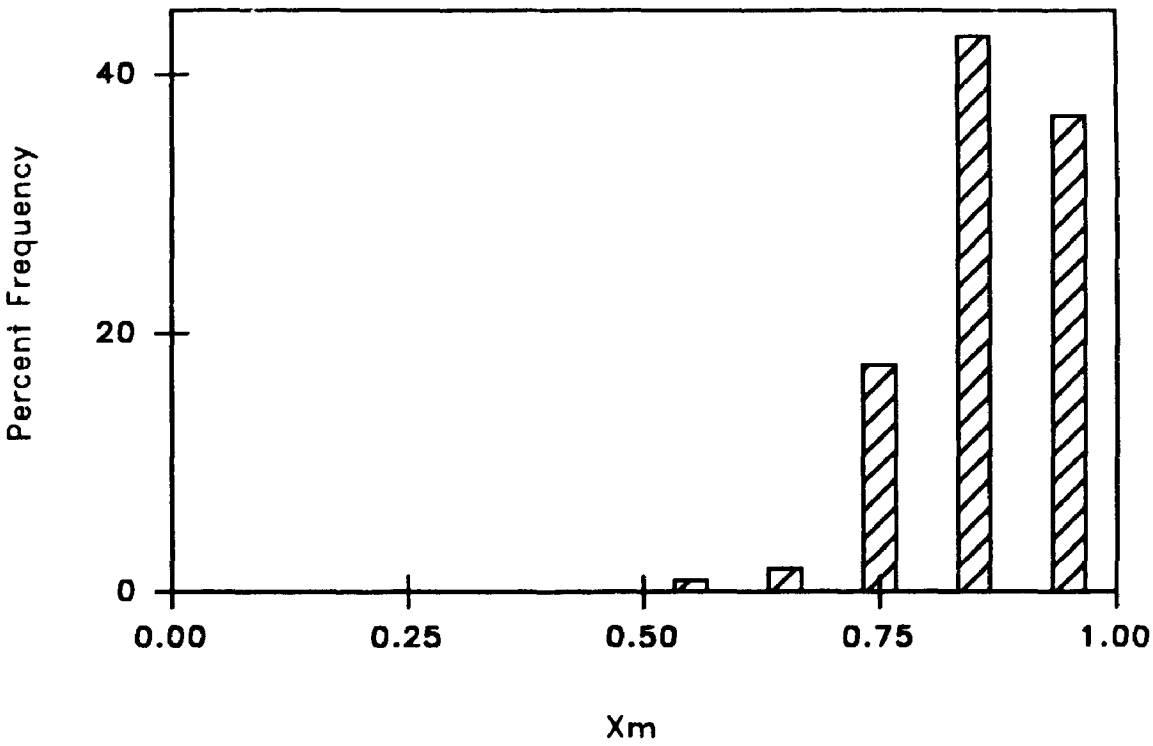
Percent Frequency
40
20
0
0.00
0.25
0.50
0.75
1.00
Xm

is heterogeneous, as suggested by Lochmüller[45]. Even with coadsorption of undecanol, a broad distribution is seen. The surface still does not mimic a homogeneous medium.

The widths of these distributions are real, and not an artifact of the technique employed. Diffusion measurements of both naphthacene and rubrene in isotropic (poly(propylene glycol) at 25°C, and anisotropic DMPC vesicles at 29°C), yet homogeneous media yield, reproducibly, a narrow range for D and Xm[60]. The values of D are, of course, quite different for each system, while Xm tends to unity in most cases. Due to inherent uncertainties in the data, distributions of diffusion coefficients and mobile fractions are expected. For simulated data with a high level of noise (10% Gaussian noise), τ_D (and therefore D) can be determined with a precision of 21%, and Xm to a precision of 7%[36]. These should represent upper limits to the standard deviations for the diffusion parameters. Typically, the standard deviation obtained for D are 40 to 45%, and 10 to 30% for Xm. These standard deviations are larger than the standard deviations obtained for individual measurements. The widths of the distributions are due to something more than just random noise alone, and is attributed to heterogeneities in both the surface structure and probe concentration.

The heterogeneity is not only on the molecular scale as shown by inhomogeneous probe distributions, but also on the micrometer (beam width) scale. In all samples, at least a small amount of microcrystalline naphthacene was visible in the microscope. The extent of crystal formation was lowest for the highly derivatized

silica gels.

The microenvironments experienced by naphthacene are present in domains smaller than the beam width. This allows for sampling of many environments simultaneously, and leads to continuous distributions of D and Xm. If the domains were larger tha. the beam width, only one environment would be probed by the beam at one time. For the case considered earlier with only two microenvironments (normal phase silica and completely coated alkyl silica) two discrete distributions for D would be expected. One distribution would have a mean value of 2.4×10^{-10} cm^2 s^{-1}, the average diffusion coefficient for naphthacene on normal phase silica. The other distribution would have a mean near 3.1×10^{-9} cm^2 s^{-1}, the calculated value for naphthacene diffusing in a completely hydrocarbon coated layer. Two discrete distributions of Xm would also be recovered. In all cases, continuous distributions in both D and Xm are recovered, indicating that the microenvironment domains are present in regions smaller than a micrometer. This can be viewed diagrammatically with Figure 3.13, where the enclosed regions represent areas smaller than the beam size.

Changes in Xm are observed on changing the method of preparation. Adsorption from solution onto C18 silica yields a much larger Xm than for a sample prepared by sublimation. This is seen even though D remains constant. The deposition process is very different in the two cases. By allowing the surface to come into contact with a wetting solvent, the hydrocarbon chains can become untangled, and more ordered[45]. As the solvent is removed, the chains will eventually settle back to the surface. As the chains settle, more of the probe

molecules are trapped in the hydrocarbon layer than if the probe were deposited by sublimation. Molecules in the hydrocarbon layer are mobile, and hence an increase in Xm is observed. As well, the formation of immobile microcrystals is more prevalent when adsorption via sublimation is employed.

Some measurements with rubrene as the probe have been performed using C18 with undecanol silica and C18 silica. Frequently, the fit to the recovery for rubrene on C18 silica was of poor quality. As well, the extent of recovery was typically low. Qualitatively, the mobility of rubrene on C18 silica is much lower than the mobility of naphthacene, and the mobile fraction for rubrene on C18 silica is estimated to be 0.2. On C18 silica with coadsorbed undecanol rubrene is far more mobile. From two samples, the diffusion coefficient is calculated to be $(4.9\pm0.6)\times10^{-10}$ cm^2 s^{-1}, and the mobile fraction is (0.61 ± 0.09). The rate of mobility is lower than that of naphthacene on a similar surface. This is an obvious effect of the four phenyl appendages which rubrene possesses over naphthacene. Rubrene is not planar, as naphthacene is, and also has a greater surface area (or molecular volume). These factors increase the frictional coefficient, and decrease the diffusion coefficient. A mobile fraction of 0.61 is explained by the combined effects of microcrystalline rubrene on the surface and a heterogeneous coating.

3.2.4 Conclusions

Naphthacene is mobile on reverse phase chromatography supports, even in the absence of a solvent. This process has been previously discounted for pyrene on derivatized silica in the absence of a solvent[51]. The mobility is greater than the mobility of naphthacene on normal phase silica by up to an order of magnitude.

Variations are observed in the diffusion parameters with the extent of derivatization and method of adsorption. As the degree of derivatization increases, both the diffusion coefficient and the mobile fraction increase. This is due to the surface coating being more homogeneous and also more fluid.

Independent of deposition method, the same value for the diffusion coefficient is recovered for naphthacene on C18 silica. However, a larger value for the mobile fraction is observed for naphthacene adsorbed from solution. A more homogeneous distribution of naphthacene is also observed for this method. With fewer microcrystals present, the mobile fraction is expected to be larger.

The largest values of D and Xm are observed for naphthacene adsorbed on a surface with at least a physisorbed derivatizing agent. This is a result of the greater homogeneity of the alkyl coating. Physisorption of long chain alcohols or fatty acids does not depend on the initial distribution or the availability of specific binding sites. This allows for the most homogeneously coated surface, and the largest values of D and Xm. However, this is not to say that the coating produces a homogeneous surface. If this were so, one may

expect the distributions obtained to be as narrow as those obtained for PAHs in homogeneous media. Since broad distributions are obtained for the diffusion parameters, even for these highly derivatized surfaces, the surface is still heterogeneous. Numerous microenvironments are experienced by naphthacene on these surfaces also. The larger values of D and Xm reflect a decrease in the microviscosity and a more homogeneous coating of the surface relative to all other surfaces.

With shorter hydrocarbon chains (C1 and C8), a very heterogeneous distribution of naphthacene is achieved. The shorter chains do not allow for many attractive forces between the chains and naphthacene. Some results for a C8 sample reveal a diffusion coefficient for naphthacene comparable to that on C18 silica, but a much smaller mobile fraction. The mobile fraction is small due to the large number of immobile microcrystals present. This mobile fraction is smaller than that for naphthacene on normal phase silica.

Significant mobility of rubrene is found on highly derivatized silica gels. Meaningful measurements have been collected for rubrene on C18 silica with coadsorbed undecanol. The diffusion coefficient is found to be 5 times smaller than the diffusion coefficient for naphthacene on the same surface. The mobile fraction for rubrene is also somewhat smaller than the mobile fraction of naphthacene. The lower mobility parameters are a result of the more complex geometric structure of rubrene.

Future studies in this area should include the investigation of diffusion of PAHs on derivatized silica, with the derivatization

carried out under more controlled conditions. Quantitative analysis of the alkyl coated surface coverage is desirable and required. At present it is not clear how this can be achieved, but certain FTIR techniques appear to be very promising[61-65].

Further derivatization of C1 and C8 silica could also be investigated. Coadsorption of smaller alcohols, 1-octanol on C8 and methanol on C1, may change the surface enough to allow for more homogeneous distributions of PAHs.

The mobility of other PAHs should also be investigated. Smaller (naphthalene, anthracene), larger (pentacene) and PAHs of similar size (pyrene, perylene) could be employed as the fluorescent probe.

REFERENCES

(1) Ron, A.; Folman, J.; Schnepp, O. *J. Phys. Chem.* **1962**, *36*, 2449.

(2) Fiat, D.; Reuben, J.; Folman, M. *J. Phys. Chem.* **1967**, *46*, 4453.

(3) Evreinov, V. I.; Golubev, V. B.; Lunina, E. V. *Russ. J. Phys. Chem.* **1975**, *49*, 564.

(4) Selivanovshii, A. K. *Russ. J. Phys. Chem.* **1976**, *50*, 990.

(5) Francis, C.; Lin, J.; Singer, L. A. *Chem. Phys. Lett.* **1983**, *94*, 162.

(6) Turro, N. J.; Zimmt, M. B.; Gould, I. R. *J. Amer. Chem. Soc.* **1985**, *107*, 5826.

(7) Bauer, R. K.; Borenstein, R.; de Mayo, P.; Okada, K.; Rafalska, M.; *Ware, W. R.;* Wu, K. C. *J. Amer. Chem. Soc.* **1982**, *104*, 4635.

(8) de Mayo, P.; Natarajan, L. V.; Ware, W. R. *Chem. Phys. Lett.* **1984**, *107*, 187.

(9) de Mayo, P.; Natarajan, L. V.; Ware, W. R. *J. Phys. Chem.* **1985**, *89*, 3526.

(10) de Mayo, P.; Natarajan, L. V.; Ware, W. R. In *Organic Phototransformations in Nonhomogeneous Media;* Fox, M. A., Ed.; American Chemical Society: Washington, DC, 1985; Chapter 1.

(11) Bauer, R. K.; de Mayo, P.; Ware, W. R.; Wu, K. C. *J. Phys.Chem.* **1982**, *86*, 3781.

(12) Bauer, R. K.; de Mayo, P.; Okada, K.; Ware, W. R.; Wu, K. C. *J. Phys. Chem.* **1983**, *87*, 460.

(13) de Mayo, P.; Okada, K.; Rafalska, M.; Weedon, A. C.; Wong, G. S. K. *J. Chem. Soc. Chem Commun.* **1981**, 821.

(14) Bauer, R. K.; de Mayo, P.; Natarajan, L. V.; Ware, W. R. *Can. J. Chem.* **1984**, *62*, 1279.

(15) Turro, N. J.; Cheng, C-C. *J. Amer. Chem. Soc.* **1984**, *106*, 5022.

(16) Beck, G.; Thomas, J. K. *Chem. Phys. Lett.* **1983**, *94*, 553.

(17) Fujii, T.; Shimizu, E. *Chem. Phys. Lett.* **1987**, *137*, 448.

(18) Fujii, T.; Shimizu, E.; Suzuki, S. *J. Chem. Soc. Faraday Trans. I* **1988**, *84*, 4387.

(19) Anpo, M.; Nishiguchi, H.; Fujii, T. *Res. Chem. Inter.* **1990**, *13*, 73.

(20) Oelkrug, D.; Flemming, W.; Füllemann, R.; Günther, R.; Honnen, W.; Krabichler, G.; Schäfer, M.; Uhl, S. *Pure and Appl. Chem.* **1986**, *58*, 1207.

(21) Oelkrug, D.; Krabichler, G.; Honnen, W.; Wilkinson, F.; Willsher, C. J. *J. Phys. Chem.* **1988**, *92*, 3589.

(22) Hara, K.; de Mayo, P.; Ware, W. R.; Weedon, A. C.; Wong, G. S. K.; Wu, K. C. *Chem. Phys. Lett.* **1980**, *69*, 105.

(23) Lochmüller, C. H.; Wenzel, T. J. *J. Phys. Chem.* **1990**, *94*, 4230.

(24) Oelkrug, D.; Uhl, S.; Wilkinson, F.; Willscher, C. J. *J. Phys. Chem.* **1989**, *93*, 4551.

(25) Pohle, W. *J. Chem. Soc. Faraday Trans. I* **1982**, *78*, 2101.

(26) Anderson, J. H.; Lombardi, J.; Hair, M. L. *J. Colloid Interface Sci.* **1975**, *50*, 519.

(27) Vinogradov, S. N.; Linnell, R. H. In *Hydrogen Bonding;* Van Nostrand Reinhold: New York, 1971; pp 11-12.

(28) Kiselev A. V.; Lygin, V. I. In *Infrared Spectra of Surface Compounds;* Wiley: New York; 1975, p 80.

(29) Bolis, V.; Fubini, B.; Coluccia, S.; Mostacci, E. *J. Thermal Anal.* **1985**, *30*, 1283.

(30) Naono, H.; Fujiwara, R.; Yagi, M. *J. Colloid Interface Sci.* **1980**, *76*, 74.

(31) Kondo, S.; Tomoi, K.; Pak, C. *Bull. Chem. Soc. Japan* **1979**, *52*, 2046.

(32) *UV Atlas of Organic Compounds,* Copyright Verlag Chemie Weinheim; Buttersworth: London, 1966, Vol. 3, p E4/2.

(33) Robertson, J. M.; Sinclair, V. C.; Trotter, J. *Acta Cryst.* **1962**, *15*, 289.

(34) Eltekov, Yu. A.; Khopina, V. V.; Kiselev A. V. *J. Chem. Soc. Faraday Trans. I* **1972**, *68*, 889.

(35) Galkin, G. A.; Kiselev, A. V.; Lygin, V. I. *Russ. J. Phys. Chem.* **1968**, *42*, 765.

(36) Petersen, N. O.; Felder, S.; Elson, E. L. In *Handbook of Experimental Immunology;* Weir, D. M., Ed.; Blackwell Scientific Publications: Oxford, 1986; Vol. 3, Chapter 24.

(37) Bjarneson, D. W.; Petersen, N. O. *J. Amer. Chem. Soc.* **1990**, *112*, 988.

(38) Peri, J. B.; Hensley, A. L. *J. Phys. Chem.* **1968**, *72*, 2926.

(39) Alchemy II, TRIPOS Associates, St. Louis, Mo.

(40) Saito, I.; Matsuura, T. In *Singlet Oxygen;* Wasserman, H. H. and Murray, R. W., Eds.; Academic Press: London, 1979, Chapter 10.

(41) Kirkland, J. J. *J. Chromatogr. Sci.* **1971**, *9*, 207.

(42) Lochmüller, C. H.; Wilder, D. R. *J. Chromatogr. Sci.* **1979**, *17*, 574.

(43) Wise, S. A.; Bonnett, W. J.; Guenther, F. R.; May, W. E. *J. Chr. Sci.* **1981**, *19*, 457.

(44) Colin, H.; Guiochin G. *J. Chromatogr. Sci.* **1978**, *158*, 183.

(45) Lochmüller, C. H.; Colborn, A. S.; Hunnicutt, M. L.; Harris, J. M. *Anal. Chem.* **1983**, *55*, 1344.

(46) Genieser, H-G.; Gabel, D.; Jastorff, B. *J. Chromatogr. Sci.* **1982**, *244*, 368.

(47) Carley, A. F.; Moroney, L.; Roberts, M. W. *Faraday Symp. Chem. Soc.* **1981**, *15*, 39.

(48) Simko, S. J.; Miller, M. L.; Linton, R. W. *Anal. Chem.* **1985**, *57*, 2448.

(49) Davies, J. A.; Sood, A. *Makromol. Chem.* **1985**, *186*, 1631.

(50) Sander, L. C.; Callis, J. B.; Field, C. R. *Anal. Chem.* **1983**, *55*, 1068.

(51) Bogar, R. G.; Thomas, J. C.; Callis, J. B. *Anal. Chem.* **1984**, *56*, 1080.

(52) Ståhlberg, J.; Almgren, M.; Alsins, J. *Anal. Chem.* **1988**, *60*, 2487.

(53) Lisichkin, G. V.; Runov, V. K.; Staroverov, S. M.; Fadeev, A. Yu. *Dokl. Akad. Nauk SSR. (Engl. Trans.)* **1988**, *299*, 313.

(54) Avnir, D.; Busse, R.; Ottolenghi, M.; Wellner, E. *J. Phys. Chem.* **1985**, *89*, 3521.

(55) Sagiv, J. *J. Amer. Chem. Soc.* **1980**, *102*, 92.

(56) von Tscharner, V.; McConnell, H. M. *Biophys. J.* **1981**, *36*, 421.

(57) Arkles, B. In *Silicon Compounds, Register and Review*; Petrarch Systems: Bristol, Pa. 1987, pp 54-55.

(58) Elson, E. L.; Reidler, J. A. *J. Supramol. Struct.* **1979**, *12*, 481.

(59) Newman, F. J.; Feher, D. A. *J. Amer. Chem. Soc.* **1990**, *112*, 1931.

(60) Balcom, B. J. Ph. D. Dissertation, The University of Western Ontario, 1990.

(61) Bush, S. G.; Jorgenson, J. W.; Miller, M. L.; Linton, R. W. *J. Chromatogr.* **1983**, *260*, 1.

(62) Bush, S. G.; Jorgenson, J. W. *J. Chromatogr.* **1990**, *503*, 69.

(63) Kratochvíla, J.; Salajka, Z.; Kazda, A.; Kadlc, Z.; Souček, J.; Gheorghiu, M. *J. Non-Cryst. Solids* **1990**, *116*, 93.

(64) Gorski, D.; Klemm, E.; Fink, P.; Hörhold, H.-H. *J. Colloid. Interface Sci* **1988**, *126*, 445.

(65) Van Der Voort, P.; Gillis-D'Hamers, I.; Vansant, F *J. Chem. Soc. Faraday Trans.* **1990**, *86*, 3751.

CHAPTER FOUR

PHOTOCHEMISTRY AND PHOTOPHYSICS

4.1 Photochemistry and Photophysics of Naphthacene in Solution

4.1.1 Introduction

Irradiation of many polycyclic aromatic hydrocarbons (PAHs) in degassed solutions yield dimers of the parent PAH. Unsubstituted and some substituted PAHs form dimers readily[1-7], whereas highly substituted PAHs do not. Birks and co-workers have investigated the dimerization of many PAHs[4,5], and have found anthracene, naphthacene and pentacene dimerize upon irradiation in degassed solutions. Evidence for dimer formation is presented in the form of decreasing absorbance of the parent aromatic hydrocarbon, and the increase of a new absorbance band attributed to the dimer[4]. Other groups have investigated the dimerization process in more detail. Wei and Livingston have found the dimerization process is reversible. Irradiation of dimers in solution with ultraviolet radiation yields the parent aromatic hydrocarbon[3]. Spectroscopic characterizations of some PAH dimers are presented by Bouas-Laurent and colleagues[1,2]. They provide spectral information on the two dimers of naphthacene, and a crossed naphthacene-anthracene dimer. The two naphthacene dimers (Figure 4.1) have slightly different physical properties, as revealed by absorption spectroscopy, melting points and solubility[1].

In oxygenated solutions, the photoproduct formed is an

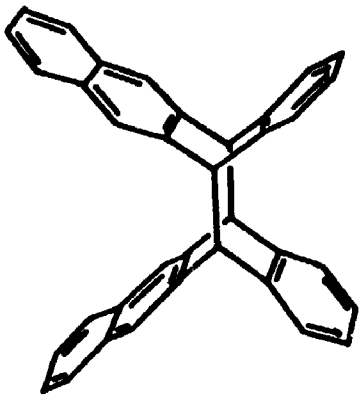

a

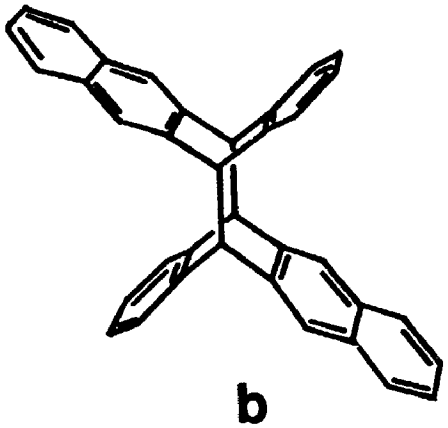

b

endoperoxide of the PAH[8-17]. The structure of the endoperoxide of naphthacene is shown in Figure 4.2. Photoperoxidation involves a Diels-Alder reaction between excited singlet oxygen ($^1\Delta_g$) and ground state PAH[8]. Generation of singlet oxygen is through triplet-triplet annihilation of ground state oxygen ($^3\Sigma_g^-$) and the first excited triplet state of the PAH[10-13]. For singlet oxygen sensitization to occur, the triplet state of the PAH must be at least 7880 cm^{-1} above the ground state[18]. This value corresponds to the energy of singlet oxygen above that of ground state oxygen.

Stevens and Algar have studied the photoperoxidation of many PAHs in solution, among them naphthacene[11-13]. These investigations focused more on physical aspects, such as quantum yields, fluorescence lifetimes and quenching parameters. They report the quantum yield of triplet state naphthacene to be 0.63 in benzene at 25^0C[13]. This high quantum yield, and the energy of the triplet state (10 250 cm^{-1})[12] indicate that naphthacene should be an efficient singlet oxygen sensitizer.

The endoperoxides of naphthacene and other PAHs have been prepared and used in thermal and photochemical decomposition studies[8,14-17]. A variety of products are obtained from the decomposition of the peroxide, which are analyzed spectroscopically. Interestingly, very little spectroscopic data for naphthacene endoperoxide appears in the literature. Spectroscopic data (NMR, UV-VIS, MS) for the endoperoxide of naphthacene and the dimers of naphthacene are presented in this thesis.

Investigations into the photophysical properties of numerous PAHs

Figure 4.2: Structure of naphthacene endoperoxide.

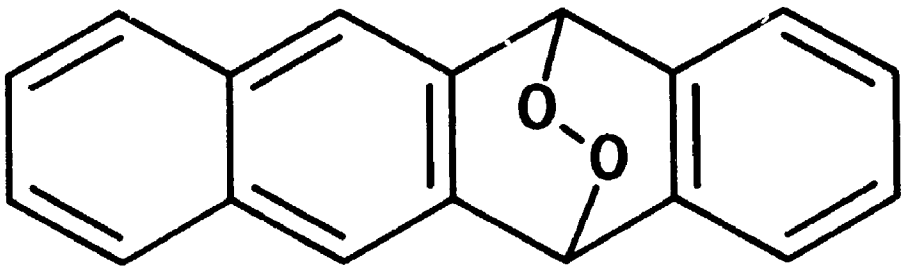
O
O

have been performed[19-21]. In dilute solution, PAHs decay following a single exponential decay law. When adsorbed on surfaces, the photophysical characteristics change drastically[22-39]. Typically, the decay does not follow a single exponential, but is characterized by the sum of many exponential functions. The fluorescence lifetime of naphthacene in various solvents is measured in order to set a basis for interpretation of photophysical data for naphthacene adsorbed on silica.

An understanding of the photochemistry of naphthacene is required for thorough analysis and interpretation of the diffusion results. To gain this understanding, the photochemistry of naphthacene both in solution and adsorbed on silica is investigated. The kinetics of photobleaching and fluorescence lifetimes of naphthacene in solution are discussed in this section.

4.1.2 Experimental

Solutions used in kinetic studies were prepared in spectroscopic grade solvents from BDH unless otherwise specified. The photochemical destruction of naphthacene in cyclohexane, isopropanol and $CDCl_3$ (MSD Isotopes) was followed by UV-VIS spectroscopy. A Shimadzu UV-VIS 160 spectrometer was used to measure all absorption spectra. Initial concentrations of naphthacene were in the 10 to 50 μM range.

Irradiation of solutions was achieved by use of an Argon ion laser set to the 476.5 nm line, with exit powers of 25 or 50 mW. All solutions were stirred and wrapped in foil during irradiation.

Approximately 50 ml of solution was used, with aliquots taken periodically. Absorption spectra for each solution in quartz cuvettes was recorded after referencing the spectrometer with the appropriate solvent. Particular attention was given to the visible region of the spectrum, which has absorption bands of naphthacene only. All three photoproducts (two dimers and one peroxide) absorb in the ultraviolet region only, with maximum absorbance at 237 nm in cyclohexane and 238 nm in $CDCl_3$.

Solutions were degassed by stirring vigorously while under vacuum followed by bubbling with nitrogen for 30 minutes. Increased oxygen concentrations were achieved by bubbling the solution with air for 30 minutes. To some solutions, DABCO (1,4 diazabicyclo(2.2.2)octane), a singlet oxygen quencher[40], was added at concentrations of 0.1 M. The concentration of DABCO in cyclohexane will be much less than 0.1 M due to DABCO being only slightly soluble. All solutions prepared in $CDCl_3$ were degassed by the above procedure and sealed in a cuvette with a septum. These solutions were submitted for NMR analysis after irradiation.

High Performance Liquid Chromatography (HPLC) was also attempted in order to follow the kinetics. The HPLC component system included two Waters 510 pumps controlled by a Waters automated gradient controller. A Gilson 231 programmable sample injector and dilutor were interfaced with the Waters system. A Waters 490 multiwavelength detector was employed to drive a Goerz SE 120 analog chart recorder (two channels) and a Waters 740 Integrator (one channel). Naphthacene was observed at 470 nm, and the photoproducts were observed at 240 nm.

Irradiation for HPLC experiments was achieved with a 150 W Xe lamp (PRA), which was filtered with an aqueous 0.57 M $NiCl_2$ solution and a 430 nm barrier filter. This removed all ultraviolet radiation, and served to dissipate a large amount of heat generated by the lamp. Samples were injected with the automatic injector (15 μl), or manually (10 μl). In each case a 20 μl sample loop was used.

Both reverse phase and normal phase HPLC was used. For reverse phase HPLC, a Waters C_{18} radial compression column was used with a mobile phase of a variable acetonitrile-water mixture. Use of a gradient controller allowed for changing proportions of the two solvents as a function of time. The gradient employed started at 50/50% v/v and was increased linearly to 100% acetonitrile over 10 minutes. This was kept constant for 2 minutes and then the gradient was reset for the next injection. A flow rate of 1.5 ml min^{-1} was used throughout the gradient. For normal phase HPLC, a Waters radial compression silica column was used with a mobile phase of 100% isopropanol at a flow rate of 2 ml min^{-1}. All solvents, of spectroscopic grade, were filtered and degassed prior to use. Water was doubly distilled deionized, filtered and degassed.

Solutions for NMR characterization of the photoproducts were prepared in $CDCl_3$ (MSD Isotopes). Stirred solutions were irradiated with the 476.5 nm line of an Argon ion laser, set to 100 mW output power. The solubility of naphthacene in most organic solvents is exceedingly low. Consequently, NMR is not a useful tool to follow the kinetics, but NMR remains a very useful tool for characterization of the photoproducts. All NMR spectra, except one, were collected on a

Varian Gemini 200 MHz spectrometer. Both one and two dimensional ^{1}H NMR spectra of the photoproducts were collected. Only one dimensional NMR spectra of naphthacene were collected. One spectrum of naphthacene dimers was collected on a Varian XL300 (300 MHz) spectrometer to resolve two pairs of overlapping singlets which appeared on spectra collected on the 200 MHz spectrometer.

An aerated solution of naphthacene in $CHCl_3$ was irradiated and used to test for the presence of peroxides, by the oxidation of iodide to iodine[41]. Controls of hydrogen peroxide in water, naphthacene in $CHCl_3$, I_2 in $CHCl_3$, and an aqueous solution with no peroxide present were used for comparison. The test for peroxides was positive with the solution of naphthacene irradiated in the presence of oxygen.

Mass spectroscopy (MS) analyses were achieved with a Finigan MAT 8230 mass spectrometer. All samples submitted for MS analysis were in the form of $CDCl_3$ solutions. All three were run using chemical ionization MS (CI-MS). The dimer solution was also run using fast atom bombardment MS (FAB-MS)

Fluorescence lifetime measurements were performed using a Coherent 25 W mode locked Nd:YAG laser. This laser was used to synchronously pump a cavity dumped dye laser (Rhodamine 6G). The output from the dye laser is frequency doubled (potassium diphosphate crystal), to give a final excitation wavelength of 290 nm. A barrier filter was used to remove any light in the visible spectrum, and neutral density filters were used to attenuate the beam as required. Emission was monitored at 470 nm using the single photon counting technique[42]. Data was collected until the counts in the peak channel

reached 2×10^4. The data is initially stored in a multichannel analyzer, and then transferred to a computer for further analysis.

4.1.3 Results and Discussion

4.1.3.1 Spectroscopic Characterizations

Characterization of the photoproducts is done with various spectroscopic techniques. The NMR spectra of naphthacene, naphthacene dimers and oxidized naphthacene are all very different. The chemical shifts and physical appearance of the spectra are summarized in Tables 4.1 - 4.3. The NMR spectrum of naphthacene shows three types of protons (Table 4.1), while those of the dimers (Table 4.2) and peroxide (Table 4.3) show six.

Generation of the photoproducts is achieved by irradiation with the 476.5 nm line of an Argon ion laser. An aerated solution of naphthacene in $CDCl_3$ requires only 5 minutes of irradiation before the characteristic yellow color of naphthacene has disappeared. The chemical shifts and physical appearance of the signals for endoperoxide of naphthacene are presented in Table 4.2. Two dimensional ^1H NMR of the peroxide shows coupling between the signals at 7.46 and 7.82 ppm, and between signals at 7.46 and 7.30 ppm, which aids in peak assignment. The NMR spectrum also reveals that only one oxidation product is formed, that is oxygen adds only to one of the center rings and not to the outer rings.

The irradiation time required to photolyze all the naphthacene in

Table 4.1: ^{1}H NMR Data for Naphthacene.

Shift / ppm	N_H^a	Description[b]	Protons[c]
8.65	4	multiplet	5, 6, 11, 12
7.98	4	multiplet	1, 4, 7, 10
7.38	4	multiplet	2, 3, 8, 9

[a]Number of protons by integration.

[b]Phvsical description of the signal.

[c]Positions of protons labelled in Figure 4.3.

Figure 4.3: NMR assignment labels for naphthacene to accompany Table 4.1.

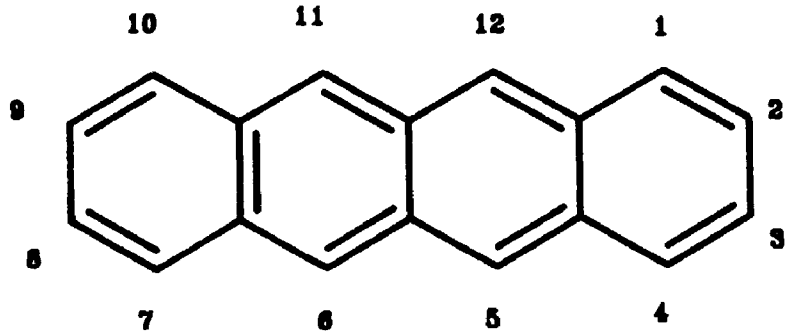
10
11
12
1
9
2
8
3
7
6
5
4

Table 4.2: ^{1}H NMR Data for Naphthacene Endoperoxide.

Shift / ppm	N_H^a	Description[b]	Protons[c]
7.82	4	overlapping sing, mult	7, 10 (m) 6, 11 (s)
7.46	4	overlapping multiplets	1, 4 8, 9
7.30	2	multiplet	2, 3
6.13	2	singlet	5, 12

[a]Number of protons by integration.

[b]Physical description of the signal: sing represents a singlet; mult represents a multiplet.

[c]Positions of protons labelled in Figure 4.4.

Figure 4.4: NMR assignment labels for naphthacene endoperoxide to accompany Table 4.2.

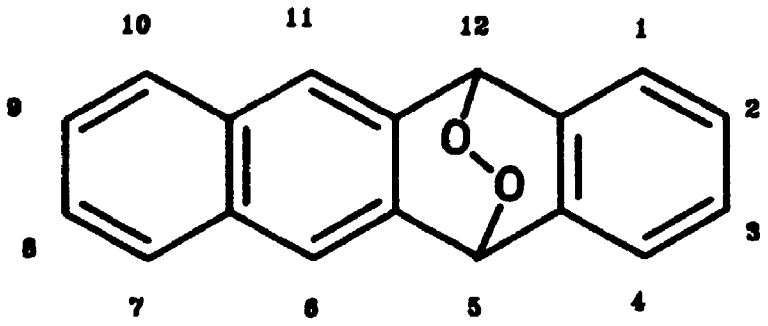
10
11
12
1
9
2
O
O
8
3
7
6
5
4

Table 4.3: ^{1}H NMR Data for Naphthacene Dimers.

Shift / ppm	N_H^a	Description[b]	Protons[c]
7.56	4	multiplet	(7, 10, 7′, 10′) (7, 10, 1′, 4′)
7.38[d]	4	singlet	(6, 11, 6′, 11′) (6, 11, 5′, 12′)
7.25	4[e]	multiplet	(8, 9, 8′, 9′) (8, 9, 2′, 3′)
6.91	4	multiplet	(1, 4, 1′, 4′) (1, 4, 7′, 10′)
6.64	4	multiplet	(2, 3, 2′, 3′) (2, 3, 8′, 9′)
4.83	4	singlet	(5, 12, 5′, 12′) (5, 12, 6′, 11′)

[a]Number of protons by integration.

[b]Physical description of the signal.

[c]Positions of protons labelled in Figure 4.5. Numbers in upper brackets for planosymmetric dimer, lower brackets for centrosymmetric dimer.

[d]Two unresolved singlets.

[e]Signal masked by solvent. Number of protons set to 4 by default.

Figure 4.5: NMR assignment labels for naphthacene dimers to accompany Table 4.3. Top: planosymmetric dimer, bottom: centrosymmetric dimer. Dimers drawn planar and without double bonds for sake of clearness.

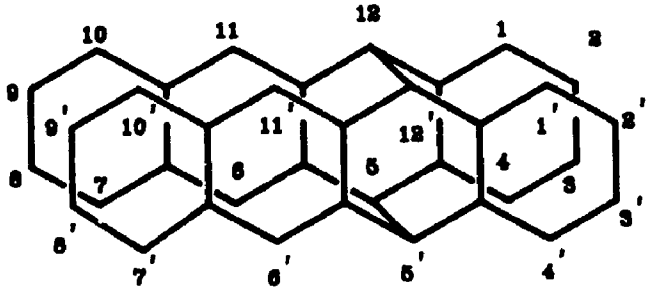
10
11
12
1
2
9
9'
10'
11'
12'
1'
2'
8
7
6
5
4
3
3'
8'
7'
6'
5'
4'

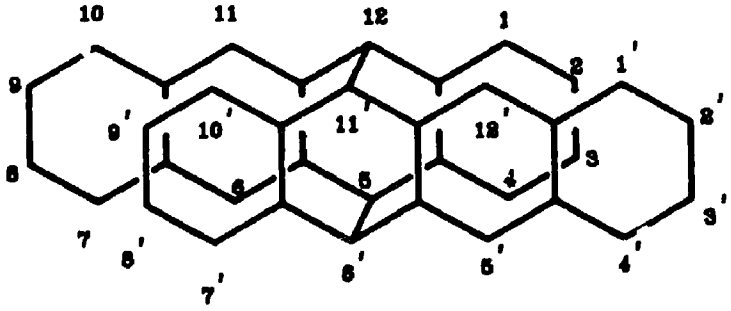
10
11
12
1
2
1'
9
9'
10'
11'
12'
2'
3
8
6
5
4
3'
7
8'
7'
6'
5'
4'

degassed solutions is much longer. After 45 minutes of irradiation, a degassed solution of naphthacene in $CDCl_3$ still has the characteristic yellow color of naphthacene, and the NMR reveals the reaction is only 56% complete. The NMR spectrum of this solution has signals characteristic of naphthacene and two photoproducts which are different from the peroxide (Table 4.3). The products formed are two naphthacene dimers (Figure 4.1). The protons at the bridgehead positions for the two dimers have similar, but slightly different chemical shifts. A spectrum of the same solution with further irradiation (2 hours total) was collected on a 300 MHz spectrometer. This resolves the signal at 4.83 ppm (bridgehead protons) into two singlets, positioned at 4.83 and 4.82 ppm (integration gives a ratio of 1:3.57). As well, the singlet at 7.38 ppm (protons on the naphthalene moiety β to the bridgehead protons) is also resolved into two singlets positioned at 7.38 and 7.37 ppm (integration gives a ratio of 3.53:1). The ratios provides a measure of the relative amounts of the two dimers in solution. We cannot, however, say that the dimers are formed in this ratio, as the centrosymmetric dimer has been found to be less soluble than the planosymmetric dimer[1] and some precipitate was present in the NMR tube. Two dimensional NMR reveals coupling between signals at 6.64 and 6.91 ppm, and between signals at 7.25 and 7.56 ppm. Also present in this spectrum are peaks corresponding to the oxidized product. Even though great care was taken to minimize the admittance of oxygen into the solution, some obviously entered when the first sample for NMR analysis was taken. Even with the presence of a very small amount of oxygen, the peroxide

forms readily.

Molar extinction coefficients for the photoproducts of naphthacene are determined from the absorption spectra. The final concentration of the products are estimated from the initial and final concentrations of naphthacene. From the spectra, the molar extinction coefficient for the peroxide is calculated to be 85 400 M^{-1} cm^{-1} at 237 nm, and for a solution of both dimers, ε = 137 000 M^{-1} cm^{-1} at 237 nm in cyclohexane. This latter value is in good agreement with the extinction coefficient reported by Wei and Livingston[3].

An isosbestic point is present in the absorption spectra of aerated solutions. The presence of an isosbestic point indicates that the extinction coefficients of the reactants and products are equal at that wavelength. The isosbestic point in the naphthacene system occurs at 255 nm in cyclohexane for aerated solutions. Stevens and Algar have reported an isosbestic point in the absorption spectra of oxygenated cyclohexane solutions of naphthacene at 258 to 259 nm[13].

Mass spectra of the three species reveal the following: the spectrum of naphthacene shows a parent peak at m/e = 228, expected 228. The spectrum of the oxidized product has parent peak at m/e = 262, with the most intense peak at m/e = 228, and second most at m/e = 260. If the product is a peroxide, the expected value of m/e is 260. Both FAB-MS and CI-MS show intense peaks for the dimer at m/e = 228, and smaller peaks at 455 (CI) or 468 (FAB). The expected value of m/e for naphthacene dimers is 456. Similar results for the naphthacene dimers were obtained by Iannone and Scott[43]. Using both chemical ionization and FAB-MS, they found the dimers to cleave quantitatively

to the monomer giving a peak at m/e = 228.

4.1.3.2 Kinetics of Photolysis in Solution

Table 4.4 presents decay parameters for the disappearance of naphthacene in solution as a function of irradiation time, oxygen content and illumination intensity. The slopes presented in Table 4.4 are calculated by linear least-squares fitting of semi-log plots of the absorbance of naphthacene against irradiation time (Figure 4.6). For solutions with a significant amount of dissolved oxygen, the slope gives a measure of the rate constant for oxidation. The total rate of reaction will depend on the illumination intensity, the lifetime of singlet oxygen, and the solubility of oxygen in the solvent for a given initial naphthacene concentration. In both cyclohexane and isopropanol which have not been treated in any way, the slopes are very nearly the same. The small difference is due to differences in the lifetime of singlet oxygen in each solvent (17 μs[44,45] versus $\approx$10 μs[46]), and the solubility of oxygen in each. In solvents where the lifetime of singlet oxygen is much higher ($CHCl_3$ 60 μs; $CDCl_3$ 300 μs[44,45]) the rate of decay is very rapid, with all the naphthacene reacting within a few minutes. Quantitative measurements of the kinetics of oxidation of naphthacene in these solvents have not been done. Increasing the oxygen content in cylcohexane and isopropanol is achieved by bubbling the solution with air prior to irradiation. A small rate increase is seen in cyclohexane, and the rate in isopropanol is nearly doubled. Since the slopes are changing with

Table 4.4: Calculated Slopes From Semi-log Plots of Naphthacene Photolysis in Solution.

Solvent[a]	$[N]_0/\mu M$[b]	Slope/10^{-4} s^{-1} [c]	N[d]	R^2 [e]
		No treatment		
CHX	17	-2.80	16	0.995
IPA	28	-4.68	16	0.997
		Air bubbled		
CHX	26	-3.57	17	0.991
IPA	22	-8.49	10	0.991
		N_2 Bubbled		
CHX	14	-2.72	13	0.998
CHX[f]	16	-1.41	11	0.998
CHX[f]	30	-1.75	13	0.998
CHX	30	-3.44	15	0.998
IPA	38	-6.19	9	0.988
$CDCl_3$	20	-8.75	7	0.989
		N_2 Bubbled; DABCO added		
CHX	17	-0.83	13	0.995
IPA	38	-3.17	13	0.996
$CDCl_3$	20	-1.77	9	0.997

[a]Solvents: CHX is cyclohexane; IPA is isopropanol.

[b]Initial concentration of naphthacene.

[c]Errors on slopes calculated to be ±10%.

[d]Number of data points used in the fit.

[e]Correlation coefficient.

[f]25 mW laser intensity for these two; all others 50 mW.

Figure 4.6: Semi-log plot of naphthacene absorbance (points) as a function of irradiation time. The solid line represents the line of best fit given by linear regression. Data for a solution of naphthacene in nitrogen bubbled cyclohexane.

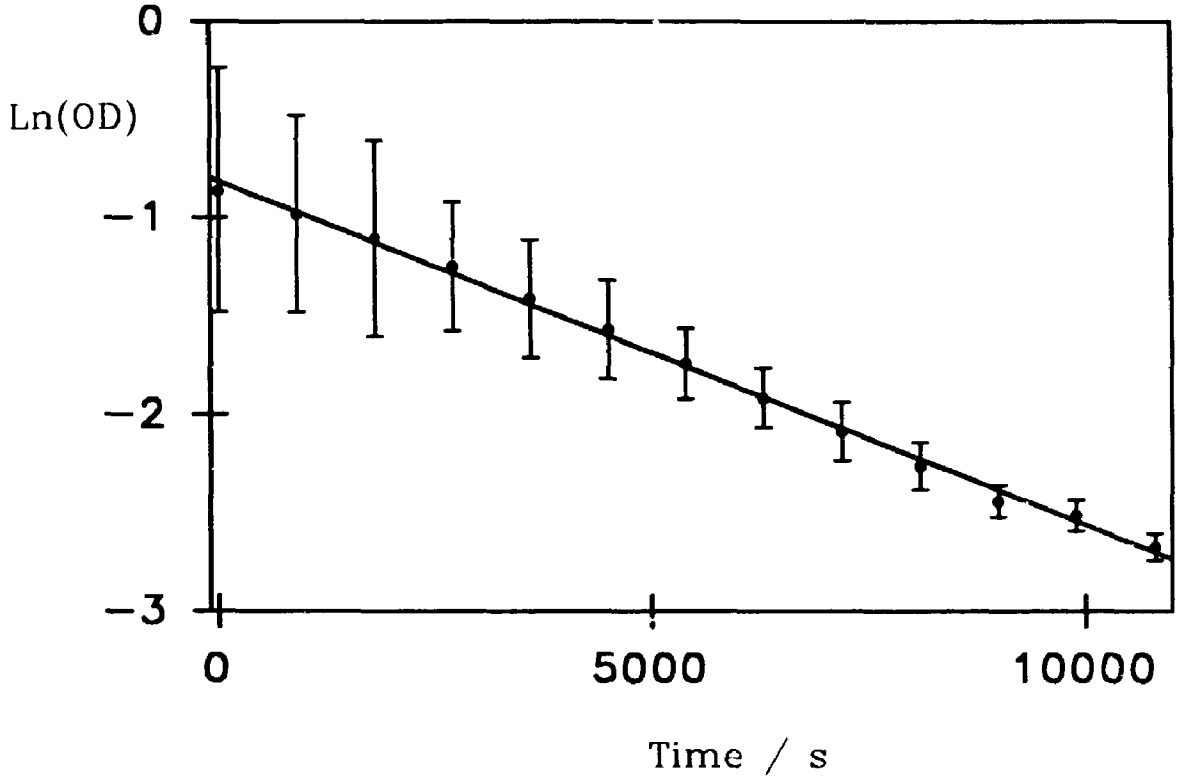
0
Ln(OD)
−1
−2
−3
0
5000
10000
Time / s

oxygen content, the slopes must not represent the intrinsic rate constant k (Equation 4.1), but a measure of $k*[O_2]$:

$$\text{Rate} = k*[O_2]*[N] \qquad (4.1)$$

where the square bracket represents the molar concentrations of naphthacene (N) and oxygen (O_2).

In solutions with limited oxygen content, the reaction should involve dimerization of naphthacene. Livingston has proposed a mechanism for the dimerization of anthracene[47], and we assume the same mechanism for naphthacene. The mechanism is:

$$^1N \xrightarrow{I_a} {}^1N^* \qquad (1)$$

$$^1N^* \longrightarrow {}^1N + h\nu_f \qquad (2)$$

$$^1N^* \longrightarrow {}^3N \qquad (3)$$

$$^1N^* \longrightarrow {}^1N \qquad (4)$$

$$^1N + {}^1N^* \longrightarrow N_2 \qquad (5)$$

$$^1N + {}^1N^* \longrightarrow {}^1N + {}^1N \qquad (6)$$

$$^3N^* \longrightarrow {}^1N \qquad (7)$$

where the * represents an excited state, I_a represents the rate of photon absorption, and N_2 represents naphthacene dimers.

Steady state analysis of this mechanism gives the decay of naphthacene to be:

$$\frac{d}{dt}[^1N] = \frac{-2\, I_a\, k_5[^1N]}{(k_d + (k_5 + k_6)[^1N])} \qquad (4.2)$$

where $k_d = (k_2 + k_3 + k_4)$. Reactions 5 and 6 are bimolecular, which are generally slower than unimolecular processes (*eg.* 2, 3, 4). If this holds, then Equation 4.2 reduces to a truly first order process in naphthacene. Data for solutions bubbled with nitrogen are

fit quite well to a first order decay (Table 4.4). To ensure we are measuring the kinetics of dimer formation and not that of peroxidation due to residual oxygen in the system, two steps are taken. First, DABCO, a singlet oxygen quencher, is added, and then the solutions were bubbled with nitrogen. In the three solvents used, the kinetics are found to be first order, albeit somewhat slower than the kinetics in solutions just bubbled with nitrogen. The slower kinetics may be due to DABCO interfering in some manner with the dimerization process. Second, solutions of naphthacene are prepared in $CDCl_3$, sealed and degassed in cuvettes. First order kinetics are observed for these solutions also. After irradiation, the NMR spectra of these samples are recorded. The NMR has signals characteristic of the dimers only.

Decreasing the laser power by a factor of two reduces the slope of the semi-log plot by the same factor (Table 4.4), as expected from Equation 4.2. This has been examined only for naphthacene in degassed cyclohexane solution. The initial slope for a 30 μM solution irradiated with a 50 mW laser beam is -3.44×10^{-4} s^{-1}. Decreasing the power to 25 mW gives a slope of -1.75×10^{-4} s^{-1}, a decrease by a factor of 1.97.

HPLC is also used in attempts to follow the kinetics of photolysis of naphthacene in solution. Both normal and reverse phase columns are used in the HPLC experiments. Only aerated solutions are run with reverse phase HPLC. On reverse phase columns, with an acetonitrile water mixture run under gradient conditions, naphthacene elutes after 11.3 minutes and the peroxide after 9.8 minutes. Repeated injections of the same solution onto a reverse phase column

does not give the same integrated areas for the corresponding peaks. The retention times are quite stable, but without reproducible areas, the kinetics cannot be followed by HPLC with any confidence.

The retention time of naphthacene using normal phase HPLC with isopropanol as the mobile phase is 3.9 minutes, and that of the dimers is 2.0 minutes. Injection of a freshly prepared solution of oxidized naphthacene shows no discernible peak on the chromatogram. There is a drift in the baseline after 8 minutes, which may be due to the photoproduct, but this is not a certainty. There is also no means to measure the concentration (by integration area) of the peroxide using normal phase HPLC. Injection of a solution of oxidized naphthacene which has sat at room temperature in the dark for three days yields one peak at 1.9 minutes. This species could be any of a number of products[14-17], and has not been identified. The above mentioned difficulties do not allow for use of reverse phase or normal phase HPLC as a quantitative tool for following the kinetics of photobleaching of naphthacene in solution.

4.1.3.3 Photophysics of Naphthacene in Solution

In dilute solutions, the decay from the first excited singlet state is expected to be a first order process, and should follow a single exponential decay. The decay profile for naphthacene in cyclohexane is presented in Figure 4.7. In solution, naphthacene decays according to a single exponential decay law, with lifetimes for various solvents given in Table 4.5. The lifetime changes with

Figure 4.7: Fluorescence decay profile of naphthacene in cylcohexane. Excitation wavelength 290 nm; emission wavelength 470 nm.

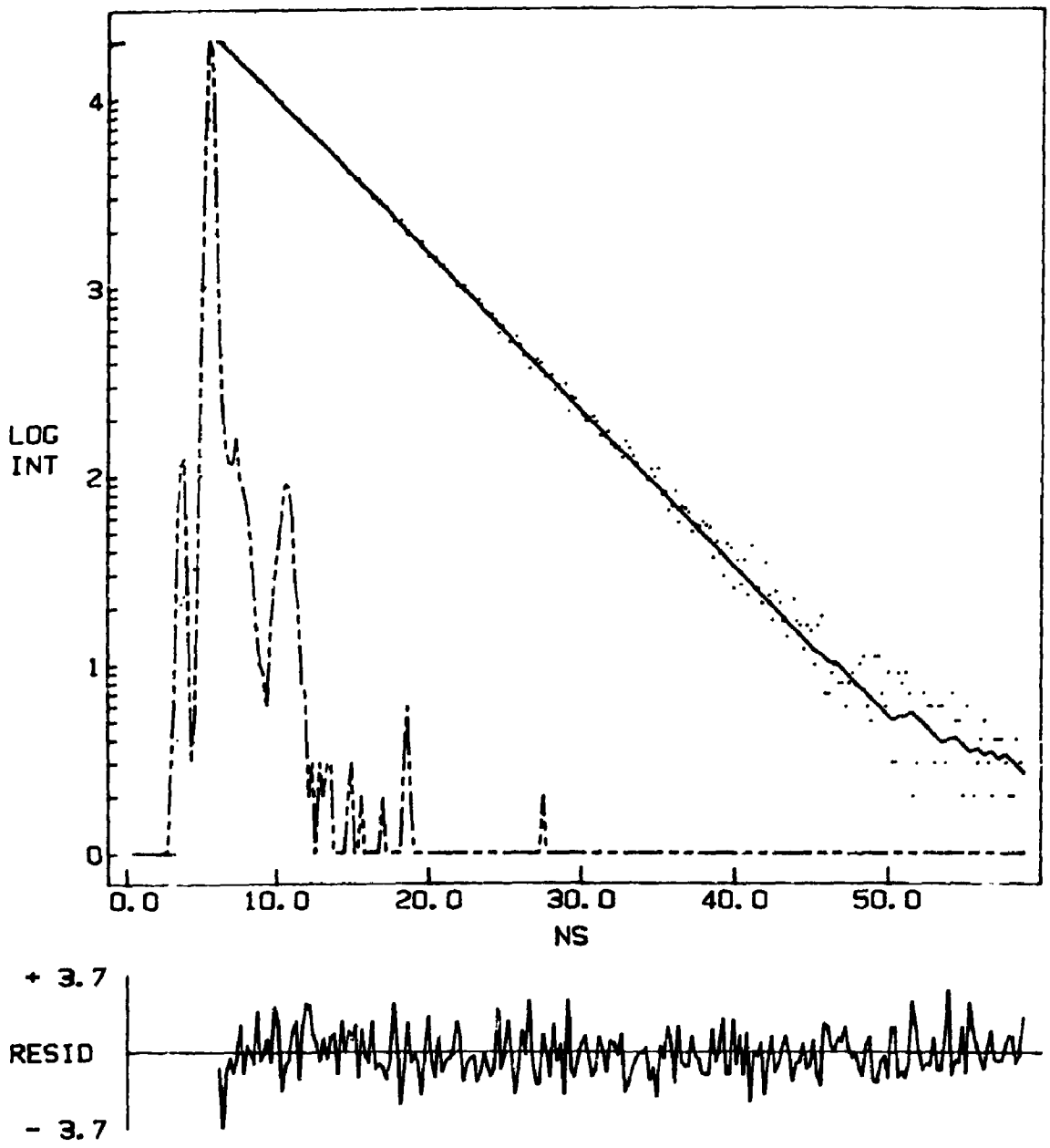
LOG
INT
4
3
2
1
0
0.0
10.0
20.0
30.0
40.0
50.0
NS
+ 3.7
RESID
- 3.7

Table 4.5: Fluorescence Lifetimes of Naphthacene in Solution.

Solvent	Lifetime / ns
Toluene	3.79
Acetonitrile	4.50
Methanol	4.75
Cyclohexane	5.26
Water	6.46[a]

[a]Average value of three lifetimes calculated using Equation 4.5.

solvent, but is in the range of 3 to 6 ns for naphthacene in various organic solvents. The decay of naphthacene in triply distilled water is shown in Figure 4.8. This decay requires at least three exponentials to obtain an acceptable fit. The solubility of naphthacene is exceedingly low in organic solvents, and even less so in water. The multi-exponential decay of the aqueous solution may be due to aggregates of naphthacene forming due to low solubility.

4.1.4 Conclusions

In solution, naphthacene photolyzes to different products depending on the initial conditions. If oxygen is present, the reaction proceeds quite quickly and the rate is dependent on the lifetime of singlet oxygen. The photoproduct obtained, an endoperoxide of naphthacene (Figure 4.2), is identified by NMR data and a qualitative test for peroxides. Very little spectroscopic data for this peroxide is present in the literature. A more complete set of spectral data (UV-VIS, NMR, and MS) is presented here. The process of photoperoxidation of naphthacene is found to proceed via a mechanism which is first order in naphthacene.

In degassed solutions, two photoproducts are obtained, the planosymmetric and centrosymmetric dimers (Figure 4.1). The rate of dimer formation is much slower than the rate of peroxide formation. The kinetics of dimerization in solution is found to be first order in naphthacene. Previous characterizations of the dimers by spectroscopic techniques presented in the literature are more complete

Figure 4.8: Fluorescence decay profile of naphthacene in water. Excitation wavelength 290 nm; emission wavelength 470 nm.

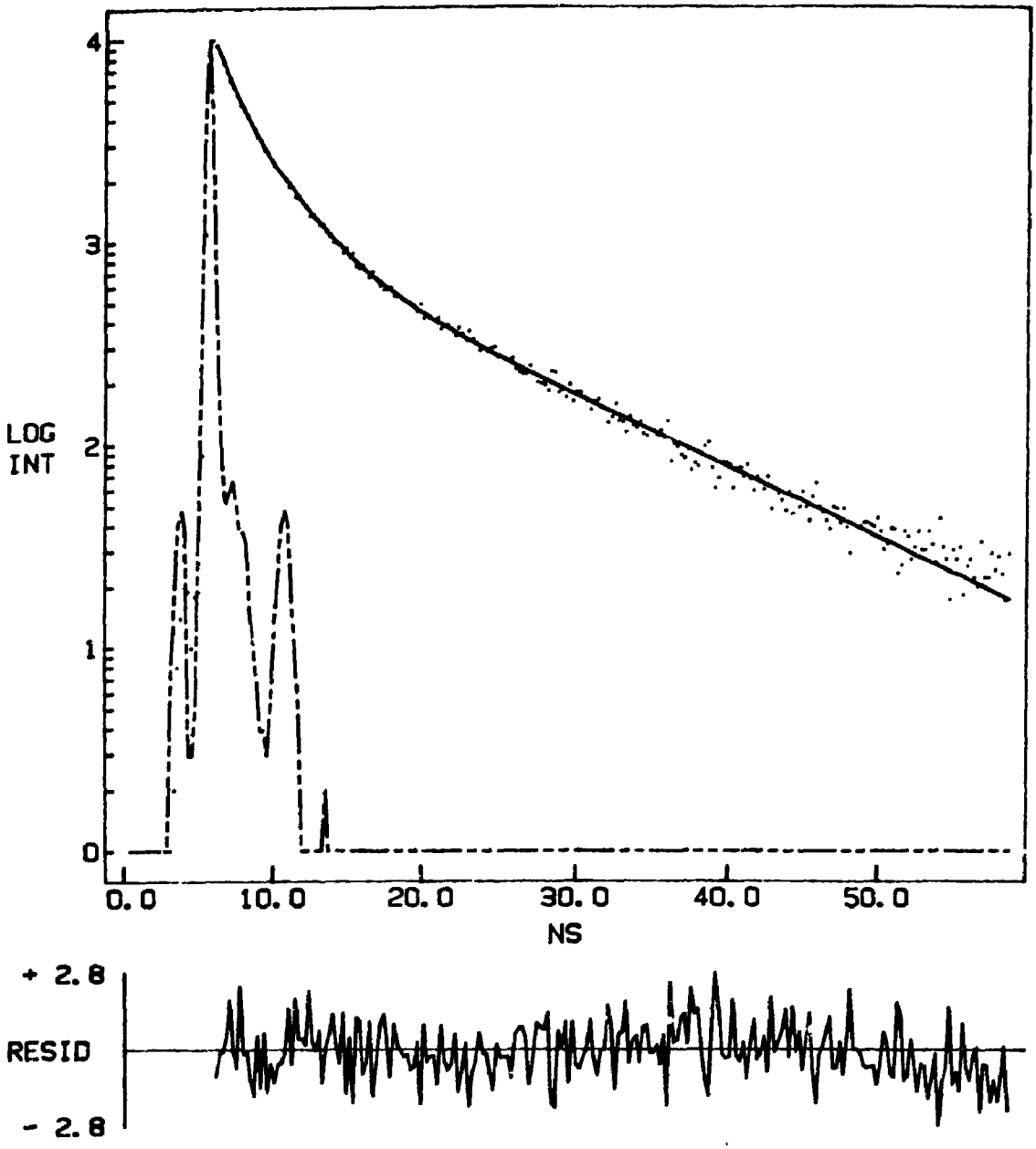
LOG
INT
4
3
2
1
0
0.0
10.0
20.0
30.0
40.0
50.0
NS
+ 2.8
RESID
- 2.8

than for the peroxide, but the data available is dated, and all is not in complete agreement with data presented here. In particular, NMR data obtained by Bouas-Laurent and co-workers[1] shows fewer signals than found here. Further NMR data, along with UV-VIS and MS data, are presented here. The dimerization of naphthacene in solution is found to be first order in naphthacene.

The fluorescence lifetime of dilute naphthacene in organic solvents is in the range 3 to 6 ns, and the decay is a single exponential. In very dilute aqueous solutions, the average lifetime is calculated to be 6.3 ns, based on fit to a three exponential function. The decay of naphthacene in water is not a single exponential, possibly due to aggregation of naphthacene.

4.2 Photochemistry and Photophysics of Adsorbed Naphthacene

4.2.1 Introduction

In degassed solutions, naphthacene dimerizes upon irradiation[1-7]. This reaction does not proceed as fast as the oxidation reaction, but is still fairly rapid. The kinetics of this reaction in solution are found to be first order in naphthacene, and are expected to be the same on the surface.

An understanding of the photochemistry of adsorbed naphthacene is required in order to interpret the measured diffusion parameters correctly. In oxygenated solutions, naphthacene is oxidized upon irradiation into an endoperoxide[8-17]. This reaction proceeds rapidly

via first order kinetics in solution, and the rate is greatly dependent upon the lifetime of singlet oxygen. On a surface, the kinetics should be first order in naphthacene.

We use Continuous Fluorescence Microphotolysis (CFM) to measure the kinetics of photobleaching for naphthacene adsorbed on C18 silica. Qualitative analysis of the data by graphical techniques reveals that the photochemistry cannot be described as purely first or second order in naphthacene, and rather a combination of the two is probably occurring.

The photophysics of various adsorbed PAHs has been investigated by numerous groups[22-39]. Photophysical examinations of these systems can give information on the heterogeneity of the environments experienced by the adsorbate. Pyrene adsorbed on various surfaces has been studied extensively, from both time resolved and steady state fluorescence perspectives. On dry silica gel, pyrene exhibits only monomer emission at low concentrations, and both monomer and excimer emission at higher concentrations[22,24-28,31]. The fluorescence lifetime of pyrene on dry silica at low concentrations cannot be described by a single exponential, due to heterogeneities of the system. As the surface is altered with coadsorbates (e.g. decanol), the decay of pyrene can be fit to a single exponential, which yields a lifetime similar to the lifetime of pyrene in solution[29,31].

Fitting of decay data collected from fluorophores in heterogeneous media has routinely achieved by an iterative least squares fit to a sum of two to four exponential functions[28,29,31]. This method can give misleading results. A four exponential function

can be used to fit a great variety of decays, giving acceptable fit statistics (*eg.* χ^2 values and random residuals). Using this method of fitting results in an estimation of up to four discrete lifetimes for the fluorophores. In heterogeneous environments (micelles, surfaces), a distribution of continuous lifetimes should be expected rather than a small set of discrete lifetimes[48,49]. Recently, two new methods have been developed to recover underlying lifetime distributions in fluorescence decay data[48-50]. These methods, the Exponential Series Method (ESM) and the Maximum Entropy Method (MEM), generate pre-exponential factors for a chosen set of lifetimes. Decay data collected for naphthacene adsorbed on dry silica gel and in crystalline form are presented and analyzed using ESM.

4.2.2 Experimental

For all Continuous Fluorescence Microphotolysis (CFM) experiments, naphthacene was adsorbed on C18 silica from cyclohexane solution. The surface concentration was maintained at 0.1% monolayer. To elucidate any effects of oxygen, the concentration of oxygen was varied, by allowing air into the vacuum line at various pressures (0, 160, 360, 570 torr) through a tube containing a drying agent (Drierite).

Effects of diffusion on the rate of naphthacene disappearance was probed by changing the beam width. Using a 140 mm focusing lens in conjunction with three objective lenses (10×, 20×, 40×) gave three beam widths of 4.8 1.5 and 1.0 μm. For a given level of attenuation,

each beam width has a different power density, which will affect the rate of decay of naphthacene. The total power reaching the sample was altered by changing the attenuation of the laser beam. Four different neutral density filters (1.08, 1.58, 1.75, and 2.11 OD) were used, with additional neutral density filters (1.03, 0.55, 0.37, and 0 OD respectively) placed in the optical path after the sample to keep the total attenuation constant. For each combination of oxygen pressure, beam size and laser beam attenuation, three procedures were collected using a time base of 500 ms/ch over 512 channels. Qualitative analysis of the data was accomplished by graphical techniques.

Fluorescence decay data for naphthacene adsorbed on dry normal phase silica gel (preheated to 25^{0}C, 250^{0}C, 600^{0}C) at a 0.1% monolayer surface concentration were measured using the single photon counting technique[42]. Naphthacene was deposited on the silica via sublimation. A Coherent 25 W mode locked Nd:YAG laser was used to synchronously pump a cavity dumped dye laser (with Rhodamine 6G). A repetition rate of 0.5 MHz was used. The output of the dye laser was frequency doubled by second harmonic generation (potassium diphosphate crystal) to give a final excitation source in the near ultraviolet (290 nm). A barrier filter was used to remove any visible light from the excitation source, and neutral density filters were used to attenuate the beam as required.

Data was collected to precisions high enough to use ESM. Typically, data was collected until there was at least 10^{5} counts in the peak channel.

4.2.3 Results and Discussion

4.2.3.1 Continuous Fluorescence Microphotolysis

Figure 4.9 shows decay profiles of naphthacene on C18 silica from CFM experiments. These same profiles are presented in Figure 4.10 as the semi-log plots, which are not linear. One may infer that the kinetics are other than first order, which may be an erroneous conclusion[51]. The photophysics (*vide infra*) and photochemistry of species in heterogeneous media is not as well defined as in homogeneous media. A reaction may follow a first order pathway, but the rate constant may be distributed about some mean value due to heterogeneities of the system. In our case, the Gaussian intensity profile of the laser beam provides for added heterogeneities. Fluorophores located near the center of the beam will react faster than those away from the center. Semi-log plots of this type of data need not be linear[51]. A means to test for first order decays is given by normalization of the data to the initial concentration[51]. A first order decay follows Equation 4.3:

$$C(r,t) = \bar{C} \exp(-k(r)\, t) \qquad (4.3)$$

If the initial concentrations of different experiments are very different, the decay described by Equation 4.3 may look visually very different. Normalization to the initial concentration gives:

$$C'(r,t) = \exp(-k(r)\, t) \qquad (4.4)$$

where $C'(r,t) = C(r,t)/\bar{C}$, t is time and k(r) is a first order rate constant which is a function of position due to the Gaussian intensity

Figure 4.9: Sample CFM experiments for naphthacene on C18 silica. (Experimental conditions: 1.0 μm beam width, 1.58 OD laser attenuation; 360 torr air pressure).

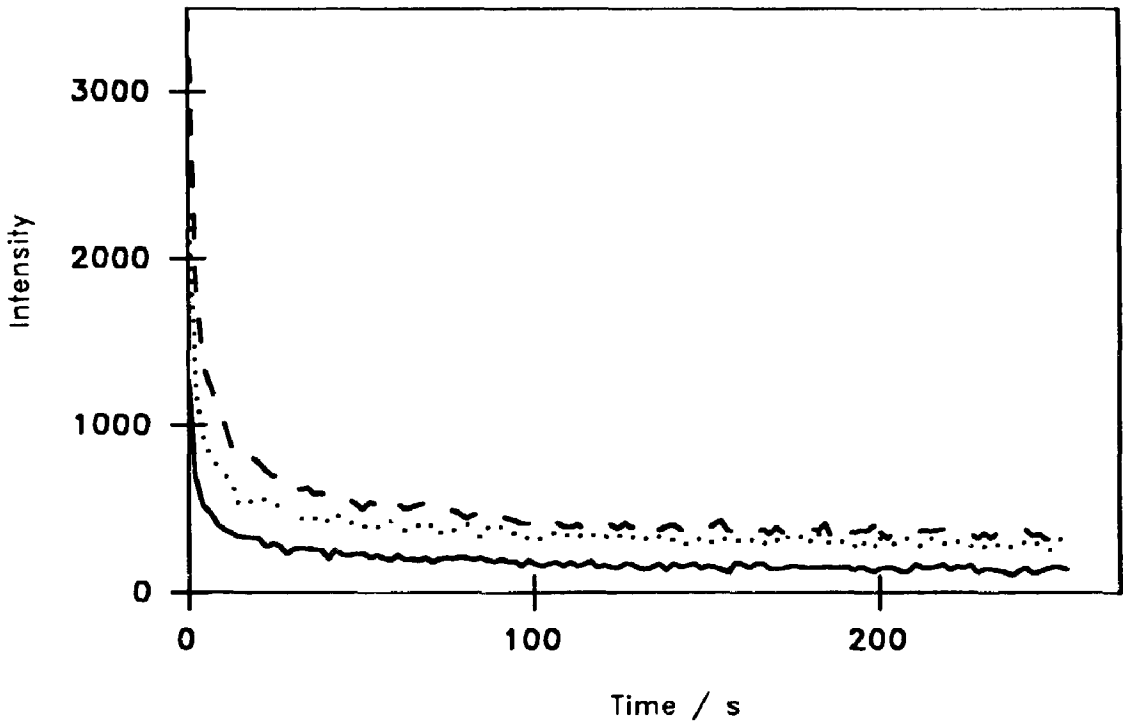
3000
2000
1000
0
Intensity
0
100
200
Time / s

Figure 4.10: Semi-log plots of CFM data from Figure 4.9.

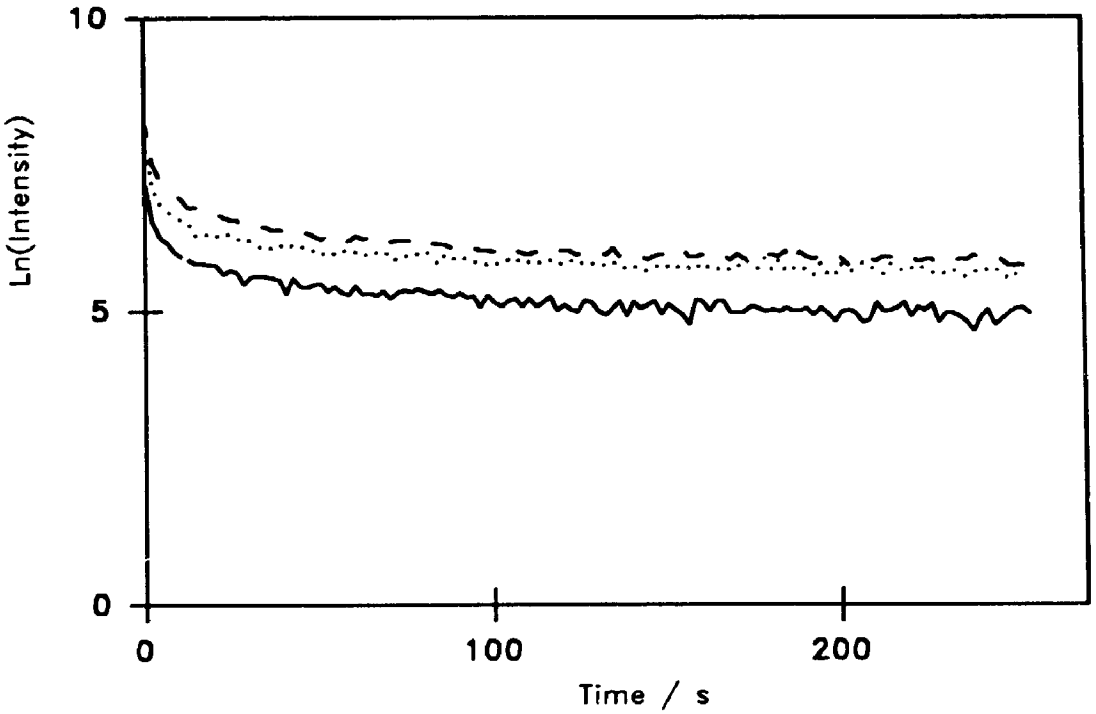
10
5
0
Ln(Intensity)
0
100
200
Time / s

profile. Equation 4.4 describes a common curve for kinetics in heterogeneous environments regardless of initial concentration. If the kinetics are first order, the normalized curves should be superimposable[51]. Figure 4.11 shows two sets of data normalized to the initial concentrations. Figure 4.11a reveals that under the conditions stated (360 torr air pressure, 1.0 μm beam, 1.58 OD attenuation) the kinetics appear to be first order, while Figure 4.11b shows that under other conditions (570 torr air pressure, 1.51 μm beam, 1.08 OD attenuation), the kinetics are not always first order in naphthacene.

If the kinetics are second order in naphthacene, a linear relationship would exist between the reciprocal of the intensity and total irradiation time. Figure 4.12 reveals that these plots are not linear. The non-linearity could be due to heterogeneities of the system. There is no simple way to normalize the data as in the first order case to allow a direct comparison.

Diffusion of fluorophores into the illuminated region can also cause first or second order plots to deviate from linearity. Diffusion will increase the intensity, while photobleaching will decrease the intensity. Presently, we have not fit the data to a model of a given kinetic order coupled with diffusion. From the normalization above and Figure 4.11, it is clear that in some cases we see first order kinetics, and in others we see non-first order kinetics.

The experiments done here are a preliminary set, designed to explore the photochemistry from a qualitative, or at best,

Figure 4.11a: Normalized CFM plots. Data from Figure 4.9 normalized to the initial concentration. The plots are superimposable, which indicates first order kinetics.

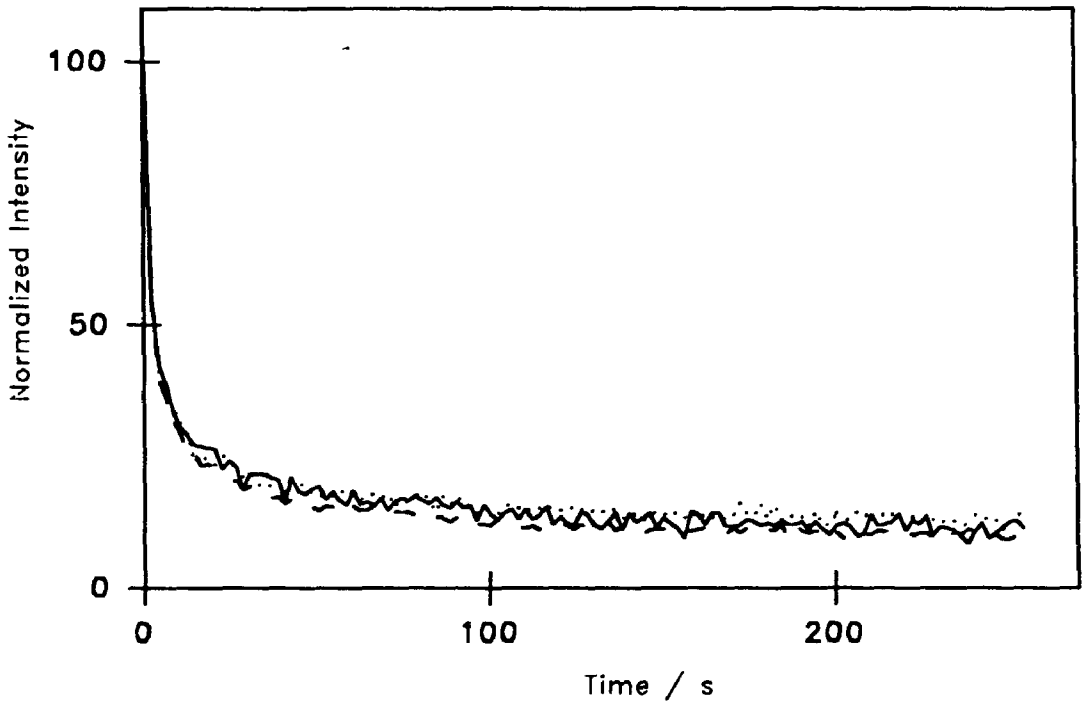
100
50
0
Normalized Intensity
0
100
200
Time / s

Figure 4.11b: Normalized CFM plots. Data normalized to the initial concentration. The plots are not superimposable, which indicates non-first order kinetic processes are occurring. (Experimental parameters: 1.5 μm beam width; 570 torr air pressure, 1.08 OD laser attenuation).

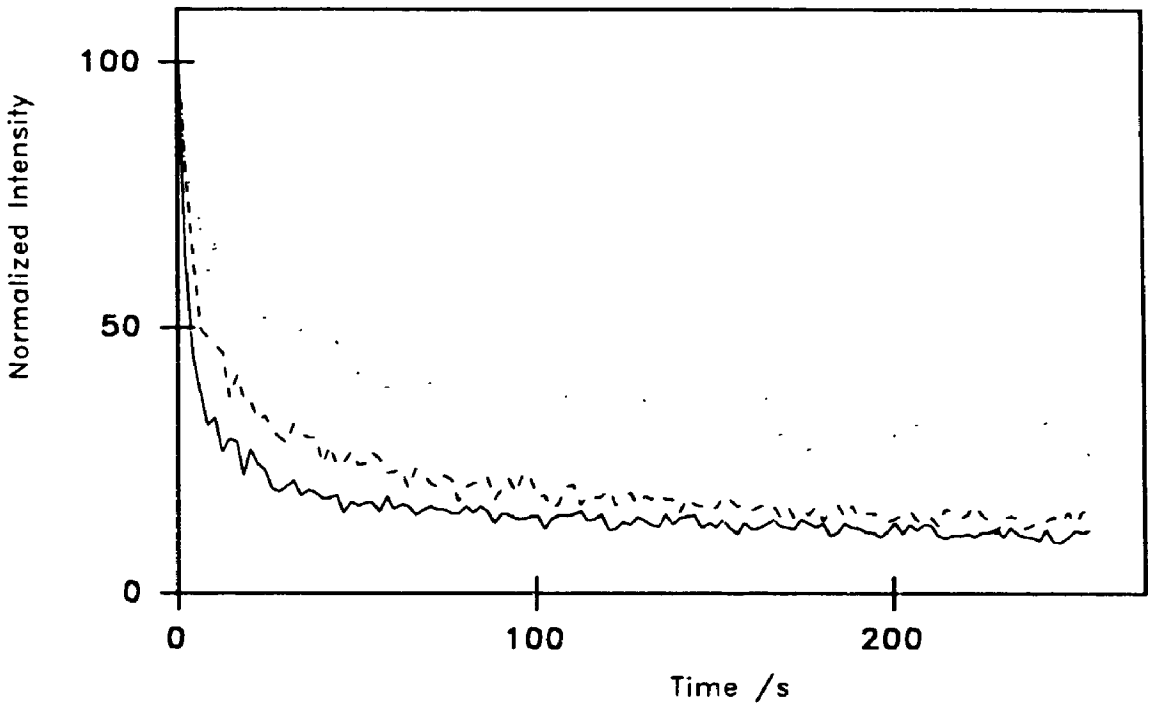
100
50
0
Normalized Intensity
0
100
200
Time /s

Figure 4.12: Plots of the reciprocal intensity as a function of irradiation time. Same data presented in Figure 4.11b.

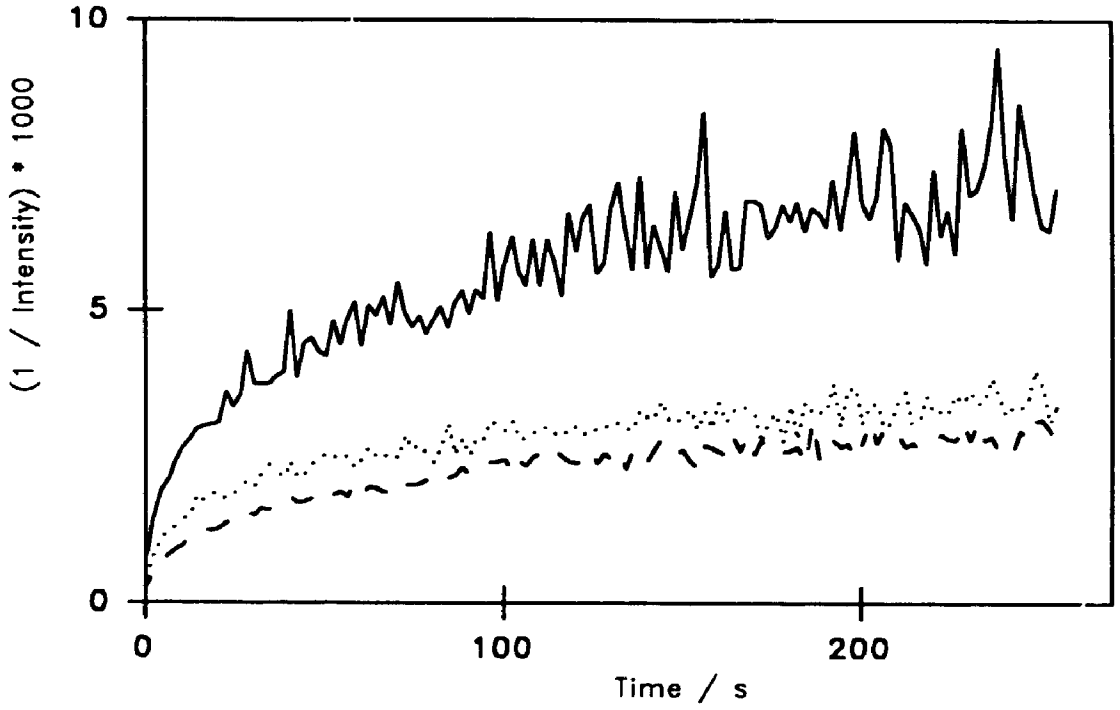
10
5
0
(1 / Intensity) * 1000
0
100
200
Time / s

semi-quantitative perspective. Changing experimental parameters such as oxygen content, beam width and illumination intensity allows for further qualitative assessments.

In general, as the oxygen content increases, the initial rate of bleaching and the total extent of bleaching increase. This is shown in Figure 4.13 for four CFM experiments which vary only in the oxygen content. The effects seen by the addition of oxygen are explained by the photochemistry. Photo-oxidation occurs more rapidly in solution than photodimerization, and this should also be the case on the surface. Oxygen is probably more mobile on the surface than naphthacene, and will be present on the surface and in the vapor phase for those samples with increased oxygen content. These factors enhance the probability of photo-oxidation occurring over that of photodimerization, and increase the rate of reaction. As the oxygen content is increased the kinetics do not all tend to first order, judging by the normalization procedure described above.

No consistent effect is observed upon varying only the beam width (Figure 4.14). As the beam width increases, the power density decreases, and one would expect the rate of decay to decrease. In the cases examined, no significant effect was noticeable among experiments with the same oxygen content and laser attenuation.

As the illumination power is increased, the rate of bleaching and the overall extent of bleaching both increase (Figure 4.15). Both photochemical pathways (peroxidation and dimerization) proceed through the first excited singlet state. An increase in the illumination should increase I_a (Equation 4.2), and therefore the rate of reaction.

Figure 4.13: Effects of oxygen concentration on the rate and extent of photobleaching in CFM. (Experimental parameters: 1.0 μm beam width; 1.58 OD laser attenuation). Air pressure: 0 torr (———); 160 torr (— —); 360 torr ( ); 570 torr (– – –).

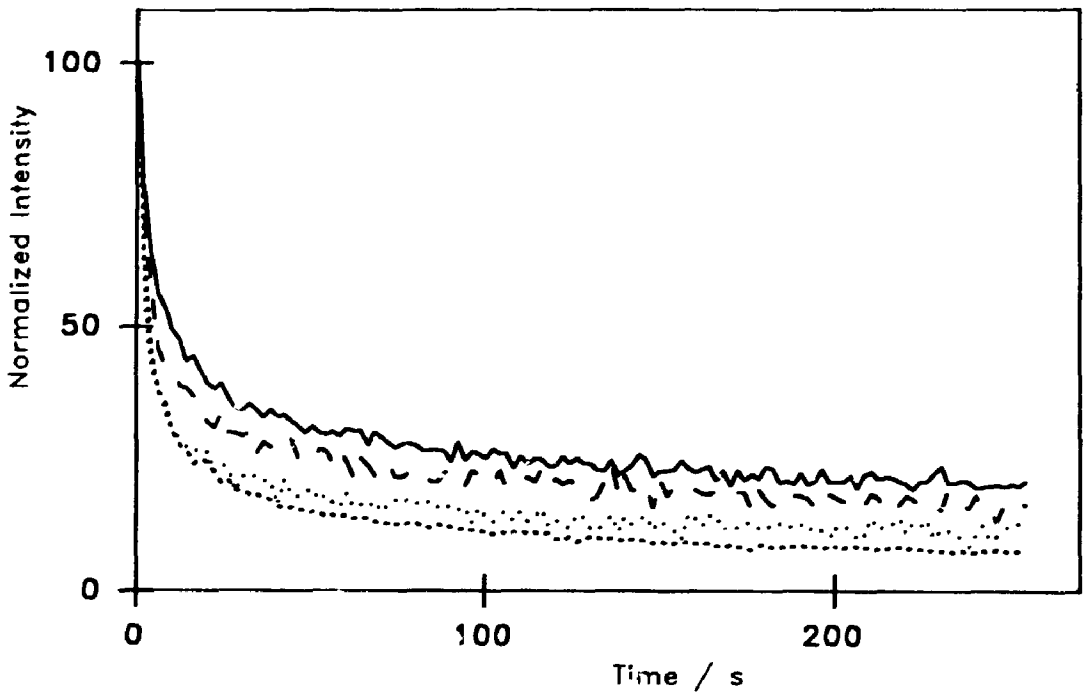
100
50
0
Normalized Intensity
0
100
200
Time / s

Figure 4.14: Effect of beam width on the rate and extent of photobleaching in CFM. (Experimental conditions: 1.08 OD laser attenuation; 570 torr air pressure. Beam widths: 1.0 μm (———); 1.5 μm (— —); 4.8 μm ( )).

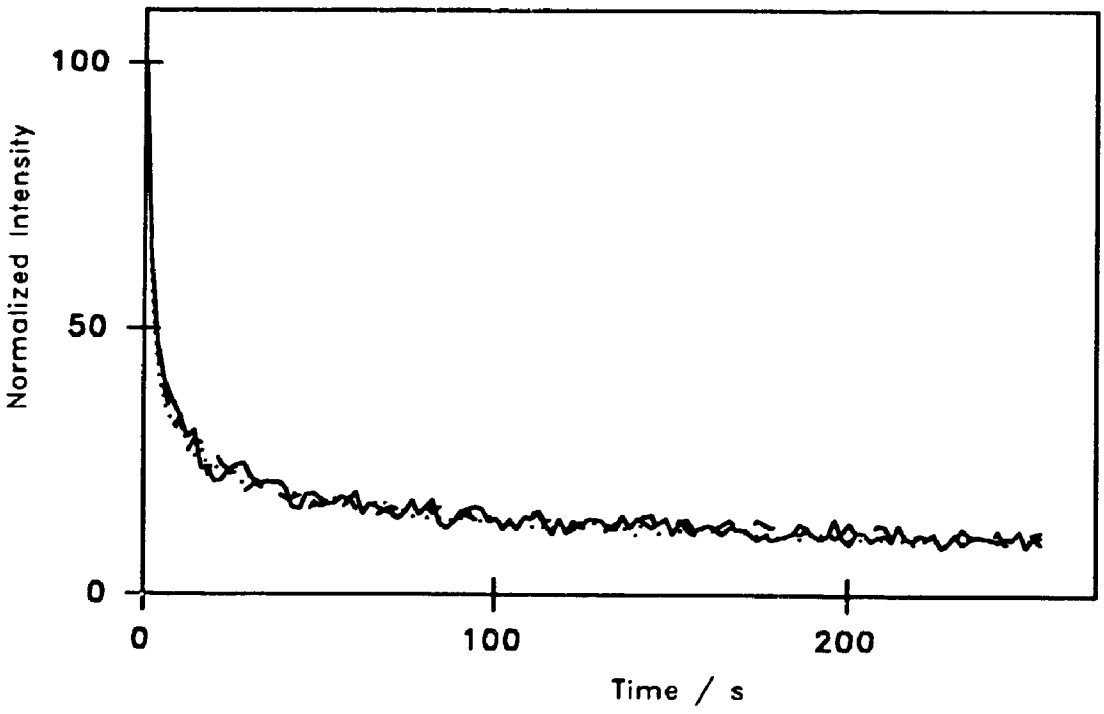
100
50
0
Normalized Intensity
0
100
200
Time / s

Figure 4.15: Effect of laser attenuation on the rate and extent of photobleaching in CFM. (Experimental conditions: 0 torr air pressure; 1.0 μm beam width. Laser attenuation: 2.11 OD (———); 1.75 OD (— —); 1.58 OD (·); 1.08 OD (– – –)).

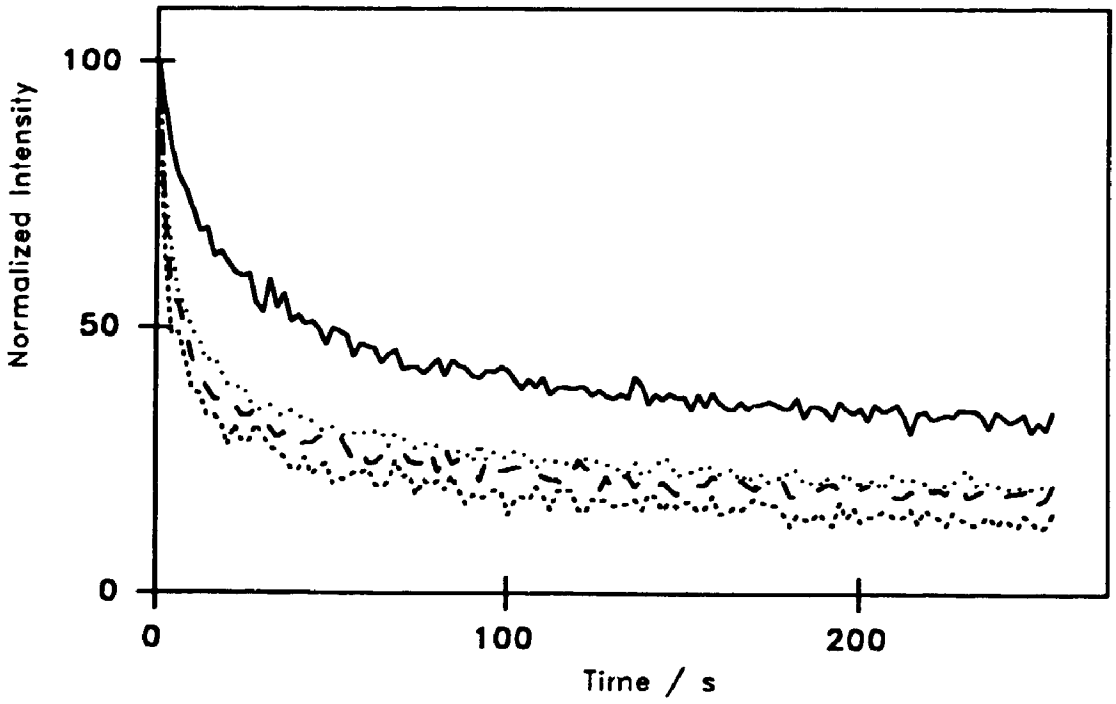
100
50
0
Normalized Intensity
0
100
200
Time / s

An increased rate over the same length of time leads to a greater number of molecules reacting, *i.e.* the number of half lives is increased.

4.2.3.2 Fluorescence Decay of Naphthacene on Silica

Figure 4.16 shows the decay profile for naphthacene adsorbed on silica gel preheated at 25°C. The average lifetimes (calculated via Equation 4.5), based on fits to four exponential functions, for naphthacene on various silica gels and in crystalline form are presented in Table 4.6.

$$\bar{\tau} = \frac{\sum_i a_i \tau_i^2}{\sum_i a_i \tau_i} \qquad (4.5)$$

The average lifetimes in Table 4.6 are larger than the lifetimes found for naphthacene in organic solutions (Table 4.5). In each case, there are rapidly decaying components ($\tau < 1$ ns), slowly decaying components ($\tau > 10$ ns), and components decaying at intermediate rates. The rapidly decaying components are probably due to scattered light. The long lifetime components are thought to arise from the silica support. To test this, the decay from silica is measured and subtracted from two samples (see Table 4.6). These two samples still have a long lifetime component. Changes in average lifetimes or decay rates can only be explained by considering all possible relaxation mechanisms, which include fluorescence (f), intersystem crossing (isc) and non-radiative pathways (nr):

Figure 4.16: Fluorescence decay profile for naphthacene adsorbed on silica pretreated at room temperature. Excitation wavelength 290 nm; Emission wavelength 470 nm.

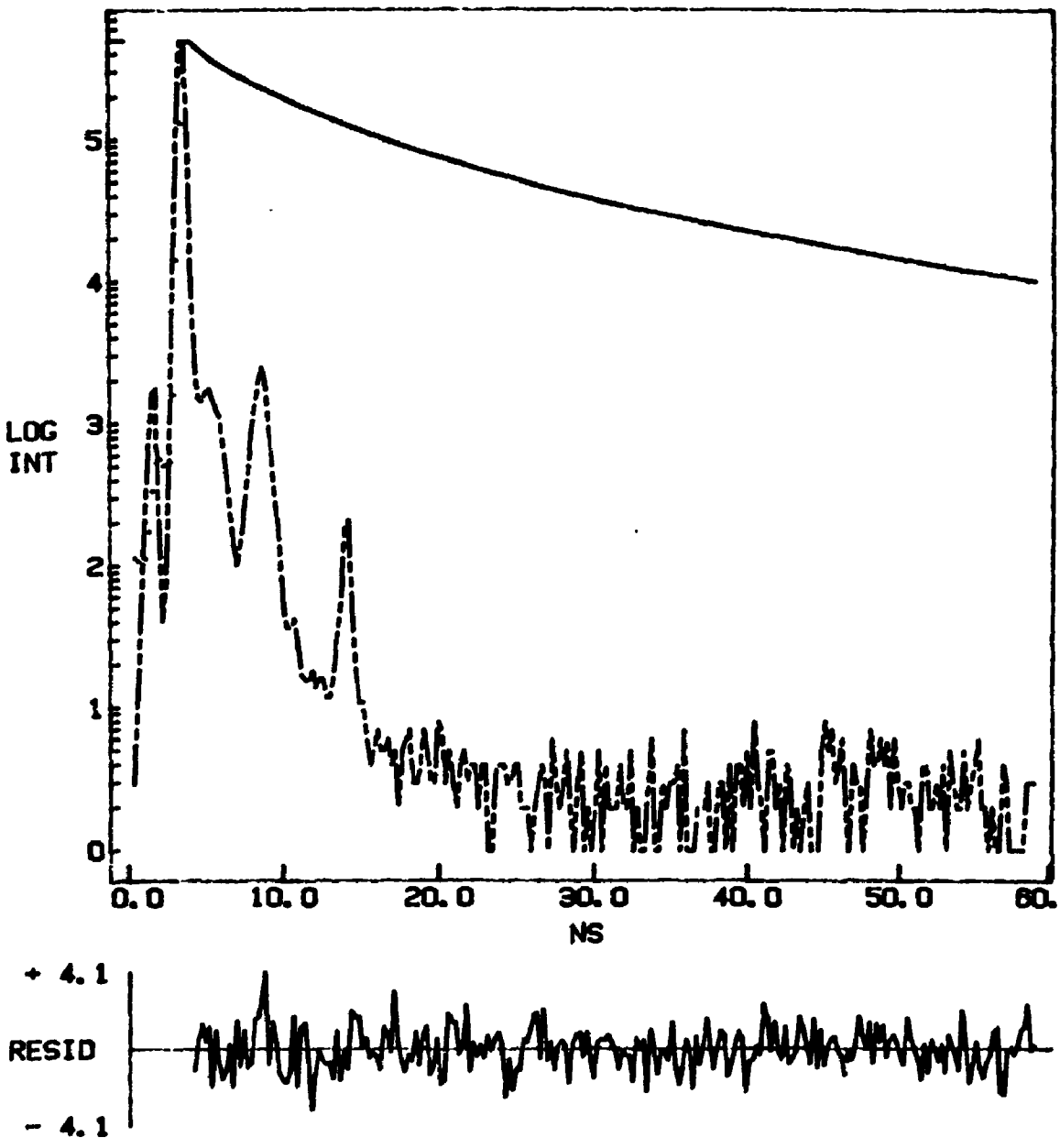
LOG
INT
5
4
3
2
1
0
0.0
10.0
20.0
30.0
40.0
50.0
60.
NS
+ 4.1
RESID
- 4.1

Table 4.6: Fluorescence Lifetimes for Naphthacene Decay in Crystalline Form and Adsorbed on Silica.

Preparation[a]	$\langle\tau\rangle^b$ / ns	CPC[c] / 10^3
Powder	4.31	200
Crystals from solution	2.28	100
25°C silica	15.96	500
25°C silica	8.25	500
25°C silica[d]	12.74	650
25°C silica[d]	12.82	700
250°C silica	6.00	500
250°C silica	5.10	500
600°C silica	15.05	500
600°C silica	13.36	500

[a]Sample description.

[b]Average lifetime calculated from Equation 4.5.

[c]Counts in the peak channel.

[d]Silica blank subtracted.

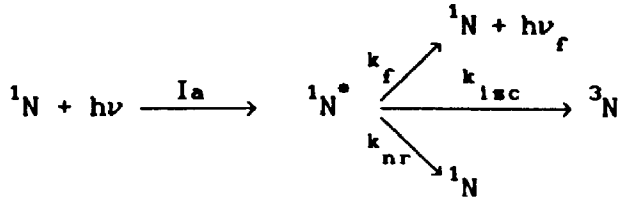

(4.6)

where I_a is the rate of absorption of light with energy $h\nu$, the k's are rate constants, and $h\nu_f$ is the energy of fluorescence. The total rate constant for decay (k_d) from the first excited singlet state is given by Equation 4.7, with the lifetime (τ_d) defined by k_d^{-1}.

$$k_d = k_f + k_{isc} + k_{nr} \tag{4.7}$$

Single photon counting gives a measure of the total decay (k_d) from the excited state. For an increase in the rate of decay, at least one of the pathways in 4.6 must be enhanced. Conversely, a decrease implies inhibition of one of the pathways. Compared to the rate of decay in solution (k_d = 0.2 to 0.3 ns^{-1}), an increase is seen for crystalline naphthacene (k_d = 0.25 to 0.5 ns^{-1}), while a decrease is observed for naphthacene adsorbed on silica ($k_d \leq 0.2$ ns^{-1}).

Fitting the data to a small number of discrete lifetimes is misleading since a distribution of lifetimes should be expected[48,49]. To recover underlying distributions in the decay data, the Exponential Series Method (ESM) is employed. ESM consists of choosing a set number of lifetimes logarithmically spaced over a selected range, and calculating the pre-exponential factors (a_i's) of a series of exponential functions[48-50]:

$$f(t) = \sum_{i=1}^{n} a_i \exp(-t/\tau_i) \tag{4.8}$$

where f(t) represents the fluorescence intensity as a function of time.

Recovered distributions for naphthacene in crystalline form and adsorbed on silica gel pretreated at various temperatures are presented in Figure 4.17. All plots show rapidly decaying components (with $\tau < 1$ ns), which is an artifact. These components are present in most ESM analyses, and are due to scattered light. Focusing on the lifetimes with $\tau \geq 1$ ns, ESM results for crystalline naphthacene (Figure 4.17a) shows two distributions, with peak values near 1 ns and 3.5 to 4 ns. ESM recovers slightly different distributions for powdered naphthacene and naphthacene crystallized from solution.

Other PAHs in crystalline form have not been examined using ESM. To use these techniques (ESM and MEM) properly, simulations of data should be carried out to test the ability of ESM to distinguish between a distribution of lifetimes and a set of discrete lifetimes. This is not a straight forward simulation process for crystalline materials since there are many parameters very difficult to incorporate into simulations, such as photon re-absorption and re-emission. The experiments are done here with crystalline naphthacene solely to establish a basis for qualitative comparison of ESM results obtained for naphthacene adsorbed on silica. From work using the fluorescence microscope, it is evident that naphthacene forms crystalline domains on dry silica gel. Hence, it is necessary to examine the decay of naphthacene crystals in order to make direct comparisons to data accumulated for naphthacene on silica.

For naphthacene on dry silica gel, ESM recovers one distribution, with peak values in the 4 to 7 ns range, and a spike at higher lifetime values (10 to 40 ns). Extending the lifetime range does not

Figure 4.17a: Lifetime distributions recovered by ESM for crystalline naphthacene. Top: naphthacene powder; bottom: naphthacene crystallized from cyclohexane solution. Lifetime range: 0.1 to 20 ns; number of lifetimes: 100.

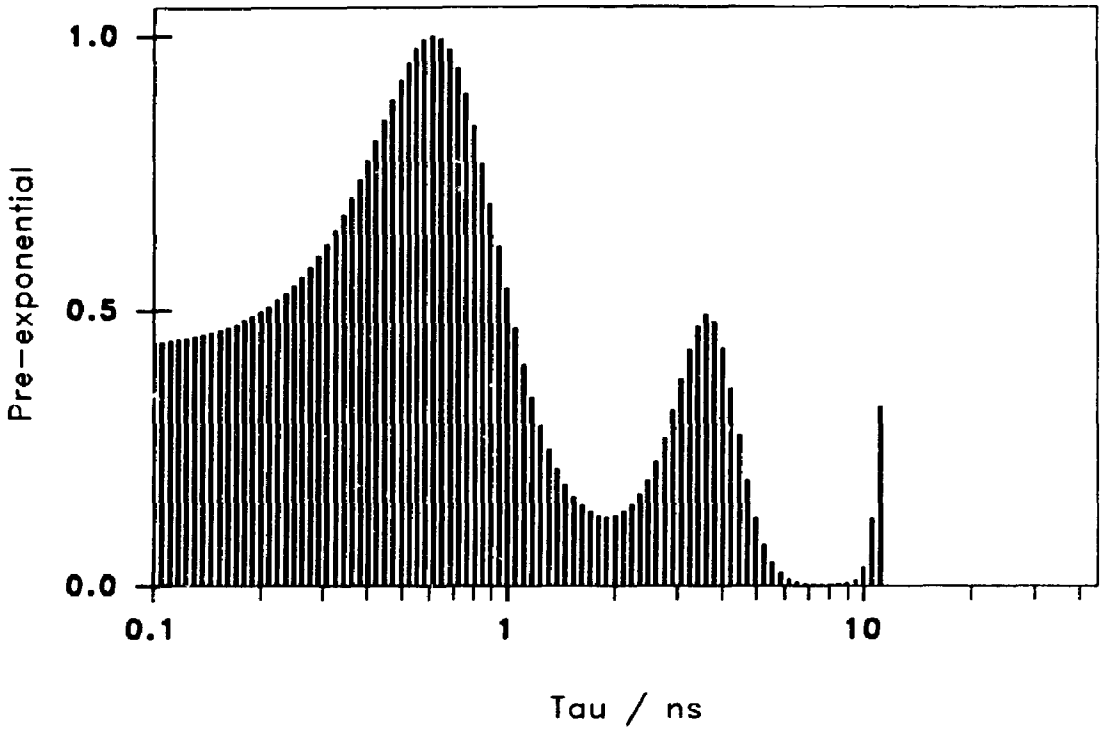
1.0
0.5
0.0
Pre-exponential
0.1
1
10
Tau / ns

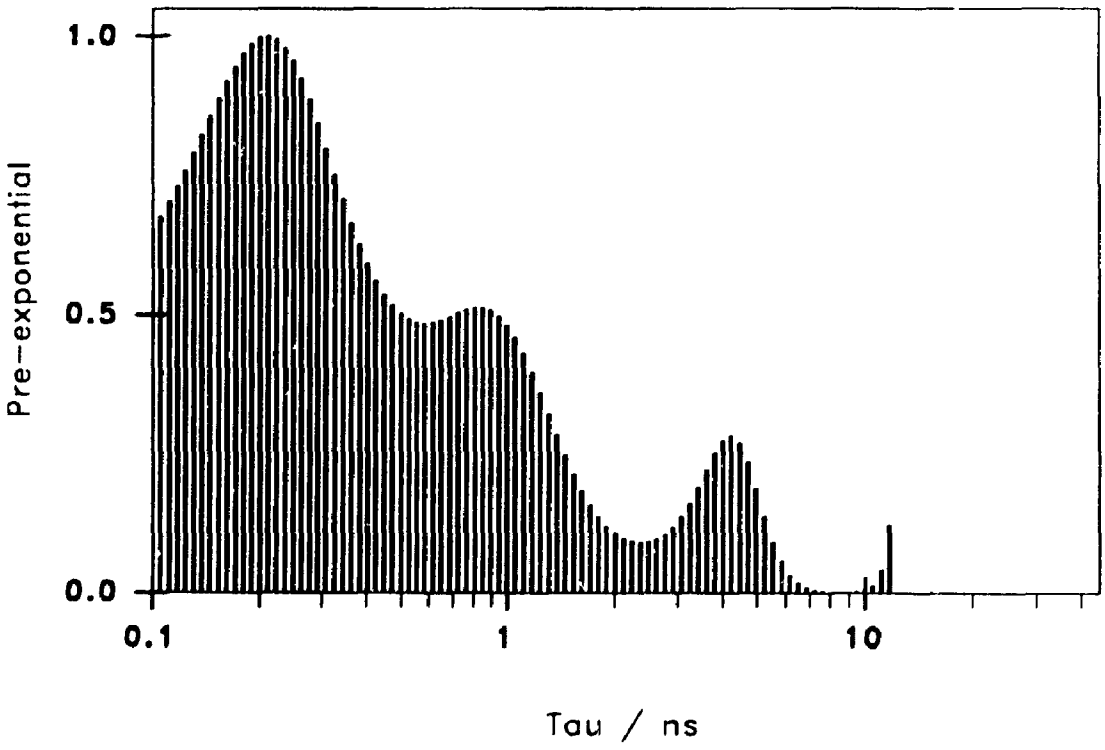
1.0
0.5
0.0
Pre-exponential
0.1
1
10
Tau / ns

Figure 4.17b: Lifetime distributions recovered by ESM for naphthacene adsorbed on silica pretreated at room temperature. Lifetime range: 0.5 to 40 ns; number of lifetimes: 100.

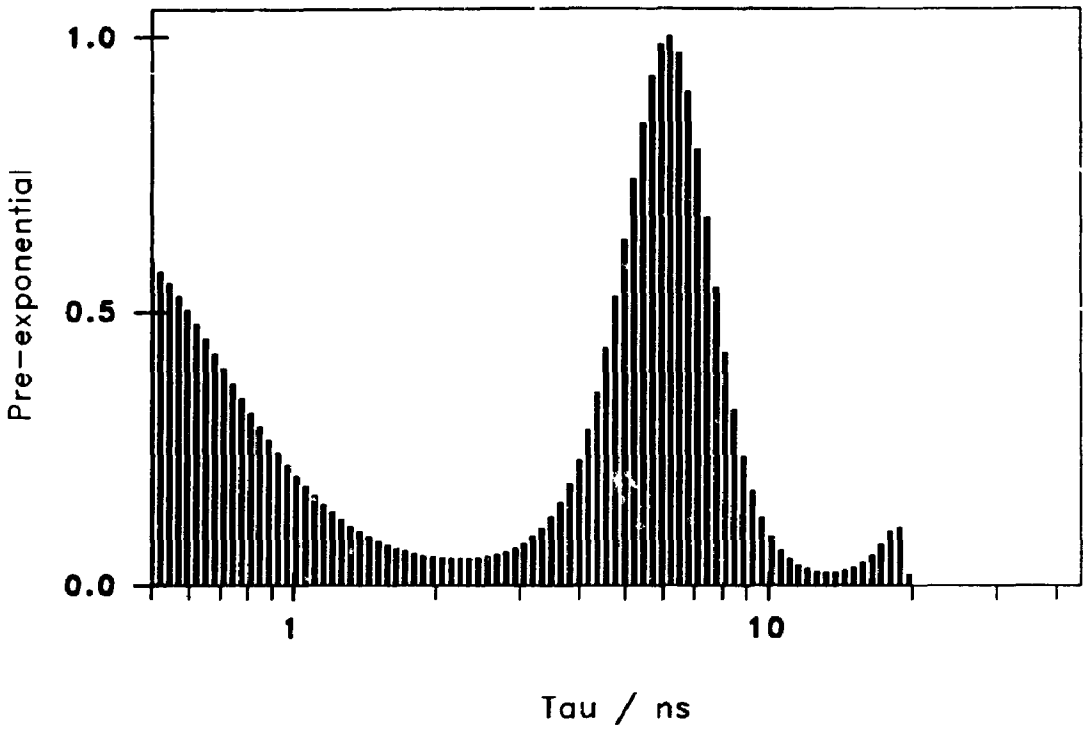
1.0
0.5
0.0
Pre-exponential
1
10
Tau / ns

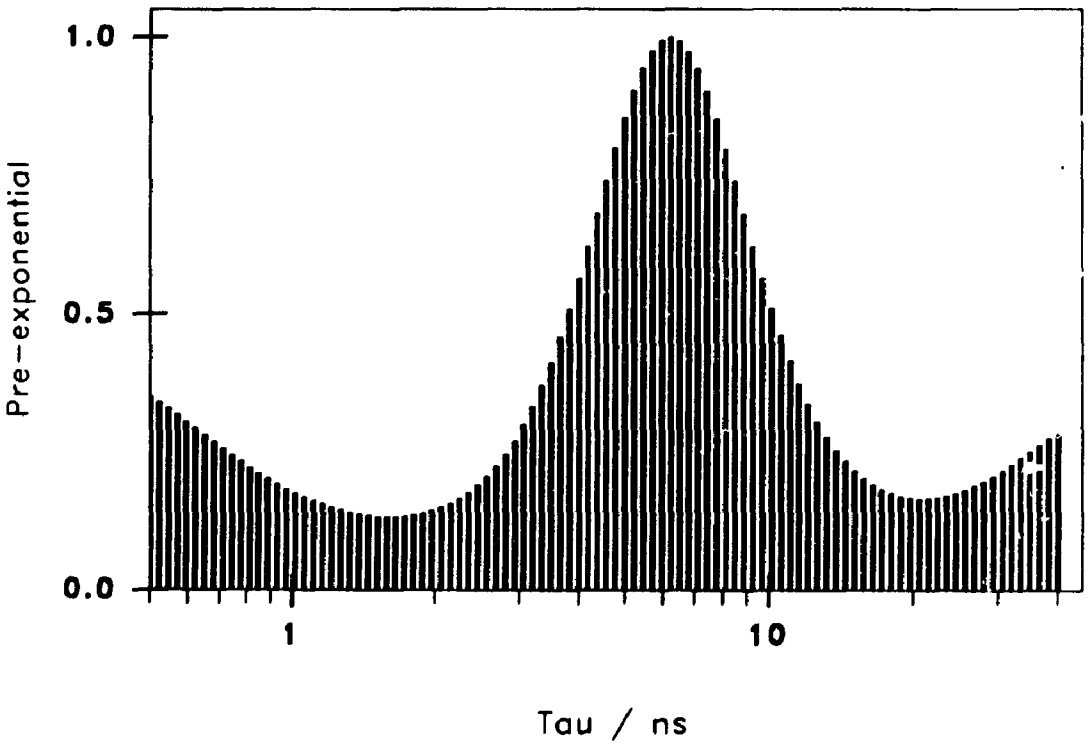
1.0
0.5
0.0
Pre-exponential
1
10
Tau / ns

Figure 4.17c: Lifetime distributions recovered by ESM for naphthacene adsorbed on silica pretreated 250^{0}C. Lifetime range: 0.5 to 40 ns; number of lifetimes: 100.

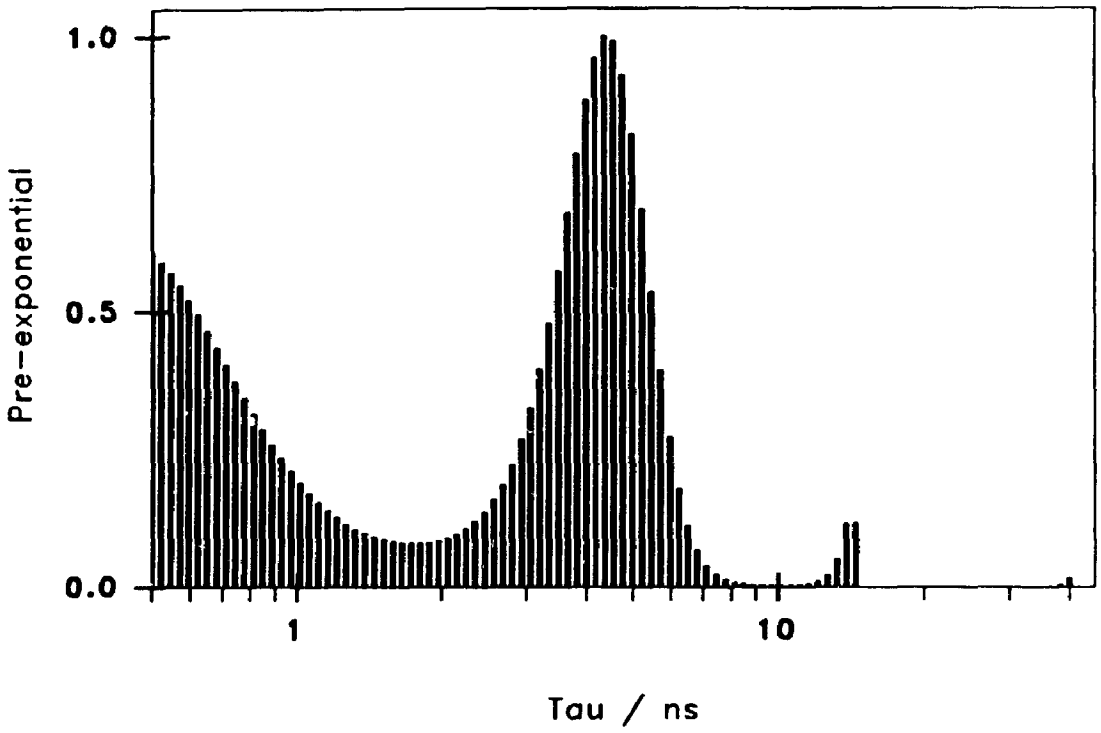
1.0
0.5
0.0
Pre-exponential
1
10
Tau / ns

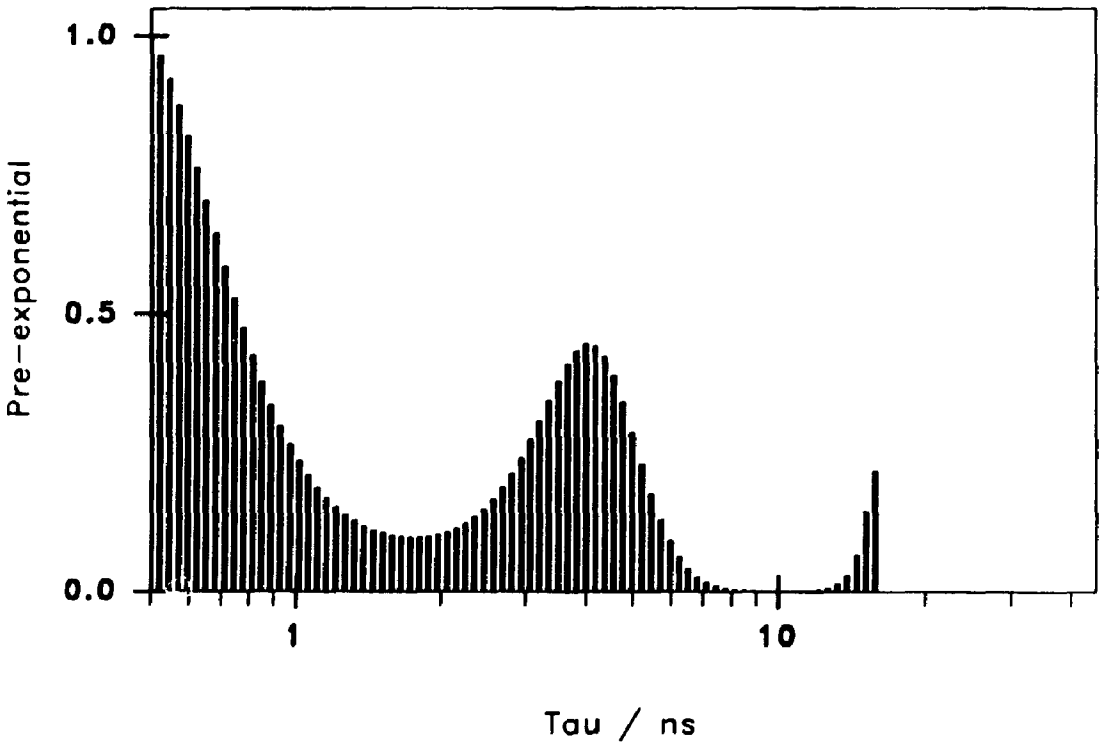
1.0
0.5
0.0
Pre-exponential
1
10
Tau / ns

Figure 4.17d: Lifetime distributions recovered by ESM for naphthacene adsorbed on silica pretreated 600^{o}C. Lifetime range: 0.5 to 40 ns; number of lifetimes: 100.

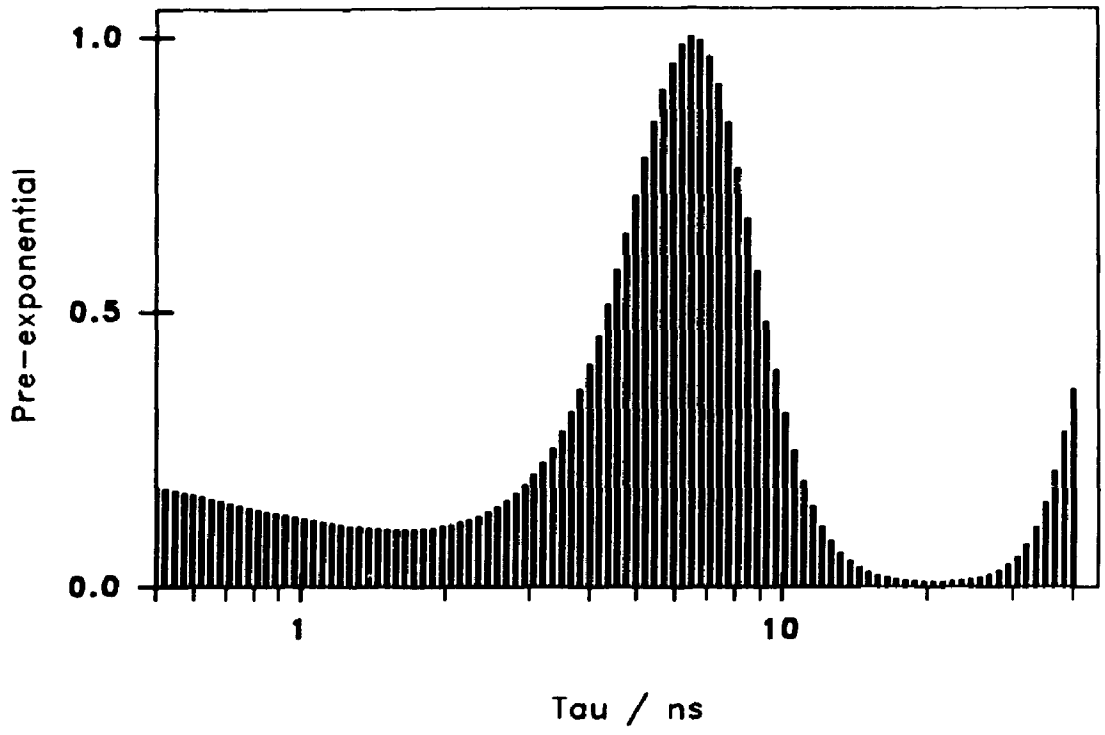
1.0
0.5
0.0
Pre-exponential
1
10
Tau / ns

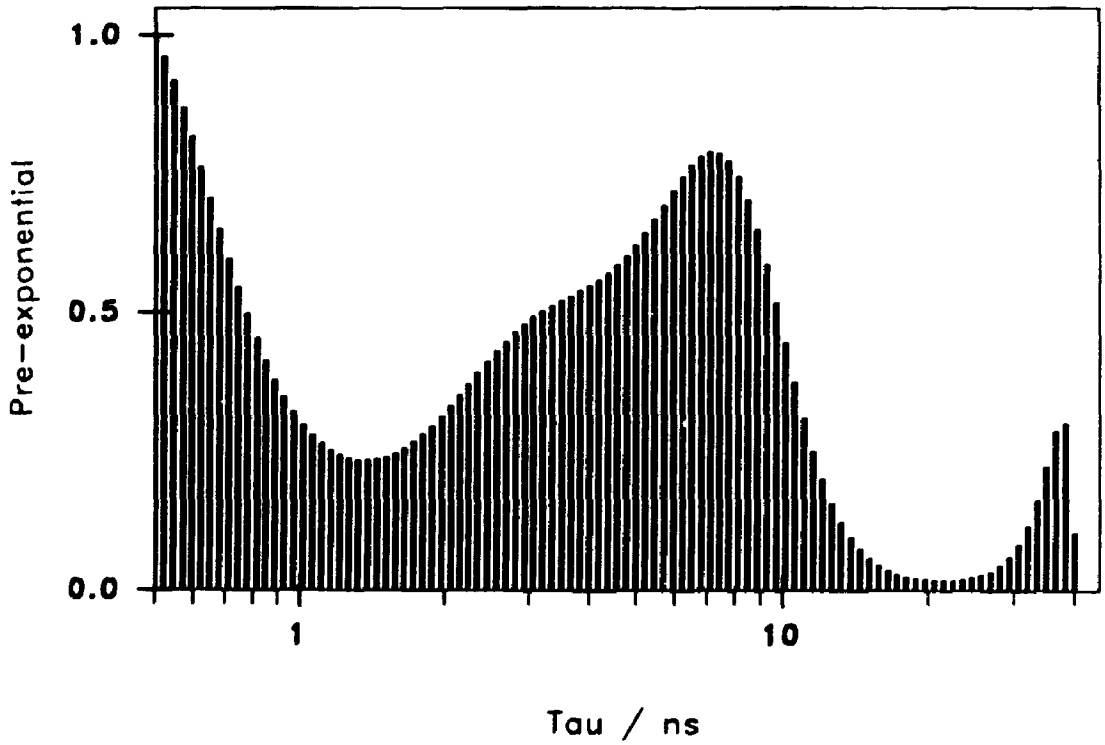
1.0
0.5
0.0
Pre-exponential
1
10
Tau / ns

change the position or the intensity of the spike. The spike may be real, but simulations would have to be performed to test for this. The distributions in the 4 to 7 ns range are of interest. A consistent trend in the peak value of these distributions is not observed with pretreatment temperature. The distributions for the samples heated at 25°C (Figure 4.17b) have peak values near 6.2 ns, those for silica heated to 250°C (Figure 4.17c) are near 4 ns, and those for the 600°C samples (Figure 4.17d) are at 6 to 7 ns. With other PAHs, a consistent trend is usually seen, with the peak values decreasing with pretreatment temperature[52]. It is unclear why a consistent trend is not seen with naphthacene.

Some differences are seen in the ESM results for samples of adsorbed naphthacene prepared under the same conditions. The most obvious case is that for naphthacene adsorbed on silica heated to 600°C (Figure 4.17d). These differences could be caused by small variations in sample preparation or by aging of the samples.

A very interesting observation is that the position of the distributions recovered by ESM are in the same lifetime range as naphthacene in organic solvents (Table 4.5). For a large number of PAHs examined, the lifetime is significantly decreased upon adsorption on silica[52]. One other PAH, perylene, shows little change of lifetime between the adsorbed samples and solution[52]. A common factor between naphthacene and perylene is that the emission from both is in the lower energy part of the visible spectrum. Most other PAHs emit in the near UV to the blue end of the visible spectrum, at larger energies. It has been postulated that PAHs whose emission is at

higher energies can be quenched by an interaction of some kind with the surface. For this to occur, there must be spectral overlap between the emission of the PAH and the absorption of whatever surface mode causes the quenching. This implies the active surface modes should be detectable through normal absorption spectroscopies. The nature of these modes is unknown and they have not yet been detected. Molecules with emission in the visible region cannot be quenched by the surface, because of poor spectral overlap.

These preliminary experiments are done to investigate a possible link between photophysical examinations and the diffusion measurements discussed in Chapter 3. Analyses using ESM generally give one distribution, with a peak value in the 4 to 7 ns range. However, from the FPR experiments, we know that there must be at least two naphthacene populations on dry silica, a mobile one and an immobile one (Table 3.1). From the ESM result, it appears that we cannot distinguish between the photophysical properties of these two populations. Little evidence for a lifetime distribution due to crystalline naphthacene on the surface is found. The difference in the peak values for the distributions obtained for crystalline naphthacene and naphthacene on silica heated to 25^{o}C and 600^{o}C is large enough that recovered distributions should appear skewed or as two overlapping distributions. This is possibly seen in one of the 600^{o}C samples (Figure 4.17d), but not in any of the others. The photophysical experiments are by no means complete. Simulations should be carried out to determine if ESM can distinguish between the recovered distributions and a possible set of discrete lifetimes. It

would also be necessary to test if the spike recovered at larger lifetimes is real. These tasks have not been completed.

4.2.4 Conclusions

The kinetics of photobleaching of adsorbed naphthacene are found to be neither first nor second order, regardless of the oxygen content. A combination of processes with different kinetic pathways is probably occurring. Graphical analysis of CFM results show the rate of photobleaching increases with oxygen content and laser intensity. A consistent trend between the initial rate and power density (or beam size) is not observed.

A more quantitative approach to CFM can be taken. Further development of the theory pioneered by Peters *et al.*[53,54] and extended by Ferrières and colleagues[55] is required. If a Gaussian intensity beam is to be used, any effects due to the non-uniform beam intensity must be determined. The central intensity of the Gaussian beam is higher than the intensity at greater radial distances. Hence, the rate of absorption, and therefore, the rate of photochemistry should be greatest an the center of the beam. A method for deconvolution of this effect must be developed in order to interpret CFM data correctly.

Fluorescence decay of naphthacene adsorbed on silica gel is best described by a distribution of lifetimes, and not a small set of discrete lifetimes. ESM analyses reveals one distribution for naphthacene on silica in most cases. The fluorescent lifetime of

adsorbed naphthacene is not significantly changed from that of naphthacene in organic solvents. FPR results reveal at least two populations for naphthacene on silica gel. ESM does not give any evidence of distinguishing between the two.

A direct link between the measured diffusion parameters for naphthacene on dry silica gel (Chapter 3.1) and the photophysical results cannot be made. From the experiments reported here, there is no obvious direct relationship between the two dimensional diffusion coefficient and bimolecular quenching data presented elsewhere[25]. The nature of the two measurements (FPR and quenching experiments) is such that the species being examined are similar (a PAH), but the processes being followed in each case are very different.

Future research with these systems is desirable. Both CFM and ESM can be approached from a more quantitative viewpoint. Kinetic modeling of these systems should be carried out. For future CFM work, the effects of the Gaussian laser beam intensity should be deconvoluted from the signal, or one should use a beam of uniform intensity.

REFERENCES

(1) Lapouyade, R.; Nourmamode A.; Bouas-Laurent, H. *Tetrahedron* **1980**, *36*, 2311.

(2) Bouas-Laurent, H.; Castellan, A. *J. Chem. Soc., Chem. Commun.* **1970**, 1648.

(3) Wei, K. S.; Livingston, R. *Photochem. Photobiol.* **1967**, *6*, 229.

(4) Birks, J. B.; Appleyard, J. H., Pope, R. *Photochem. Photobiol.* **1963**, *2*, 493.

(5) Birks, J. B.; Aladekomo J. B. *Photochem. Photobiol.* **1963**, *2*, 493.

(6) Fournie, G.; Dupuy, F.; Martinaud, M.; Nouchi, G.; Turlet, J. M. *Chem. Phys. Lett.* **1972**, *16*, 331.

(7) Katul, J. A.; Zahlan, A. B.; *J. Chem. Phys.* **1967**, *47*, 1012.

(8) Saito, I.; Matsuura, T. In *Singlet Oxygen;* Wasserman, H. H.; Murray, R. W., Eds.; Academic Press: London, 1979, Chapter 10.

(9) Bloodworth, A. J.; Eggelte, H. J. In *Singlet* O_2; Frimer A. A., Ed.; CRC Press: Boca Raton, 1985, Volume II, Chapter 4.

(10) Stevens, B. In *Singlet Oxygen Reactions with Organic Compounds and Polymers;* Rånby, B.; Rabek, J. F. Eds; John Wiley and Sons: Chicester, 1978. Chapter 8.

(11) Stevens, B.; Algar, B. E. *Chem. Phys. Lett.* **1967**, *1*, 58.

(12) Stevens, B.; Algar, B. E. *J. Phys. Chem.* **1968**, *72*, 2582.

(13) Stevens, B.; Algar, B. E. *J. Phys. Chem.* **1968**, *72*, 3468.

(14) Schmidt, R.; Brauer, H. D. *J. Photochem.* **1986**, *34*, 1.

(15) Brauer, H. D.; Schmidt, R. *J. Phootochem.* **1984**, *27*, 17.

(16) Rigaudy, J.; Sparfel, D. *Bull. Chim. Soc. Fr.* **1977**, *7-8*, 742.

(17) Rigaudy, J.; Sparfel, D. *Tetrahedron,* **1978**, *34*, 113.

(18) Ogryzlo, E. A. In *Singlet Oxygen Reactions with Organic Compounds and Polymers;* Rånby, B.; Rabek, J. F. Eds; John Wiley and Sons: Chicester, 1978. Chapter 2.

(19) Birks, J. B. In *Photophysics of Aromatic Molecules;* Wiley-Interscience: London, 1970.

(20) Birks J. B. (Ed) *Organic Molecular Photophysics, Volumes 1 and 2;* John Wiley and Sons: London, 1975.

(21) Berlman, I. B. In *Fluorescence Spectra of Aromatic Molecules;* Academic Press: New York, 1965; Second Edition, p. 132.

(22) Francis, C.; Lin, J.; Singer, L. A. *Chem. Phys. Lett.* **1983**, *94*, 162.

(23) Turro, N. J.; Zimmt, M. B.; Gould, I. R. *J. Amer. Chem. Soc.* **1985**, *107*, 5826.

(24) Bauer, R. K.; Borenstein, R.; de Mayo, P.; Okada, K.; Rafalska, M.; *Ware, W. R.;* Wu, K. C. *J. Amer. Chem. Soc.* **1982**, *104*, 4635.

(25) de Mayo, P ; Natarajan, L. V.; Ware, W. R. *Chem. Phys. Lett.* **1984**, *107*, 187.

(26) de Mayo, P.; Natarajan, L. V.; Ware, W. R. *J. Phys. Chem.* **1985**, *89*, 3526.

(27) de Mayo, P.; Natarajan, L. V.; Ware, W. R. In *Organic Phototransformations in Nonhomogeneous Media;* Fox, M. A., Ed.; American Chemical Society: Washington, DC, 1985; Chapter 1.

(28) Bauer, R. K.; de Mayo, P.; Ware, W. R.; Wu, K. C. *J. Phys.Chem.* **1982**, *86*, 3781.

(29) Bauer, R. K.; de Mayo, P.; Okada, K.; Ware, W. R.; Wu, K. C. *J. Phys. Chem.* **1983**, *87*, 460.

(30) de Mayo, P.; Okada, K.; Rafalska, M.; Weedon, A. C.; Wong, G. S. K. *J. Chem. Soc. Chem Commun.* **1981**, 821.

(31) Bauer, R. K.; de Mayo, P.; Natarajan, L. V.; Ware, W. R. *Can. J. Chem.* **1984**, *62*, 1279.

(32) Turro, N. J.; Cheng, C-C. *J. Amer. Chem. Soc.* **1984**, *106*, 5022.

(33) Beck, G.; Thomas, J. K. *Chem. Phys. Lett.* **1983**, *94*, 553.

(34) Fujii, T.; Shimizu, E. *Chem. Phys. Lett.* **1987**, *137*, 448.

(35) Fujii, T.; Shimizu, E.; Suzuki, S. *J. Chem. Soc. Faraday Trans. I* **1988**, *84*, 4387.

(36) Anpo, M.; Nishiguchi, H.; Fujii, T. *Res. Chem. Inter.* **1990**, *13*, 73.

(37) Oelkrug, D.; Flemming, W.; Füllemann, R.; Günther, R.; Honnen, W.; Krabichler, G.; Schäfer, M.; Uhl, S. *Pure and Appl. Chem.* **1986**, *58*, 1207.

(38) Oelkrug, D.; Krabichler, G.; Honnen, W.; Wilkinson, F.; Willsher, C. J. *J. Phys. Chem.* **1988**, *92*, 3589.

(39) Oelkrug, D.; Uhl, S.; Wilkinson, F.; Willscher, C. J. *J. Phys. Chem.* **1989**, *93*, 4551.

(40) Youngs, R. H.; Brewer, D. R. In *Singlet Oxygen Reactions with Organic Compounds and Polymers;* Rånby, B.; Rabek, J. F. Eds; John Wiley and Sons: Chicester, 1978. Chapter 6.

(41) Pasto D. J.; Johnson D. R. In *Laboratory Text for Organic Chemistry;* Prentice-Hall Inc.: Englewood NJ, 1979, p 29.

(42) O'Connor, D. V.; Phillips, D. In *Time-correlated Single Photon Counting;* Academic Press: London, 1984.

(43) Iannone, M. A.; Scott, G. W. *Chem. Phys. Lett.* **1990**, *171*, 569.

(44) Belluš, D. In *Singlet Oxygen Reactions with Organic Compounds and Polymers;* Rånby, B.; Rabek, J. F. Eds; John Wiley and Sons: Chicester, 1978. Chapter 9.

(45) Monroe, B. M. In *Singlet* O_2*;* Frimer, A. A. Ed.; CRC Press: Boca Raton, 1985, Volume I, Chapter 5.

(46) Estimate based on lifetimes for singlet oxygen for other alcohols in references 44 and 45.

(47) Livingston, R. In *Photochemistry in the Liquid and Solid States;* Daniels, F., Ed.; John Wiley and Sons: New York, 1960; pp 76-82.

(48) James, D. R.; Ware, W. R. *Chem. Phys. Lett.* **1986**, *126*, 7.

(49) Siemiarczuk, A.; Wagner, B. D.; Ware, W. R. *J. Phys. Chem.* **1990**, *94*, 1661.

(50) James, D. R.; Liu, Y.-S.; Petersen, N. O.; Siemiarczuk, A.; Wagner, B. D.; Ware, W. R. *SPIE* **1987**, *743*, 117.

(51) Albery, W. J.; Johnson, C. R.; Wilde, C. P.; Darwent, J. R. *J. Amer. Chem. Soc.* **1985**, *107*, 1854.

(52) Liu, Y.-S; Ware, W. R. personal communication.

(53) Peters, R.; Brünger, A.; Schulten, K. *Proc. Natl. Acad. Sci.* **1981**, *78*, 962.

(54) Brünger, A.; Peters, R.; Schulten, K. *J. Chem. Phys.* **1985**, *82*, 2147.

(55) Ferrières, X.; Lopez, A.; Altibelli, A.; Dupou-Cezanne, L., Lagouanelle, J-L.; Tocanne, J-F. *Biophys. J.* **1989**, *55*, 1081.

CHAPTER FIVE

Summary

We use Fluorescence Photobleaching Recovery (FPR) to measure the mobility (both rate and fraction of mobile molecules) of naphthacene adsorbed on various silica surfaces at low coverages. This set of experiments represents the first time FPR has been employed to measure mobilities in completely non-biological systems. We find polycyclic aromatic hydrocarbons to have significant mobility on all silica surfaces. In particular, the mobility of adsorbed naphthacene is examined in detail. The diffusion coefficient for naphthacene on normal phase silica is invariant of the silica preparation (pretreatment temperature, addition of water), and is measured to be 2.4×10^{-10} cm^2 s^{-1}. The mobile fraction has a significant dependence on the silica preparation, and varies from 33 to 67%.

These results (invariant diffusion coefficient and variable mobile fraction) indicate that the same population of naphthacene is being measured in each case, but the relative amount of molecules in this population changes with silica preparation. We propose a model based solely on geometric factors to predict which population of naphthacene is the mobile one. From this model it appears that molecules bound to three silanol groups are the mobile species being measured. The best experimental test for this model would be to measure the mobility of other linear PAHs (naphthalene, anthracene, pentacene). We expect little change in the diffusion coefficient, but significant change in the mobile fraction with the number of rings in

the PAH. The diffusion of pentacene on silica has been unsuccessfully examined due to the photophysical (low quantum yield of fluorescence) and photochemical (readily oxidizes) nature of this PAH.

Results obtained with rubrene on silica were found to be inconsistent between samples, but qualitative assessments are justified. Rubrene shows significant mobility with a diffusion coefficient larger than that of naphthacene (5×10^{-10} cm^2 s^{-1}), and a mobile fraction near 40%.

On all normal phase silica surfaces the surface distribution of naphthacene is heterogeneous. This is seen as microcrystalline domains on the surface in the microscope. The portion of naphthacene in these domains depends on the silica preparation. This affects the mobile fraction, as these domains are not mobile.

Derivatization of the silica surface with alkyl chains produces a hydrophobic surface, on which naphthacene is distributed less heterogeneously. Both the diffusion coefficient (6.6×10^{-10} cm^2 s^{-1}) and mobile fraction (50%) are increased over the value measured for naphthacene on normal phase silica pretreated at room temperature. Hence, the surface is coated in hydrocarbon chains, but the coating is not complete. More homogeneous coatings are obtained by physisorption of long chain alcohols or acids on the surface. On these surfaces, the diffusion coefficient is 2.5×10^{-9} cm^2 s^{-1}, and the mobile fraction approaches 90%.

The recovered diffusion parameters for naphthacene on all surfaces mentioned above are found to be broad distributions. The

widths of the distributions are larger than would be expected from inherent uncertainties in the calculation of the diffusion parameters. We attribute the widths to heterogeneities on the surface, and in the distribution of naphthacene.

The photochemistry and photophysics of naphthacene in solution and on the surface are also examined. The fluorescence decay of naphthacene in solution follows a single exponential decay law, with lifetimes in the 3 to 6 ns range. On the surface, the decay is best described as a distribution of lifetimes. Very little quenching is observed for naphthacene in going from a homogeneous solution to a heterogeneous surface. Many other PAHs have much shorter lifetimes on the surface than in solution. This may be due to certain surface interaction which may cause quenching in PAHs that emit in the near ultraviolet, but not for those which emit at lower energies.

The photolysis of naphthacene in solution leads to either an oxidation product (endoperoxide), or two dimers. Formation of both types of photoproducts follow mechanisms first order in naphthacene, but the rate of oxidation is much greater than that of dimerization.

On the surface, the kinetics of photolysis are not as simple. Qualitative analysis of data collected via Continuous Fluorescence Microphotolysis indicates that naphthacene does not always follow first order kinetics on the surface. To examine any systematic errors in the measured diffusion parameters the theoretical basis of FPR is expanded to include second order bleaching processes. Previously, only first order processes were considered. We find, through

simulations, that use of the theory developed for first order bleaching kinetics will adequately fit data generated after a second order bleaching process. Little effect is seen in the value of the mobile fraction. As the extent of bleaching increases, the value of the diffusion coefficient is increasingly underestimated. Unfortunately, the functional form developed for fitting of data with a theory based solely on second order processes involves a series which is divergent under normal experimental conditions. We propose that the original theory will give a good estimate of the diffusion parameters, but if the photobleaching is known to follow a second process, a correction factor for the diffusion coefficient should be employed.